FREE.

UNCLASSIFIED
CONTRACT NO. NGR 22-009-065

THERMAL CONTACT CONDUCTANCE IN A VACUUM

M. MICHAEL YOVANOVICH

Engineering Projects Laboratory
Massachusetts Institute of Technology

DSR Report No. 4542-39

(Heat Transfer Laboratory Series)

National Aeronautics and Space Administration

November 1965

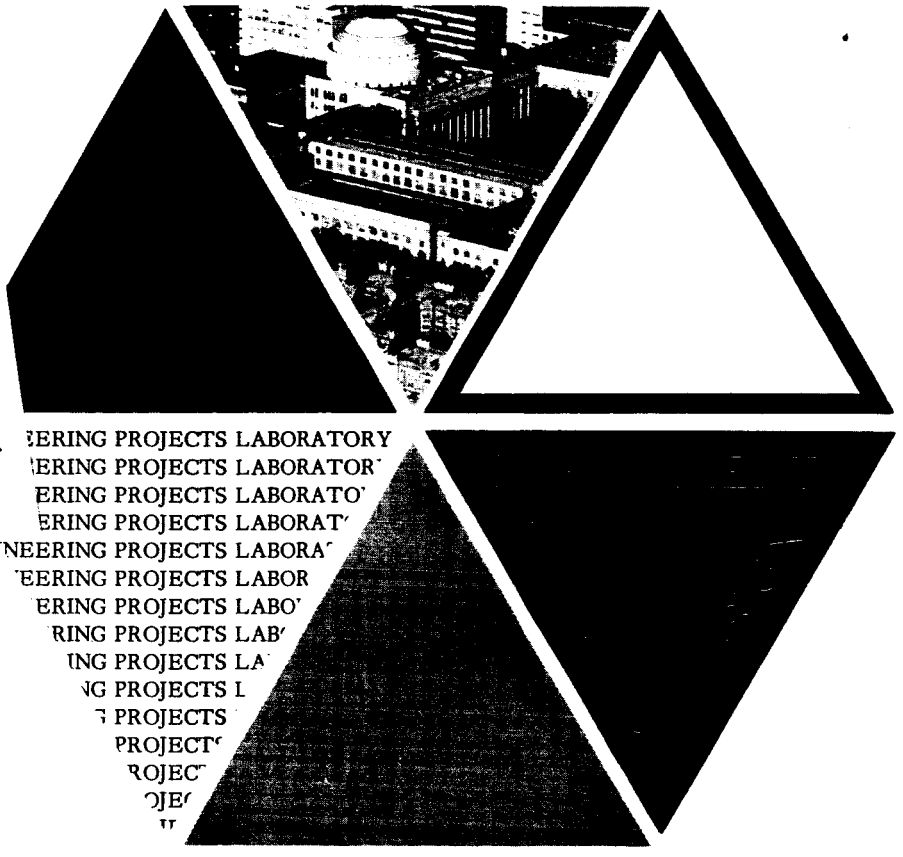

THERMAL CONTACT CONDUCTANCE IN A VACUUM

by

MILAN MICHAEL YOVANOVICH

ABSTRACT

The object of this work is to develop analytically equations by which one could predict the thermal contact conductance between contiguous surfaces operating in a vacuum environment. In this work the solution to the problem is obtained by considering that any surface can be modelled as being either: 1) nominally-flat but rough, 2) a smooth surface having cylindrical waviness, 3) a smooth surface having spherical waviness, or 4) a surface having either cylindrical or spherical waviness plus roughness. Since the radiative heat transfer and the conduction through the interstitial fluid are negligible, the conduction of heat across the metal contact spots is the dominant mechanism. It is considered that the prediction of thermal contact conductance must be approached by: 1) examining the surface geometry, 2) proposing mathematical models for the solution of the heat transfer problem, 3) determining the surface parameters from deformation analysis, and 4) obtaining experimental data to substantiate the proposed models.

The surface analysis is actually a critical examination of profiles of real surfaces as obtained by profilometers. From such profiles it is proposed that real surfaces can be idealized by assuming that any surface is a combination of a wavy and rough component.

The thermal analysis is based upon the models proposed and the solutions for the steady-state condition are obtained for the various models and the appropriate boundary conditions. Certain surface parameters appear in the thermal contact conductance equations, which require that an analysis of the deformation of the surface under load be undertaken.

The deformation analysis is separated into two regimes: 1) purely elastic and 2) purely plastic. The surface parameters are then determined as functions of the applied load for the proposed models under the restrictions of pure elastic or pure plastic deformation.

Since real surfaces yield elastically and plastically under load, test data are obtained to correlate the heat transfer equation with the applied load.

Thesis Supervisor: Warren M. Rohsenow

Title: Professor of Mechanical Engineering

TABLE OF CONTENTS

TABLE OF CONTENTS (Cont'd)

TABLE OF CONTENTS (Cont'd)

ACKNOWLEDGEMENTS

The author wishes to acknowledge the assistance and advice of his thesis supervisor, Professor Warren M. Rohsenow, and the many long and fruitful discussions with Professor Henri Fenech.

The author also wishes to extend his gratitude to Mr. Frederick Johnson for his help in the construction and the operation of the surface generator.

The author is also grateful to Mr. Bora Mikic for many stimulating discussions pertaining to contact conductance.

The author wishes to express his sincere appreciation for the financial support of the National Aeronautics and Space Administration under Research Grant NGR-22-009-065.

This work was done in part at the Computation Center at the Massachusetts Institute of Technology, Cambridge, Massachusetts.

NOMENCLATURE

Symbols	Description	Unit
a	radius of heat channel	in.
c	radius of contact spot	in.
h	contact conductance	BTU/hr-ft^2
k	thermal conductivity	BTU/hr-ft-^{o}F
k_1	material constant	1/psi
ℓ	length in direction of no waviness	in.
n	contact spots per unit area	no/in^2
p	apparent pressure	psi
A	total area	in^2
C	compliance	in
E	modulus of elasticity	psi
H	microhardness	psi
L	wave pitch	in
N	total number of contact spots	no
P	total load	lb
R	contact resistance	^{o}F/BTU/hr
S	surface	ft^2
T	temperature	^{o}F
W	load per unit length of contour contact	lb/in
Y	separation of mean lines	in

NOMENCLATURE (Cont'd)

Subscripts

o	zero load
1	surface 1
2	surface 2
a	apparent
c	contour
c	cylindrical waviness
m	mean value
r	real
r	roughness component
s	spherical waviness

Greek Symbols

ϵ_1^2	ratio of real to contour area
ϵ_2^2	ratio of contour to apparent area
σ	root mean square roughness
$\dot{\sigma}$	root mean square slope

LIST OF TABLES

LIST OF FIGURES

Chapter 1

INTRODUCTION

1.1 Historical Background

It has been established that the surfaces of solid bodies which are pressed together actually touch only at isolated spots and that the real contact area is a small fraction of the total or apparent area. Thus the heat transfer across the interface formed by the contiguous surfaces is in part confined to the contacting spots resulting in converging and diverging flow lines at each contact spot, and in part through the fluid which may be present in the gaps. In a vacuum environment the heat transfer is accomplished by two modes: conduction through the metal contact and radiation across the gap. During the past fifteen years many papers and reports on the subject have appeared, stimulated by recent technological developments in the power reactor field and aerospace work. The very high heat fluxes encountered in reactor design required that knowledge about the thermal conductance between the fuel elements and the metal cladding be obtained in order to achieve acceptable overall thermal efficiencies.

The aerospace industry on the other hand, required information about the thermal conductance between lightweight materials operating in a vacuum.

The majority of the papers dealt with experimental data obtained for various surface geometries under a range of loads and environmental pressures. The result is that all the experimental investigations, even those in which the surface geometry was clearly defined, are applicable only to the specific cases tested, and there is no way for another investigator to apply these data to other situations (see references).

It was recognized by some that a more fundamental approach was required in order to understand more fully this difficult problem, and so several analytical works have appeared on the scene, the most noteworthy are listed in the Bibliography (11, 12, 16, 24).

In one way or another each report dealt with a specific aspect of the thermal conductance problem and gave a better understanding of it. However, it should be noted that some experimenters (15, 19, 20) have found each theory to be inadequate in correlating data in some area of their testing.

This report is concerned with the analytical and experimental determination of the thermal conductance of rough, wavy surfaces in a vacuum environment.

1.2 Review of Thermal Conductance Literature

1.2.1 Studies of Thermal Conductance with Interstitial Fluid

Tachibana (30) in one of the earlier papers tried to find an empirical relationship between the contact resistance and the coarseness of the surface finish in the presence of air, oil and parafin. He concluded that the effects of surface finish can be accounted for by the mean height of the coarseness. He also stated that even if the surface finish is relatively smooth locally, a small degree of out-of-flatness makes the contact resistance larger. When a large area is in contact, the contribution to the gaps by bending of the surface is greater than that by the coarseness of the finish. Under such conditions, the conductance can only be determined by taking into account the bending of the surface over the whole contact surface.

Held (31) made an analytic study and obtained some experimental data to check out the theoretical work. He considered only nominally-flat, rough surfaces with a random distribution of peaks; with initial plastic deformation of peaks and then elastic deformation of those peaks coming into contact with a further increase in load. He observed that the conductance due to the air in the gaps was remarkably high, representing an overwhelming proportion of the total conductivity. This is not surprising since his surfaces were very rough and the apparent pressures were quite low.

Kouwenhoven and Potter (32) investigated the thermal resistance between two steel surfaces in the presence of air. Argon was used as the interstitial fluid for the high temperature tests to eliminate oxidation of the surfaces. Specimens varying in roughness from 3 to 4150 x 10^{-6} inches were used, and the thermal resistance results were reported at two temperature levels for pressures ranging from 195 to 2455 psi. They concluded that thermal resistance decreases exponentially for rough surfaces. The rate of decrease becomes less until at 3 x 10^{-6} inches, the resistance is practically independent of pressure. They reported that the temperature level has only a small effect on thermal resistance contrary to data obtained by other investigators. Their final conclusion was that there is need for more accurate data of the actual surface areas in contact, as this remains one of the greatest unknown factors in the problem.

Barzelay et al., in two reports (40, 41) reported the results of many tests which were conducted to determine the factors influencing the thermal conductance across the interface between aluminum and stainless steel structural joints. The type of joints investigated included: bare metal-to-metal contact: contact surfaces coated with zinc-chromate primer; contact surfaces separated by thin foils of good conductors; contact surfaces separated by thin sheets of insulation; contact surfaces joined by strength-giving bonds and rivited joints. The factors investigated were heat flow, temperature drop, temperature level, and surface

condition. In the first report (40) contact pressures were held constant at about 7 psi in order to permit a thorough investigation of the other parameters. The second report (41) considered the effect of pressure ranging from 5 to 425 psi.

They concluded that their experimental results gave evidence of the following conclusions: the thermal conductance increases with the mean temperature level, and remains approximately constant with changes in heat flow; the thermal conductance of the interface with pressure, being appreciable at low pressures but levelling off at higher pressures; at any pressure level the thermal conductance generally increases as the r.m.s. of the surface roughness decreases; however, surface roughness alone is not a dominant parameter in determining thermal conductance of contacts, for overall flatness has a more important role in determining the configuration of surface matching; when subject to repeated heating and loading cycles the materials reveal a pronounced but varied loss and recovery of strength which causes corresponding changes in thermal conductance; in general interfaces formed between rough surfaces give more consistent data than those between smooth surfaces; because of thermal stresses caused by temperature gradients and uneven heat flow, a certain amount of warping of the specimens occurs at the interface and may influence the conductance value far more than either roughness or initial flatness.

1.2.2 Studies of Thermal Conductance in Vacuum

Boeschoten and Van der Held (42) investigated the contact conductance between surfaces of aluminum-aluminum and steel-uranium. The interstitial fluid was air, helium or hydrogen, varying in gas pressure from 1 mm Hg to 760 mm Hg. The temperature of the interface was maintained at about 300°F for all experiments.

They concluded that at low contact pressures of about 15 psi, the heat conduction takes place principally across the gaps, whereas at higher contact pressures the metallic contact spots become dominant. From thermal conductance and hardness measurements, they concluded that the contact spots are about 30 microns in radius on the average, whereas about 640 such spots are found per square inch at a contact pressure of 225 psi. The contact pressure has little influence on the size of the contact spots, but the number varies proportionally with the contact pressure; and above a certain value of the contact pressure, a confluence of the contact spots takes place with a corresponding decrease in their number. They stated that it seems that the size of the contact spots is independent of the materials from which the joint is formed, a value of about 30 microns being found for a great variety of metals, and independent of the applied load and the size and the shape of the joints.

Kaspareck and Dailey (39) obtained empirical data of the thermal conductance of various dissimilar metals operating in a vacuum of

10^{-2} mm Hg. Surface finishes ranged from 5 to more than 200 x 10^{-6} inches CLA (Center Line Average), and a flatness deviation of about 700 x 10^{-6} inches with contact pressures up to 1020 psi.

They concluded that a valid evaluation of surface flatness must be undertaken with a well-defined program to determine the relationship of flatness deviation to contact conductance. Data obtained from this experimental program cannot be utilized to determine an average temperature differential over the entire component mounting surface because of insufficient knowledge concerning the average contact pressure. They emphasized the relationship between surface characteristics, (i.e., flatness deviation, surface finish) and contact conductance. To evaluate flatness deviation and surface finish, each must be taken separately, and then combined in a closely controlled test.

E. Fried, et al., (18) in an attempt to determine the interface thermal contact resistance of materials used in space vehicles, investigated the effects of surface finish and flatness of aluminum and magnesium plates operating at a chamber pressure of 10^{-6} mm Hg. Surface finishes from 6 to 65 x 10^{-6} inches r.m.s. and contact pressures up to 35 psi were considered. They concluded that the flatness of the surface was a very important variable for thermal contacts in a vacuum but were unable to explain qualitatively how this parameter should be considered.

Fried, in a subsequent report (19), made an attempt to semi-empirically correlate the thermal contact conductance versus the apparent pressure by assuming the deformation to be elastic. The model which was proposed consisted of a spherical contact against a flat plate. This was considered to represent the asperities individually and the cumulative effect of a group of asperities on an elastic substrate. The Hertz equation of elastic deformation for spherical contacts was considered to be applicable, in particular after the initial contact was made during which a number of the asperities have been plastically deformed. The initial effect must be determined experimentally. Fried concluded that the thermal conductance when plotted against the apparent pressure indicated a definite two-regime behavior with a pronounced point of change of slope. The exact reason for this change in slope has not yet been defined, although it is believed that possibly it represents the change from purely elastic to elastic-plastic deformation behavior. He also made note of the fact that flatness deviation effects were significant in controlling the thermal conductance of metallic contacts in a vacuum.

Bloom (15), in a very extensive report obtained experimental data for several space craft materials operating at space conditions of temperature and pressure. The apparent pressure ranged from 100 to 1000 psi and the surfaces had finishes ranging from 3 to 130 x 10^{-6} inches r.m.s. while the flatness deviation ranged from 100 to 500 x 10^{-6} inches. He

showed empirical relationships of thermal conductance versus apparent pressure, thermal conductance versus interface temperature, and thermal conductance versus roughness. He then made an attempt to correlate his data with the Fenech and Rohsenow Theory (16) and the Clausing and Chao Theory (12). He found that the calculated conductance values using both first and second-order equations as proposed by Fenech resulted in the theoretical predictions falling far below actual data values. The differences between theory and test were greatest at low apparent pressures, but tended to diminish as the contact pressure exceeded 1000 psi.

He also discovered that for the case of aluminum, the theory and test for smooth specimens were in good agreement up to a contact pressure of 500 psi. The theory predicted far higher values of the conductance than obtained from tests for pressures exceeding 500 psi. For the case of stainless steel, both theory and data are in good agreement up to 200 psi; then theory begins to exceed data. The tendency for theory to predict much larger values of thermal conductance than data usually occurred when more than 42 percent of the total apparent area was in macroscopic contact.

He concluded that the reason for the discrepancy between theory and data could be attributed to the following: 1) the conductance due to the asperities was considered to be negligible according to Clausing, 2) the macroscopic conductance area predicted by the Hertz equation is only valid for elastic spherical indentations.

In an effort to reconcile the discrepancy between theory and test, he attempted to combine Fenech's microscopic theory with Clausing's macroscopic theory, but found that this resulted in theoretical values only slightly lower than before for the higher pressure data.

Bloom concluded that a microscopic theory should be developed in which the conductance values that it predicts can prevent the total conductance from diverging to infinity at contact pressures greater than 5000 psi, or a better macroscopic theory should be developed which does not diverge so rapidly.

1.2.3 Review of Analytic Studies of Thermal Contact Conductance

One of the earlier analytical and theoretical investigations of thermal contact conductance of metal surfaces was due to Cetinkale and Fishenden (11). In this analysis the contacting surfaces were nominally flat but rough, and the contact areas were assumed to be uniformly distributed, each contact spot was assumed to be fed by a larger coaxial cylinder. The voids at the interface were assumed to be of uniform thickness and filled with a fluid of uniform conductivity. The steady-state temperature distribution was obtained by the relaxation method.

After having considered the material resistance and the fluid resistance, they developed an equation for the interface conductance which had several parameters that were to be determined empirically. The actual area of contact was determined by considering that the softer of

the two metals will flow plastically until the mean contact spot pressure is equal to its Meyer hardness. They stated that their parameters were independent of the metal or fluid and were constant for a given type of surface roughness.

Fenech and Rohsenow (16) in a later investigation made a mathematical analysis of the thermal contact conductance by proposing an idealized shape of contact and then solving the boundary value problem by subdividing the contact region and satisfying average boundary conditions between each region. The thermal conductance was then expressed in terms of the thermal conductivities of the contacting metals and of the fluid filling the voids, the real area in contact, the number of contact points per unit area, and the volume average thickness of the void gaps.

A method was given for the determination of the above physical properties of a contact. To use this method the following measurements are necessary: two recorded profiles, perpendicular to one another; and a Knoop hardness test on the softer of the two metals making the contact.

Experiments were performed with the following types of artificial contact models: 1) solid cylinders with a neck machined into them, thereby providing one contact spot of a specified radius, 2) specimens whose surface consisted of several machined pyramids. Fairly good agreement with experimental results was reported for interstitial fluids such as air, water, and mercury.

They concluded that two further requirements were necessary to account for the elastic deformation of the surface sublayers and permanent changes in the surface profile. Since these two effects had been neglected, they stated that caution should be exercised in using the actual graphical method at pressures sufficiently high to make these effects important.

The most recent analytical investigation due to Clausing and Chao (12) is based upon the fact that real surfaces exhibit out-of-flatness as well as roughness. They proposed that the apparent area can be separated into a contact and a noncontact region. The contact region is defined as that portion of the contact surface where the density of microcontacts is high and is called the microscopic contact area. The noncontact area contains few or no microscopic contact areas. They suggested that the thermal contact resistance for any interface in a vacuum may be represented by three resistances in series: large scale or macroscopic constriction resistance, small scale or microscopic constriction resistance and the film resistance. For "clean" engineering surfaces they stated that the macroscopic resistance should be orders of magnitude larger than the microscopic resistance. They assumed that the macroscopic contact area can be determined by purely elastic considerations and thus obtained a dimensionless group termed the elastic conformity modulus which relates the dimensionless radius ratio of the

contact to the applied load, the surface parameters, and the material properties.

They obtained experimental data for several surfaces having roughness of about 4 x 10^{-6} inches and flatness deviation ranging from 40 to 900 x 10^{-6} inches. The tests were conducted in a chamber evacuated to 5 x 10^{-6} mm Hg. The apparent pressure ranged from a few psi to about 1000 psi while the mean interface temperature ranged from 160°F to 340°F.

There was good agreement between theory and test for all but the aluminum specimens. For this set of tests, best agreement was obtained between the theoretical curve and the aluminum specimens having a roughness of 45 and 80 x 10^{-6} inches respectively and a flatness deviation of 220 x 10^{-6} inches.

They concluded that the macroscopic constriction effect is significant and dominates the thermal contact resistance of many engineering surfaces. Their theory leads to a pair of dimensionless parameters for correlating data, and calculations have indicated that the microscopic constriction resistance is of secondary importance for many engineering surfaces.

1.3 Review of Surface Deformation Literature

The re-occurring conclusion of the thermal conductance literature reviewed under Section 1.2 is that only by having a better and complete understanding of the deformation of the roughness and the wavy components can there be a better understanding of the thermal conduction problem.

A cursory examination of the references of subjects related to contact resistance shows that indeed many papers and reports have been written regarding the description of surfaces, the deformation of contacting surfaces under applied load, and the determination of various physical parameters such as number of contact spots and the real area of contact. Some investigators have approached the problem from the purely elastic deformation standpoint (44, 50, 58, 61, 64) while others have considered the problem from the purely plastic deformation standpoint (46, 54, 62, 63). Recently several papers have considered that the deformation of real surfaces can only be solved by considering both elastic and plastic deformation of the roughness and wavy components (49, 51, 52, 55, 57).

Chapter 2

SURFACE ANALYSIS

2.1 Description of Surfaces

It has been established that the surfaces of solid bodies which are brought together under load actually touch only at isolated spots and that the real area of contact is a small fraction of the total or apparent area.

A careful examination of profiles of real surfaces obtained by means of surface analyzers, such as the one described by Henry (9) or by any of the several commercial machines available, reveals that real surfaces of solid bodies are both rough and wavy.

The roughness component, often referred to as the microscopic roughness, is due to the irregularities in the surface which result from the inherent action of production processes. These are deemed to include traverse feed marks and the irregularities within them. Roughness can range from 2×10^{-6} inches r.m.s. for very smooth surfaces to 600×10^{-6} inches r.m.s. for the roughest surfaces.

Waviness or macroscopic roughness is that component of the surface profile upon which roughness is superimposed. The waviness may result from such factors as machine or work deflections, vibrations, chatter, heat treatment, or warping strains. The length of these waves,

depending on quite a number of conditions, varies from 0.04 to 0.40 inches and the height accordingly varies from 80 x 10^{-6} to 1600 x 10^{-6} inches. The waviness component can appear as cylinders or spherical caps, and may or may not be periodic in character.

2.2 Nominally Flat Surface

The nominally flat surface is characterized by having a series of peaks and valleys. The heights of the asperities seldom exceed 200 x 10^{-6} inches. The most characteristic range of the included angle at the peak is between 160^{o} and 164^{o}. The smallest included angle which occurs with the roughest surfaces would never be smaller than 150^{o}. The crests or peaks of the asperities are surfaces of very gentle curvature and not as shown in Figure 1. The vertical scale is exaggerated with respect to the horizontal scale by a factor of 10, so that the sides of the peaks and valleys appear much steeper than they really are, and the curvature of the peaks and valleys are greater than they are represented in Figure 1.

2.3 Wavy Surface

The wavy surface is characterized by large protuberances which are orders of magnitude larger than the asperities found on nominally flat surfaces. These waves which have been designated as flatness deviations by Clausing (12) have base widths which are generally two orders of magnitude larger than the wave height. This results in waviness which is

very gentle with regard to the slope, and produces peaks and valleys of relatively large curvature.

2.3.1 Cylindrical Waviness

This waviness or macroscopic roughness is characterized by being essentially two dimensional, having a characteristic pitch L, a radius of curvature R, and a finite length ℓ in the direction of no waviness.

It is obvious that for cylindrical waviness

$$N_c = \frac{A_a}{L^2} = \frac{A_a m^2}{L \ell} \tag{2.1}$$

where N_c is the number of cylindrical contours to be found on the apparent area, and the form factor $m^2 = \ell/L$.

When two identical wavy surfaces having cylindrical waves are brought together so that they touch along a line parallel to the axis of the waves, then the contour area of contact is given by

$$A_c = N_c 2 C_2 \ell \tag{2.2}$$

where C_2 is the half width of the contact area, Figure 3.

The ratio of the contour area to the apparent area will be defined by

$$\epsilon_{2c}^2 = \frac{A_c}{A_a} = \frac{2C_2 m^2}{L} \qquad (2.3)$$

The importance of this dimensionless term will be developed in the following chapter.

2.3.2 Spherical Waviness

Spherical waviness is characterized by being three dimensional, having a characteristic pitch L and a radius of curvature R.

For spherical waviness, Figure 4, the number of contours can be expressed as

$$N_c = \frac{A_a}{\frac{\pi}{4} L^2} \qquad (2.4)$$

When two spherical caps are brought together under load, the radius of contact C_2 can be determined from the following expression

$$A_c = N_c \pi C_2^2 \qquad (2.5)$$

As for the cylindrical contours, define the ratio of the contour area to the apparent area as

$$\epsilon_{2s}^2 = \frac{A_c}{A_a} = \frac{4C_2^2}{L^2} \qquad (2.6)$$

The importance of this parameter will also be developed in the following chapter.

Chapter 3

THERMAL ANALYSIS

3.1 Contact Model for Nominally Flat Rough Surfaces

An examination of nominally flat surface profiles shows that for small compliances, as a result of moderate to light apparent pressures, the contact spots are small in number and in size. Each contact spot is assumed to be circular in area and concentric with the heat channel which feeds the spot. Since the slopes of the asperities which contribute to the contact are generally less than 10 degrees, and the radius of the contact is orders of magnitude smaller than the radius of the heat channel, the system can be regarded as one semi-infinite solid in contact with another over a small circular area.

As the load is increased, the number and size of the contact spots increase so that the model proposed for light loads is no longer applicable. In this case the influence of one contact spot on another must be considered in the analysis.

3.2 General Equation for Contact Resistance

By definition the thermal contact conductance is given by

$$h = \frac{Q}{A_a \Delta T} \tag{3.1}$$

and the thermal contact resistance, following the electrical analog, is given be

$$R = \frac{\Delta T}{Q} \tag{3.2}$$

and

$$dR = \frac{ds}{k\ dA} \tag{3.3}$$

where k is the thermal conductivity, ds is the elemental length in the direction of the heat flux vector, and dA is the elemental area perpendicular to the heat flux vector.

Combining these definitions one can then write the relationship between the thermal contact conductance and resistance as

$$\frac{1}{hA_a} = \int dR = \int_s \frac{ds}{\int_A k\ dA} \tag{3.4}$$

The problem of heat transfer with light loading reduces to that of the heat flow between two semi-infinite regions $0 < z < \infty$, $0 < z < \infty$, having thermal conductivities k_1 and k_2 (Figure 5) which are in contact over the radius c, the center of the contact being taken as the origin of the cylindrical coordinate system (r, z).

The following analysis is based upon steady-state conditions, constant thermal and material properties, clean surfaces (no oxide film resistance), no interstitial fluid, and negligible radiation across the gaps.

The differential equation of the temperature, for the axially symmetric case

$$\frac{\partial^2 T}{\partial r^2} + \frac{1}{r}\frac{\partial T}{\partial r} + \frac{\partial^2 T}{\partial z^2} = 0 \qquad (3.5)$$

must be satisfied by the following boundary conditions throughout the two regions:

$$\frac{\partial T_1}{\partial z} = 0 \quad \text{at} \quad z = 0, \quad r > c \qquad (3.6)$$

$$\frac{\partial T_2}{\partial z} = 0 \quad \text{at} \quad z = 0, \quad r > c \qquad (3.7)$$

In the absence of sources and sinks the conservation of thermal energy requires that

$$k_1 \frac{\partial T_1}{\partial z} = - k_2 \frac{\partial T_2}{\partial z}, \quad z \gg a \qquad (3.8)$$

and temperature continuity across the contact requires that

$$T_1 = T_2 \quad \text{at} \quad z = 0, \quad r < c \qquad (3.9)$$

letting

$$T_1 = T_o \quad \text{at} \quad z = \infty \qquad (3.10)$$

and

$$T_2 = 0 \quad \text{at} \quad z = \infty \tag{3.11}$$

it can be shown by substitution that

$$T_1 = T_o - \int_o^\infty \psi(m) e^{-mz} J_o(mr) dm \tag{3.12}$$

and

$$T_2 = \int_o^\infty \phi(m) e^{-mz} J_o(mr) dm \tag{3.13}$$

for any m.

Using the boundary conditions specified above, the unknowns $\psi(m)$ and $\phi(m)$ can be obtained as

$$\phi(m) = \frac{k_1}{k_2} \psi(m) \quad \text{and} \quad \psi(m) = \frac{2T_o k_2 \sin(mc)}{m\pi(k_1 + k_2)} \tag{3.14, 3.15}$$

Now T_1 can be solved for and is found to be

$$T_1 = T_o - \frac{2k_2 T_o}{\pi(k_1 + k_2)} \int_o^\infty e^{-mz} \sin(mc) J_o(mr) \frac{dm}{m} \tag{3.16}$$

and therefore

$$T_1 = \frac{T_o k_1}{k_1 + k_2}, \quad z = 0, \quad r < c \tag{3.17}$$

The contact temperature is seen to be independent of the size of the contact and uniform over the contact area.

The heat flow over the contact area is found by integration to be

$$Q = -2\pi k_1 \int_o^c r \frac{\partial}{\partial z} \left[\frac{2 T_o \ k_2}{\pi (k_1 + k_2)} \int_o^\infty \sin(mc) e^{-mz} J_o(mr) \frac{dm}{m} \right]_{z=0} dr$$

$$= \frac{4 k_1 k_2 T_o c}{k_1 + k_2} \qquad (3.18)$$

Defining the mean harmonic thermal conductivity as

$$\frac{2}{km} = \frac{1}{k_1} + \frac{1}{k_2} \qquad (3.19)$$

the heat flow can now be expressed as

$$Q = 2 k_m T_o c \qquad (3.20)$$

It is seen that the heat flow varies linearly with the radius of contact.

The thermal contact resistance can now be expressed as

$$R = \frac{T_1 - T_2}{Q} = \frac{1}{2 kmc} \qquad (3.21)$$

If there are N contact spots over the apparent area A_a, then the total resistance will be given by

$$R = \frac{1}{2 N k_m c} \tag{3.22}$$

and the thermal contact conductance using Eq. (3.4) is given by

$$h = 2 n k_m c \tag{3.23}$$

where n is the number of contact spots per unit area and c is the radius of contact.

Further reduction of Eq. (3.23) can be achieved by substituting

$$n \pi a^2 = 1 \tag{3.24}$$

where a is the radius of the heat channel feeding the contact spot. Thus the limiting value for the dimensionless number $k_m \sqrt{n}/h$ is $\sqrt{\pi}/2\epsilon$ for very light loading, and any formulation which is developed for the general case must reduce to this value in the limit as the apparent pressure becomes very small.

For the case of large apparent pressures the total contact resistance for N circular contact spots uniformly distributed over the apparent area A_a at an average distance of 2a from center to center, according to Holm (54), can be expressed as

$$R(N, c) = \frac{1}{2 \pi N k_m c} \tan^{-1} \frac{a}{c} - \frac{a}{k_m A_a} \tag{3.25}$$

This is an approximation because it has not taken into consideration the very small resistance in the shaded space, Figure 6.

Since

$$A_a = N \pi a^2 \text{ and } n\pi a^2 = 1 \qquad (3.26, 3.27)$$

by direct substitution and using Equation (4), the thermal contact conductance can be written as

$$\frac{1}{h} = \frac{2a}{k_m} \left[\frac{1}{2\,c/a} \tan^{-1} \frac{1}{c/a} - 1 \right] \qquad (3.28)$$

or

$$\frac{k_m \sqrt{n}}{h} = \frac{2}{\sqrt{\pi}} \left[\frac{1}{2\epsilon_1} \tan^{-1} \frac{1}{\epsilon_1} - 1 \right] \equiv fr(\epsilon_1) \qquad (3.29)$$

where

$$\epsilon_1^2 \equiv \frac{Ar}{A_a} = \frac{c^2}{a^2}$$

For values of $\epsilon_1 < 0.03$, $\tan^{-1} 1/\epsilon_1$ can be calculated from $(\pi/2 - \epsilon_1)$.

Equation 3.29 is graphically displayed in Figure 7 as $fr(\epsilon_1)$ versus ϵ_1 which is the ratio of the radius of contact to the radius of the heat channel feeding the contact spot.

It is interesting to note that the dimensionless heat transfer number is composed of the contact conductance, the thermal conductivity of the metals, and the square root of the number of contact spots per unit area. The parameter $\sqrt{n}$ is actually the reciprocal of the pitch between the contact spots and implicitly takes into consideration the surface geometry and the effect of the applied load.

3.3 Contact Model for Cylindrical Waviness

Since waviness found on solid bodies may be the result of machine or work deflections, it may appear as cylinders (two-dimensional characteristic), as spherical caps (three-dimensional characteristic), and may or may not be periodic.

In order to come to grips with the problem, it is proposed to idealize the first type of contact as an "ellipse" whose major axis (ℓ) is orders of magnitude larger than the minor axis ($2c_2$).

3.4 General Contact Conductance Equation for Cylindrical Waviness

The fact that for the waviness component the slopes are very gentle and the radius of curvature is very large relative to the contact width suggests that this problem can also be idealized as a contact between semi-infinite solids touching along a line. At light pressures the contact will resemble a long thin rectangular spot being fed by a large square channel.

As the load is increased, the width of the contact area will grow but never exceed a fraction of the heat channel width.

The problem of heat transfer with light loading reduces to that of the heat flow between two semi-infinite regions $0 < z < \infty$, $0 < z < \infty$, having thermal conductivities k_1 and k_2, which are in contact over the width $2c_2$ and the length ℓ, the center of the contact being taken as the origin of the rectangular coordinate system (x, y, z).

The following analysis is based upon steady-state conditions, constant thermal and material properties, clean surfaces, no interstitial fluid (vacuum), and negligible radiation across the gaps.

For the case with negligible effects in the direction of the axis of contact, the differential equation reduces to

$$\frac{\partial^2 T}{\partial x^2} + \frac{\partial^2 T}{\partial z^2} = 0 \qquad (3.30)$$

The boundary conditions are

$$+ k_1 \frac{\partial T_1}{\partial z} = -k_2 \frac{\partial T_2}{\partial z} = 0 \text{ at } z = 0, \; x > c \qquad (3.31\ a, b)$$

In the absence of sources and sinks the conservation of energy requires that

$$+ k_1 \frac{\partial T_1}{\partial z} = - k_2 \frac{\partial T_2}{\partial z} \quad , \; z \gg a \tag{3.32}$$

and temperature continuity across the contact requires that

$$T_1 = T_2 \quad \text{at} \quad z = 0 \quad x < c \tag{3.33}$$

Letting $T_1 = T_o$ and $T_2 = 0$ at $z = \infty$ (3.34 a,b)

it can be shown by substitution into the differential equation that

$$T_1 = T_o - \int_o^\infty \psi(m) e^{-mz} \cos(mx) dm \tag{3.35}$$

and

$$T_2 = \int_o^\infty \phi(m) e^{-mz} \cos(mx) dm \tag{3.36}$$

for all values of m.

Satisfying the boundary conditions (3.32) and (3.33) one can show that

$$\phi(m) = \frac{k_1}{k_2} \psi(m) \text{ and } \psi(m) = \frac{2T_o k_2}{\pi (k_1 + k_2)} \frac{J_1(mc)}{m} \tag{3.37 a,b}$$

Therefore the solutions for the temperature distribution in regions 1 and 2 can be written as

$$T_1 = T_o - \frac{2T_o k_2}{\pi(k_1 + k_2)} \int_o^\infty J_1(mc) e^{-mz} \cos(mx) \frac{dm}{m} \tag{3.38}$$

$$T_2 = \frac{2T_o k_1}{\pi(k_1 + k_2)} \int_o^\infty J_1(mc) e^{-mz} \cos(mx) \frac{dm}{m} \tag{3.39}$$

The heat flow over the contact is found by integration to be

$$Q = \int_o^c -2k_2 \frac{\partial T_2}{\partial z} \Bigg]_{z=o} dx = \frac{2}{\pi} T_o k_m c \tag{3.40}$$

It is seen that, as for the circular contact, the heat flow varies linearly with the width of the contact.

The thermal contact resistance can be expressed as

$$R = \frac{T_1 - T_2}{Q} = \frac{1}{\frac{2}{\pi} k_m c} \tag{3.41}$$

If there are N_c contact spots over the apparent area A_a, then the total resistance will be given by

$$R = \frac{1}{\frac{2N_c}{\pi} k_m c} = \frac{1}{h A_a} \tag{3.42}$$

and therefore the thermal contact conductance is given by

$$\frac{h\,L}{k_m} = \frac{\epsilon_2^2}{\pi\, m^2} \tag{3.43}$$

where L is the pitch between waves, k_m is the harmonic mean thermal conductivity of the two metals and ϵ_2^2 is the ratio of the real to apparent areas.

For the case of multiple contacts where one contact spot influences the neighboring contact spots the total contact resistance can be expressed as

$$R(N_c, c_2) = \frac{1}{2 N_c k_m c_2} \tan^{-1} \frac{L}{2 c_2} - \frac{L}{A_a} \tag{3.44}$$

and the total contact conductance can be written as

$$\frac{k_m}{hL} = \frac{2 m^2}{\epsilon_2^2} \tan^{-1} \frac{m^2}{\epsilon_2^2} - 1 \equiv f_c(\epsilon_2) \tag{3.45}$$

In the limiting case when ϵ_2^2 approaches zero, $\tan^{-1} m^2/\epsilon_2^2$ can be calculated from $(\pi/2 - \epsilon_2^2/m^2)$ and it can be shown that Equation (3.45) reduces to Equation (3.43) in the limit as ϵ_2^2/m^2 approaches zero. Equation (3.45) is shown graphically displayed in Figure 8 as $f_c(\epsilon_2)$ versus ϵ_2 with m^2 as a parameter.

3.5 Contact Model for Spherical Waviness

Although the flatness deviation is several orders of magnitude greater than the surface roughness, the pitch of the spherical waviness is also several orders of magnitude larger. When two such spherical caps come into contact, the system can be regarded as one semi-infinite solid in contact with another over a small circular area. This approximation is very good when the flatness deviation is small or when the applied load is moderate.

3.6 General Contact Conductance Equation for Spherical Waviness

The solution for the steady-state condition must satisfy Laplace's equation and the boundary conditions as specified under Section 3.2.

The equation for the total contact resistance for multiple contacts can be written as

$$R = \frac{1}{h A_a} = \frac{1}{2\pi N_c k_m c_2} \tan^{-1} \frac{L}{2C_2} - \frac{L}{k_m A_a} \qquad (3.46)$$

where C_2 is the radius of contact, L is the pitch of the spherical caps and N_c is the total number of contacts.

Since $A_a = N_c \frac{\pi}{4} L^2$ and $A_c = N_c \pi c_2^2$, the dimensionless area ratio $\epsilon_2^2 = 4c_2^2/L^2$.

The general contact conductance equation can now be written as

$$\frac{k_m}{hL} = \frac{1}{2\epsilon_2} \tan^{-1} \frac{1}{\epsilon_2} - 1 \equiv f_s(\epsilon_2) \qquad (3.47)$$

graphically displayed in Figure 9.

Note that the dimensionless heat transfer number is composed of the contact conductance, the thermal conductivity of the metals and the pitch of the spherical caps. The dimensionless heat transfer number k_m/hL is a function of ϵ_2 which, from elastic theory, depends upon the applied load, the surface geometry (d, L) and the material property E.

Chapter 4

DEFORMATION ANALYSIS

4.1 Surface Deformation

As shown in the preceding chapter, the determination of thermal contact conductance is dependent upon certain physical parameters which can only be obtained from a complete understanding of how material surfaces behave under loading. In a vacuum environment, the heat transfer between surfaces is a function of the surface finish, whether nominally flat but rough or wavy and rough, and the elastic-plastic deformation of the materials over a range of pressures.

Numerous investigations have been done to determine the real area of contact between solid bodies. Bowden (46) proposed the following simple formula

$$A_r = P_a/H \tag{4.1}$$

where P_a is the apparent pressure and H is the microhardness of the softer material. This gives the value of the real area of contact for conditions of fully plasticity without recourse to the roughness or the waviness of the surface.

Archard (43, 44, 45) in several papers determined the real area of contact by assuming spherical asperities, having a range of radii of curvature and of heights. His analysis was based upon considering the deformation to be completely elastic.

F. F. Ling (58) in one paper investigated some factors influencing the real area-load characteristics for semi-smooth touching surfaces. He based his analysis upon one surface being rigid and microscopically smooth while the other was allowed to have a large number of microscopic asperities in the form of wedges.

In Ling's second work (59) an attempt was made to determine a plausible distribution of asperities when both mating surfaces are rough. He considered uniform, linear, Guassian, and Poisson distributions in order to correlate compliance-load data, and he obtained compliance-load data for stainless steel, aluminum and brass. The surfaces were flat ranging in roughness from 6 to 20 x 10^{-6} r.m.s. while the maximum apparent pressure was only 120 psi.

An analysis was done by Greenwood (51) to determine the real contact area for nominally-flat, rough surfaces but considered only contact between a smooth surface and a rough surface having a Gaussian distribution of asperity heights. It was concluded by the authors that the nature of the contact deformation depends upon the topography of the

surface and not upon the load and established a criterion for distinguishing surfaces that touch elastically from those that touch plastically.

The elastic contact of rough spheres was considered in Greenwood's second paper (52). It is shown that for light loads and rough surfaces the behavior of surfaces in contact is quite different from that described in the classical Hertzian theory: the contact region is much larger, and the pressures much lower. As the load is increased or the surface becomes smoother, these differences become less and the Hertzian values are obtained as a limiting case.

Although the apparent contact area is greater than the Hertzian contact area, the total area of the real micro-contacts is less; conversely, the real pressures on the micro-contacts are much higher, and the apparent pressures much lower, then the Hertzian predictions.

An excellent paper on the compliance of elastic bodies in contact was written by Mindlin (61). His analysis was based upon considering two homogeneous, isotropic, elastic bodies in contact at a point. He determined the boundary of the contact to be an ellipse and gave the magnitudes of the principal axes and the relative approach or compliance of the two bodies.

Based upon the work done by previous investigators and on recent empirical data, we assumed that the real area of contact can be determined by the assumption that the deformation of the asperities is plastic and elastic, while the waviness component will deform elastically for light loads

and elastically and plastically for very high pressures. Under the influence of the applied load, the two surfaces approach each other and the highest peaks will be deformed before any of the lower ones come into contact. If all the yielding is at the tips of the peaks, one would therefore expect the highest asperities to be massively deformed by plastic deformation until the real area of contact is that given by $A_r = P_a/H$.

In fact, such behavior has not been observed, and it is evident that subsurface yielding has occurred on a scale large enough to distribute the load over a larger number of asperities than would be possible if only the higher asperities were deformed at their tips.

4.2 Elastic Deformation of Nominally Flat Rough Surfaces

Based on the thermal analysis of Chapter 3 it is quite evident that the two most important surface parameters are the number of contact spots per unit length and the ratio of the real to apparent areas.

In order to determine $\sqrt{n}$ we first obtain linear profiles of the two contacting surfaces using a profilometer. If we assume that the asperities are ergodic over the contacting surfaces, then recorded profiles along any diameter of the specimen will be representative of any other arbitrary diameter. This will allow us to obtain the three-dimensional configuration of the surfaces by recording only one profile from each surface. The initial, or no-load position is determined when contact is

first established at three spots per unit area or $\sqrt{3}$ points on each pair of profiles. This initial separation between the mean lines of each profile is carefully identified as Y_o and is generally 3 to 4 times the r.m.s. value of the contacting surfaces. To simulate an increase in pressure, the profiles are moved by small increments in a direction perpendicular to the contact plane; this relative displacement of the two profiles is termed the compliance of the two surfaces under load. This technique is best accomplished by reproducing the two profiles on transparent sheets of paper and counting the number of times the surfaces interfere with each other as the compliance is increased. The two profiles are then displaced a slight distance parallel to the contact plane and the counting procedure is repeated as the compliance is increased. The number of contact points is then taken as the average of the two counts and plotted versus the ratio of the compliance to the initial displacement, Figures 10 and 11.

J. J. Henry (21) accomplished the same result as the graphical method by recording profile voltages on magnetic tape; then recordings were fed into a general purpose analog computer which processed the input voltages in a manner analogous to the graphical analysis.

In order to relate the number of contact spots with the applied load, three M. I. T. Masters Theses (4, 7, 8) were devoted to the radiographic determination of the number of contact spots.

Because of the uncertainties encountered in the radiographic technique the values of the experimentally determined n are lower than the values determined graphically for a given apparent pressure. These uncertainties involve the facts that the phenomenon of tracer transfer at a contact point need not occur at every contact spot and that all of the receiver sample contacts receiving radioactive gold-198 need not receive a sufficient amount to activate the portion of the emulsion in their vicinity during the allotted exposure time. Just how much error is inherent in a given autoradiographic datum cannot be precisely determined.

The other alternative is to obtain test data of compliance versus apparent pressure for pairs of surfaces having different materials and surface geometries. As stated in Chapter 2, Ling (58) obtained such data for three different pairs of metals which were nominally flat but relatively smooth; also, his maximum apparent pressure was only 120 psi, much too low to be extrapolated up to 1000 psi or even 10,000 psi.

Figure 12 , $\sqrt{n}$ versus apparent pressure, represents experimental data obtained by radiographic means for nominally flat aluminum surfaces having a roughness of 120×10^{-6} inches r.m.s. and a slope of 0.120 r.m.s.

Since ϵ_1 and $\sqrt{n}$ are geometrically related to the compliance, this data will be applicable to any materials which have the same surface

$$c_1 = \left[\frac{3\pi}{4} P(k_1 + k_2) \frac{R_1 R_2}{R_1 + R_2} \right]^{1/3} \tag{4.2}$$

while the compliance of the two surfaces can be expressed as

$$C = \left[\frac{9\pi}{16} P^2(k_1 + k_2)^2 \frac{R_1 + R_2}{R_1 R_2} \right]^{1/3} \tag{4.3}$$

Solving for the radius of contact after having considered all the appropriate assumptions, the following simple geometric relation results:

$$c_1^2 = \frac{CR}{1.58} \tag{4.4}$$

The second geometric parameter can now be determined from

$$\epsilon_1^2 = \frac{A_r}{A_a} = \frac{N_1 \pi c_1^2}{A_a} + \frac{N_2 \pi c_2^2}{A_a} + \ldots \tag{4.5}$$

$$\epsilon_1^2 = \frac{\pi}{1.58} \sum_{i=o}^{m} (C_m - C_i)(n_{i+1} - n_i) R_i \tag{4.6}$$

where the summation over the subscript i is to account for the new contact points which appear when the compliance, C, increases by ΔC, an arbitrary increment, where n is the number of contact spots per unit area, and R is the radius of curvature corresponding to the compliance C. Solutions were obtained by means of the M. I. T. Digital Computer and are plotted versus the compliance ration in Figure 14 .

geometry. Therefore, once $\sqrt{n}$ versus P_a is obtained from test, then knowing $\sqrt{n}$ versus c/Y_o, one can cross plot c/Y_o versus P_a.

Figure 13 shows the experimental data obtained by Ling and test data as determined from heat transfer data for stainless steel and $\sqrt{n}$ versus P_a aluminum.

It is interesting to note that Ling's data for smooth surfaces and moderate pressures when extrapolated come very close to our data. It would appear that when c/Y_o is plotted versus P_a, the magnitude of the roughness is not an important parameter.

The second geometric parameter ϵ_1^2, which is the ratio of the real area of contact to the total or apparent area, can be determined from the classical elastic theory of Hertz. The subsequent deformation analysis will be based upon the following assumptions: (1) all asperities have spherical caps, (2) the number of asperities in contact will be determined by graphical analysis of profiles, (3) the surface is ergodic, (4) the two surfaces are of the same material, and $\nu_1 = \nu_2 = 0.3$, (5) the two surfaces are similar, i.e., $R_1 = R_2 = R$, (6) the two surfaces are symmetric about the contact plane, (7) the line of force always acts through the centers of curvature of touching asperities.

Elastic deformation theory shows that the radius of contact per pair of touching asperities can be expressed as

Similarly one can show that the apparent pressure can be related to the surface geometry (n, R), the compliance C and the elastic modulus by the following simple relationship

$$P_a = \frac{E}{1.865} \; n \; C^{3/2} \; R^{1/2} \tag{4.7}$$

or

$$\frac{P_a}{E} = \frac{1}{1.865} \sum_{i=o}^{m} (n_{i+1} - n_i)(C_m - C_i)^{3/2} \; R_i^{1/2} \tag{4.8}$$

Values of P_a versus compliance were determined with the aid of a computer and are plotted in Figure 15.

4.3 Plastic Deformation of Nominally Flat Rough Surfaces

The simplest deformation analysis applies to the case of nominally-flat, rough surfaces. It is assumed that the asperities are deformed plastically and therefore the real contact area can support only the stress at which the material begins to yield. For metallic surfaces this stress is the microhardness H of the material determined in a Knoop or Vickers test. Therefore, from a simple force balance consideration:

$$H \, A_r = P_a \, A_a \tag{4.9}$$

or

$$\frac{P_a}{H} = \frac{A_r}{A_a} = \epsilon_1^2 \tag{4.10}$$

When only the yield stress Y of the material is available, the surface parameter can be obtained from Equation (C-5) of Appendix C.

$$\epsilon_1^2 = \frac{P_a}{3Y} \tag{4.11}$$

An approximation, Figure 16 , which relates the ratio of the real to apparent areas with the geometry of the surface and the compliance as developed in Appendix B is expressed as

$$\epsilon_1^2 = \frac{A_r}{A_a} = \left(\frac{C}{Y_o}\right)^2 e^{-j^2}\left(1 - \frac{C}{Y_o}\right)^2 \tag{4.12}$$

where C is the compliance of the two surfaces, Y_o is the separation of the mean lines at zero load, and j is a multiplier (Appendix A).

4.4 Elastic Deformation of Wavy Surfaces

The thermal analysis of Chapter 3 shows that for cylindrical waviness the two surface parameters necessary for the evaluation of the contact conductance are the ratio of the real contact area to the apparent area and the length of the cylinder. For spherical waviness the two parameters are the real contact area to the apparent area ratio and the pitch of the waves.

4.4.1 Elastic Deformation of Cylindrical Wavy Surfaces

The subsequent analysis will be based upon the following postulates: (1) all the cylindrical waves are smooth and continuous, (2) the two

surfaces are similar, i.e., $R_1 = R_2 = R$, (3) the surfaces are of the same material and $\nu_1 = \nu_2 = 0.3$, (4) the two surfaces are symmetrical about the contact plane, (5) the cylindrical waves have uniform pitch, (6) the line of force always acts through the centers of curvature of the touching waves, (7) the deviation from flatness is small relative to the pitch.

From elastic deformation theory one can write the half-width of rectangular contact area as

$$c_2 = 1.08 \left[\frac{WR}{E} \right]^{1/2} \tag{4.12}$$

where W is the load per unit length in the direction of no waviness, R is the radius of curvature and E is the modulus of elasticity.

If assumption (7) is held to be valid, then the radius of curvature can be approximated by

$$R \doteq \frac{L^2}{8d} \tag{4.13}$$

where L is the pitch and d is the deviation from flatness.

One obtains from a simple force balance

$$W = P_a L^2 / \ell \tag{4.14}$$

$$c_2 = 1.08 \left[\frac{P_a L^4}{8Ed\ell} \right]^{1/2} \tag{4.15}$$

Finally one can express the cylindrical elastically deformed area ratio as

$$\epsilon_{2ce}^2 = \frac{2c_2}{L}\, m^2 = 0.765\, m \left[\frac{P_a L}{Ed}\right]^{1/2} \qquad (4.16)$$

It should be emphasized that this will be the ratio of the real contact area to the total or apparent contact area only for the case of no surface roughness and elastic deformation of the surfaces. It is interesting to note that the dimensionless number ϵ_{2ce}^2 depends upon the surface geometry (L, d), the material property E, and the applied load P_a.

4.4.2 Elastic Deformation of Spherical Wavy Surfaces

The elastic deformation analysis will be based upon the following assumptions: (1) all the spherical waves are smooth and continuous, (2) the two surfaces are similar, i.e., $R_1 = R_2 = R$, (3) the surfaces are of the same material and $\nu_1 = \nu_2 = 0.3$, (4) the two surfaces are symmetrical about the contact plane, (5) the spherical waves have a uniform pitch, (6) the line of force always acts through the centers of curvature of the touching waves, (7) the deviation from flatness is small relative to the pitch.

The radius of contact can be written as

$$c_2 = 1.28 \left[\frac{FR}{E} \right]^{1/3} \tag{4.17}$$

where F is the load at each contact, R is the radius of curvature of the spherical cap and E is the modulus of elasticity.

As for cylindrical waviness one can express the radius of curvature as

$$R \doteq \frac{L^2}{8d} \tag{4.18}$$

and

$$F = P_a \frac{\pi}{4} L^2 \tag{4.19}$$

from a simple force balance consideration.

Finally one can express the spherical elastically deformed area ratio as

$$\epsilon_{2se} = \frac{2c_2}{L} = 0.81 \left[\frac{P_a L}{Ed} \right]^{1/3} \tag{4.20}$$

Again one should remember that this expression is the real area to apparent area ratio only for the case of no surface roughness, otherwise it expresses the contour area to apparent area ratio. Note that the dimensionless number ϵ_{2se}^2 depends upon the surface geometry (L, d), the material property E, and the applied load P_a.

4.5 Plastic Deformation of Wavy Surfaces

Wavy surfaces whether cylindrical or spherical can only support the stress at which the material begins to yield if there is plastic deformation. For metallic surfaces this stress is generally equal to 2.8 - 3.0 times the yield stress Y.

4.5.1 Cylindrical Waviness

A force balance consideration gives

$$N_c 2c_2 \ell H = P_a N_c L L \tag{4.21}$$

$$\frac{2c_2 \ell}{L^2} = \epsilon_{2p}^2 = \frac{P_a}{H} \tag{4.22}$$

where P_a is the apparent pressure and H is the microhardness which is equal to 3Y.

4.5.2 Spherical Waviness

$$N_c \pi c_2^2 H = P_a N_c \frac{\pi}{4} L^2 \tag{4.23}$$

$$\frac{4c_2^2}{L^2} = \epsilon_{2p}^2 = \frac{P_a}{H} \tag{4.24}$$

It should be noted that for all three cases of nominally flat rough surfaces, cylindrical wavy surfaces and spherical wavy surfaces, the area ratio parameter is a function only of the applied load P_a, and the material strength H. It is independent of the shape or distribution of the asperities or the waviness.

Chapter 5

EXPERIMENTAL DETERMINATION OF CONTACT RESISTANCE

5.1 Description of Apparatus

The experimental apparatus is shown in Figure 17 and consists of a structure for support and loading, the test chamber, a vacuum system and an instrument console.

The physical load is obtained by means of the lever system, having a mechanical advantage of about 100, which provides dead weight loading that is transmitted to the test section by means of the bellows. Dead weight loading has the advantage of being independent of thermal strains which result when the test section is heated to operating conditions. The actual load on the test specimens is measured directly by a strain gauge dynamometer which had been calibrated against a Moorehouse Proving Ring.

When tests are run in a vacuum, the minimum load on the test section is 103 pounds (or 131 psi in the on e-inch diameter test section) due to the atmospheric pressure acting across the 3-inch diameter bellows through which the loading system is attached to the vacuum chamber.

An assembly drawing of the test section and chamber is shown in Figure 18 . The chamber is a vacuum enclosure consisting of a top plate

and upper cylinder, a baseplate which is bolted to the supporting structure, and to which is attached the vacuum system, and a lower flanged cylinder bolted to the upper cylinder and baseplate.

The test section, Figure 18 , consists of, from top to bottom: the upper cooler (part 4), spacers (5 and 6) of materials chosen to have conductivities appropriate for the test being conducted, the upper heater (7), the upper heat meter (8), the two test specimens (9, 10) the lower heat meter (16), the lower heater (17) and insulating spacer (18), the dynamometer (19), and the lower cooler (20).

Some flow of water is maintained in all coolers during testing in order to protect the top and base plates and the feedthrough. The heating elements are Kanthal resistance wire coiled and cemented between an alundum core and an outer sleeve. The heater cores are one-inch diameter stainless steel.

All thermocouples are 28-gauge chromel-alumel cemented into place using Sauereisen. Four thermocouples are inserted into each specimen up to the centerline and are uniformly spaced along the axis of the specimen. The thermocouple and ceramic sleeve occupy less than 3 per cent of a plane perpendicular to the axis of the specimen, and therefore the thermocouples do not measurably disturb the flow of heat.

The dynamometer is a 1 1/2 inch diameter by 2-inch long solid aluminum cylinder located between the lower cooler and the lower insulation. Near the base of the cylinder are attached semi-conductor strain gauges. The basic sensitivity of the dynamometer is about 1 millimeter displacement on the Sanborn recorder readout for a one-pound load.

In order to minimize radiation losses from the test section, radiation shields are provided as shown in Figure 18.

The vacuum system consists of a mechanical forepump, a 4-inch diffusion pump with a water-cooled optical baffle, and a three-way vacuum valve. The mechanical pump is capable of reducing the pressure in the chamber to about 10 microns; while the mechanical and diffusion pumps operating in series are capable of reducing the chamber pressure to about 1.5×10^{-6} mm Hg when the system is operating at about 500°F.

Pressures between 5 and 1000 microns of Hg are read with a thermocouple gauge, and the pressure range between 5 microns and 10^{-7} mm Hg is read with an ionization gauge.

The instrument console is shown in Figure 19 . Power for the four heaters and the pumps is controlled from the console. The thermocouple potentiometer, wattmeters for the heaters, and the vacuum gauge control are located on the console as are valves for controlling the water flows through the four coolers.

The apparatus for generating the cylindrical waviness consists of the specimen holder and the tool as shown in Figure 20 . The holder consists of two V-blocks, two verniers, runners and baseplate, while the tool is a long piece of tool steel 1/4-inch thick having one edge machined to the desired waviness.

5.2 Preparation of Specimens

Specimens about 1 1/2-inch are cut from 1-inch diameter bar stock. After turning the specimens on a lathe and then grinding the ends so that the specimens are 1 1/2-inch long, they are lapped to produce a flat surface with a roughness number of 3.

The surfaces are now tested for waviness with the profilometer, and if there should be any indication of surface waviness, the lapping process is repeated.

The nominally flat surfaces are then blasted with glass spheres to achieve an ergodic surface having a random distribution of asperities. These prepared specimens are stored in dessicators to prevent oxidation of the surface until the specimens are to be tested.

The wavy specimens are prepared using the apparatus described above. The specimen is placed between the V-blocks and secured into place when it has been ascertained that the specimen is level by means of the lower vernier. The cutting edge of the tool is covered with a thin layer of lapping compound and the tool is then aligned with the horizontal vernier which

is flush with the edge of the specimen. The tool under uniform pressure is run across the specimen generating the wavy, rough surface. The waviness depends upon the shape of the tool and the roughness depends upon the lapping compound used between the tool and the specimen.

By means of the horizontal vernier the tool is displaced the width of the tool across the specimen and the rubbing process is repeated. This is repeated until the desired surface geometry is obtained. The specimens are placed in a dessicator until they are to be tested.

5.3 Experimental Procedure

The surface profiles of the specimens to be tested are read out onto a Sanborn strip by means of the profilometer. Next the thermocouples are placed and secured in the specimens by means of the Sauereisen, surfaces are cleaned with acetone and the specimens are positioned and aligned in the test section under a load of about 20 psi.

After having aligned the specimens, the chamber was closed and a vacuum of about 5×10^{-6} mm Hg was attained by means of the mechanical and diffusion pumps. With a minimum interface pressure of 131 psi, all heaters were turned on producing an interface temperature of about $700^{\circ}F$. The system and the interface were allowed to outgas for about 36 hours after which there was no noticeable change with time of the contact conductance.

The outgassing of the interface having been completed, the load was increased in increments, temperature readings were taken and recorded. About two to four hours were required to achieve thermal equilibrium in the test section subsequent to increasing the load. The specimens having high heat capacitities and low thermal conductivities required maximum time for thermal equilibrium.

The temperature at the interface was generally maintained at a constant value as the load was increased by increasing the input to the heaters.

The specimens were loaded to a maximum load of about 20,000 psi and then the load was reduced in increments and the temperature readings recorded as before.

Chapter 6

COMPARISON OF PREDICTED AND EXPERIMENTAL RESULTS

To determine whether the asperities deform elastically or plastically the experimental values of h/k_m versus P_a (apparent pressure) are shown in Figure 29. In the same figure is shown the calculated values of h/k_m using Equation (3.29) where the contact ratio, ϵ, was obtained using

(a) the elastic theory outlined above and Equation (4.6)

(b) the plastic theory using the relationship $\epsilon_p^2 = P_a/H$ where H is the yield pressure, and the corresponding compliance ratio, (C/Y_o), was calculated from Equation (B-9). The number of contact points was obtained as in part (a) using Figures 10 and 11.

Figure 29 shows that the deformation of the nominally-flat, rough surfaces at light to moderate pressures is due to the plastic deformation of the asperities, but at higher pressures the actual deformation begins to deviate from the completely plastic assumption. At the light pressures the assumption of completely elastic deformation of the asperities is erroneous but at higher pressures this effect seems to be important, and is probably the reason that the experimental observations deviate from the assumption of completely plastic deformation.

As can be seen from the plots of ϵ_2 versus P_a for the cylindrical and spherical waviness, the test data values always fall between the values determined from elastic theory and plastic deformation. The values of ϵ_2 as determined by the classical Hertzian theory exceeds the test results over the entire load range, while the values of ϵ_2 as determined by plastic considerations always lies below the test results over the same load range.

Chapter 7

CRITICAL COMPARISON OF THEORY WITH PUBLISHED THEORIES AND TEST DATA

Since the phenomenon of surface interactions at large pressures is quite complex and therefore intractable, it was decided to obtain empirical information about the surface interactions under loading conditions. A survey of the literature revealed that several authors had investigated this mechanical phenomenon under various surface conditions, geometries and physical loads. Invariably the investigators were concerned with relatively smooth surfaces under very light loading so that only a small number of asperities per unit area were contacted, and therefore the deformation of these contacted asperities were completely plastic.

The most interesting and useful paper (59) showed experimental data of applied load versus surface separation for three metals. In the present work, the aluminum and stainless steel data have been replotted as the apparent pressure versus the dimensionless compliance, Figure 13.

Since empirical data of the apparent pressure against the dimensionless compliance for these metals at higher pressures were not available, it was decided to use experimental information, such as $\sqrt{n}$ versus P_a for aluminum surfaces, Figure 12, and h/k_m versus P_a (apparent pressure) for the stainless steel surfaces, Figure 29.

With the assumption that $\sqrt{n}$ versus compliance is a geometric relationship independent of the material under consideration, then the apparent pressure as a function of the dimensionless compliance for any metal can be obtained from empirical data relating the number of contact spots per unit area against the apparent pressure. The information in Figure 12 is shown cross plotted in Figure 13, and compares quite favorably with the information in Reference (59).

The heat transfer data for stainless steel surfaces yielded the plot of Figure 13 which shows again a very satisfactory correlation of data from two independent sources.

The experimental data (59) was obtained for metals which had relatively smooth surfaces, and for light apparent pressures which never exceeded 120 psi; while the other experimental data was obtained for surfaces which were, relatively speaking, much rougher and the pressures ranged from a minimum of 130 psi to a maximum of about 15,000 psi.

The good agreement under these conditions is therefore most encouraging and suggests that the basic assumptions are quite good. An examination of Figure 13 shows that when the apparent pressure is plotted against the dimensionless compliance, the effect of the surface roughness is not very strong. However, further load-compliance tests should be

made for various materials having a range of roughness before definite conclusions can be made.

The conductance equation developed by Clausing was based on the assumption that the macroscopic constriction resistance is the dominant resistance, and that the material deformation is due solely to elastic deformation, with possibly some creep being present under conditions of high interface temperature.

The conductance equation is expressed as

$$\frac{k_m}{hb_2} = \frac{\pi}{2} \frac{g(x_L)}{x_L} \tag{7.1}$$

where

$$x_L = 1.285 \left[\frac{P_a L}{E_m d_t} \right]^{1/3} \tag{7.2}$$

and $g(x_L)$ is the constriction alleviation factor.

The stringent restriction that Eq. (7.1) is valid only for $x_L < 0.65$ limits its applicability to moderate apparent pressures. As an example, for aluminum materials having a flatness-deviation of 100×10^{-6} inches and a wavelength of one inch, the equation is valid up to an apparent pressure of 60 psi. The great discrepancy between theory and experimental data which he observed for aluminum samples having a flatness-deviation

of 80×10^{-6} inches or less, is probably due to the inherent limitation in the conductance equation.

As the flatness deviation increases or the modulus of elasticity increases or the pitch decreases, the pressures for which the equation is valid also increase, for example, stainless steel having $d = 500 \times 10^{-6}$ inches and L = 1/4 inch, P_a = 3600 psi. Clausing observed that for stainless steel the best agreement between theory and test occurred at $d = 300 \times 10^{-6}$ inches and the worst agreement occurred at $d = 80 \times 10^{-6}$ inches.

Since experimental data was not obtained for the case of spherical waviness, the heat transfer data reported in Reference (12) was used to determine the actual ϵ_{2s}. The dimensionless ration ϵ_{2s} as determined from pure plastic deformation, pure elastic deformation, and by test are shown plotted versus the apparent pressure. The test values of ϵ_{2s} always lie between the limiting case of plastic and elastic deformation. It would appear from the plot of the test data that there is plastic deformation present at all times, which tends to reduce the value of ϵ_{2s} determined from pure elastic deformation. A very small amount of plastic deformation will presumably have a significant effect upon the value of ϵ_{2s}. When ϵ_{2s} determined by elastic theory has values greater than 0.10 but less than 0.40, the actual value of ϵ_{2s} lies about mid-way between

ϵ_{2se} and ϵ_{2sp} (Figure 24). The actual values of ϵ_{2s} should be correlated with ϵ_{2se} and ϵ_{2sp} by considering the effects of the applied load, the material properties, and the surface geometry.

Clausing based his analysis upon the statement that the macroscopic constriction resistance (R_L) is orders of magnitude larger than the microscopic resistance (R_s). In his report he has shown that R_L/R_s is at least 29 for aluminum and at most 156 for brass. Several investigators have obtained experimental data which show that the microscopic resistance is at least as great as the macroscopic resistance, and can often be larger under certain conditions. Let us consider a stainless steel contact having P_a = 500 psi, $\sigma = 120 \times 10^{-6}$ inches, $d = 300 \times 10^{-6}$ inches, L = 0.25 inches. The ratio of the wavy to rough conductance can be expressed as $f_r(\epsilon_1)/L \sqrt{n}\, f_s(\epsilon_2) \therefore h_{2s}/h_1 = 2.50/.082 \times 0.25 \times 80 = 1.52$ and not 65 as reported by Clausing. One cannot simply say that the microscopic conductance is orders of magnitude larger than the macroscopic conductance as seen from the sample calculation. The microscopic conductance must be determined for each case and compared with the macroscopic conductance before a decision can be made to neglect the microscopic conductance.

CHAPTER 8

SUMMARY AND CONCLUSIONS

8.1 Discussion of Results

The contact conductance for nominally-flat, rough surfaces placed in a vacuum can be correlated by the thermal conductivity of the metal and by two surface parameters: the number of contact points per unit length and the dimensionless real to apparent area ratio. Since the number of contact points per unit length is inversely proportional to the distance between contact spots, then one can say the contact conductance is inversely proportional to the pitch of the contact spots.

The number of contact spots can be determined by counting the number of contact points as two linear profiles, representing the actual surfaces, are brought together. Since the compliance of two surfaces depends upon the material properties, the applied load and possibly the surface geometry, one must resort to empirical information in order to be able to correlate the number of contact spots with the applied load.

The second surface parameter necessary for the determination of the contact conductance is more difficult to obtain by studying the interaction of two profiles representing the real surfaces. A full understanding of the deformation of the asperities is necessary for the prediction of the

real to apparent area ratio. In this work an attempt was made to determine what this ratio would be if the deformation was strictly plastic or strictly elastic. From an examination of the heat transfer test data it would appear that the actual area ratio lies between the two limiting values determined by plastic or by elastic considerations. At very light pressures it appears that the deformation is solely plastic. When the pressure is increased slightly, the elastic deformation begins to have an influence and the plastic criterion is no longer valid. At very high pressures, the values of the area ratio determined by plastic theory are larger than the values determined by elastic theory. There appears to be a pressure at which there is a transition from a region where the elastic deformation yields the greater value of the area ratio to a region where the plastic deformation yields the greater value of this surface parameter.

The cylindrical waviness contact conductance is a function of the thermal conductivity of the metals and the three surface parameters: the pitch between the waves, the ratio of the length of the wave in the direction of no waviness to the pitch, and the real to apparent area ratio. Test data reveals that the area ratio is greater than that determined by plastic theory but less than that determined by elastic theory. For particular cases where the material is soft, the pitch is large and the flatness deviation is small, elastic theory gives values of the area ratio orders of magnitude larger

than determined from test. This author believes that there is a reduction in the pressure available for the elastic deformation of the waves because of a small, but significant, change in the real area due to plastic deformation. This effect will be more pronounced with wavy surfaces which are rough rather than smooth. There is a reduction in the pressure due to shearing forces as the rough surfaces slip very slightly.

This author did not obtain test data for surfaces which had spherical waviness. Test data from reference (12) were used to check out the contact conductance equation which shows that the important parameters are the thermal conductivity of the metals, and the surface parameters: the pitch between the waves and the real to apparent area ratio.

As for the case for cylindrical waviness test data shows that the area ratio is greater than the values determined by plastic theory but less than values determined by elastic theory.

This author believes that the same reasoning can be applied for the case of spherical waviness as for cylindrical waviness to explain why there is such a discrepancy between elastic theory and test data. A full understanding of the effect of shear which results in some plastic deformation is necessary before a good correlation between test and theory can be made.

8.2 Recommendations for Future Research

For nominally-flat, rough surfaces, empirical data relating the compliance with the apparent pressure for various values of the roughness are necessary for the theory to be complete.

Some means of introducing the effect of substratum yielding is also necessary to enable one to determine the number of contact spots per unit area corresponding to a particular apparent pressure.

It is evident from an examination of the interaction of two surface profiles that for certain values of the compliance, there is a coming together of several contact spots thereby forming one large contact spot. If this should occur at many places over the entire apparent area, then possibly it would have a large effect upon the actual contact conductance.

It is recommended that test data be obtained to determine the effect of load upon the cylindrical or spherical waviness. It is necessary to know whether plastic as well as elastic deformation occurs and how much. One surface could be covered with a dye which can easily be transferred to the other surface when contact occurs, and which can easily be detected upon the second surface after contact has occurred.

A critical examination of surface profiles before and after test might also reveal whether plastic deformation has occurred and how much of the real area was due to this type of deformation.

BIBLIOGRAPHY

Section 1: M. I. T. Theses

1. Fenech, Henri, "The Thermal Conductance of Metallic Surfaces in Contact," M. I. T. Sc. D. Thesis, May, 1959.
2. Henry, John Jewett, "Thermal Resistance of Metals in Contact," M. I. T. M. S. Thesis, August, 1961.
3. Carroll, Tom Wentworth, "Statistical Calculation of Geometric Parameters for Semi-Smooth Contiguous Surfaces," M. I. T. M. S. Thesis, January, 1962.
4. Kaszubinski, Leonard Joseph, "Determination of the Number of Contacts Between Two Surfaces Pressed Together," M. I. T. M. S. Thesis, August, 1963.
5. Velissaropoulos, Pandelis D., "Apparatus for Measurement of Contact Resistance," M. I. T. M. S. Thesis, August, 1963.
6. Horn, Stefan Schulze, "Thermal Contact Resistance of Graphite," M. I. T. M. S. Thesis, September, 1963.
7. Flammang, Dennis Craig, "The Use and Comparison of Autoradiographical and Statistical Methods of Determining the Number of Contacts Between Two Surfaces Pressed Together," M. I. T. B. S. Thesis, June, 1963.
8. Foster, Edward Terence, "Prediction of Contact Population in Bimetallic Surface Junctions," M. I. T. M. S. Thesis, August, 1964.

9. Henry, John Jewett, "Thermal Contact Resistance," M. I. T. Sc. D. Thesis, August, 1964.

Section 2: Contact Resistance References

10. Carslaw, H.S. and Jaeger, J. C., "Conduction of Heat in Solids," London: Oxford University Press, Second Edition, 1959.

11. Cetinkale, T.N. and Fishenden, Dr. Margaret, "Thermal Conductance of Metal Surfaces in Contact," International Conference on Heat Transfer, Institution of Mechanical Engineers, London, 1951.

12. Clausing, A.M. and Chao, B. T., "Thermal Contact Resistance in a Vacuum Environment," National Aeronautics and Space Administration, University of Illinois, ME-TN-242-1, August, 1963.

13. Clausing, A.M., "Some Influences of Macroscopic Constrictions on the Thermal Contact Resistance," National Aeronautics and Space Administration, University of Illinois, ME-TN-242-2, April, 1965.

14. Cordier, H., "Experimental Study of the Influence of Pressure on Contact Thermal Resistance," Redstone Scientific Information Center, (RSIC-116) 1961 (Translated from Acad. des Sciences, Compts. Rendus 250, April 25, 1960).

15. Bloom, M. F., "Thermal Contact Conductance in a Vacuum Environment," Missile and Space Systems Division, Douglas Aircraft Company Report SM-47700, December, 1964.

16. Fenech, H. and Rohsenow, W.M., "Prediction of Thermal Conductance of Metallic Surfaces in Contact," ASME Transactions Paper No. 62-HT-32, Journal of Heat Transfer, September, 1962.

17. Fenech, H. and Henry, J.J., "An Analysis of a Thermal Contact Resistance," Transactions of the American Nuclear Society, November, 1963.

18. Fried, E. and Costello, F.A., "The Interface Thermal Contact Resistance Problem in Space Vehicles (Lifting Reentry Vehicles)," American Rocket Society Journal, Vol. 32, New York, 1962.

19. Fried, E., "Thermal Joint Conductance in a Vacuum," ASME Paper No. AHGT-18, March, 1963.

20. Fried, E., "Study of Interface Thermal Contact Conductance Summary Report," NASA Document No. 645D652, May 1, 1964.

21. Henry, J.J. and Fenech, H., "The Use of Analog Computers for Determining Surface Parameters Required for Prediction of Thermal Contact Conductance," ASME Paper No. 63-WA-104, Journal of Heat Transfer, September, 1964.

22. Heasley, J.H., "Transient Heat Flow Between Contacting Solids," Int. J. Heat Mass Transfer, Vol. 8, pp. 147-154, 1965.

23. Jacobs, R.B. and Starr, C., "Thermal Conductance of Metallic Contacts," Review of Scientific Instruments, Vol. 10, 1939.

24. Laming, L.C., "Thermal Conductance of Machined Metal Contacts," International Developments in Heat Transfer, ASME, 1961.

25. Petri, F.J., "An Experimental Investigation of Thermal-Contact Resistance in a Vacuum," ASME Paper No. 63-WA-156, December, 1963.

26. Rogers, G.F.C., "Heat Transfer at the Interface of Dissimilar Metals," International Journal of Heat and Mass Transfer, Vol. 2, 1961.

27. Shlykov, Yu. P., Ganin, E.A. and Demkin, N.B., "Analysis of Contact Heat Exchange," Redstone Scientific Information Center (RSIC-117), 1960.

28. Shlykov, Yu. P., and Ganin, Ye. A., "Thermal Resistance of Metallic Contacts," Int. J. Heat Mass Transfer, Vol. 7, pp. 921-929, 1964.

29. Stubstad, W.R., "Measurements of Thermal Contact Conductance in Vacuum," ASME Paper No. 63-WA-150, August, 1963.

30. Tachibana, F., "Study on Thermal Resistance of Contact Surface," Redstone Scientific Information Center (RSIC-29), June, 1963.

31. Held, W., "Heat Transfer Between Worked Surfaces," Redstone Scientific Information Center - Transaction No. 76, October, 1963 (Translated from Allgemine Warmetechnik, Vol. 8, 1957).

32. Kouwenhoven, W.B. and Potter, J.H., "Thermal Resistance of Metal Contacts," Journal of American Welding Society, Vol. 27, Part 2, 1949.

33. Powell, R.W., Lye, R.P. and Jolliffe, B.W., "Heat Transfer at the Interface of Dissimilar Materials: Evidence of Thermal-Comparator Experiments," International Journal of Heat and Mass Transfer, Vol. 5, 1962.

34. Weills, N. D. and Ryder, E. A., "Thermal Resistance Measurements of Joints Formed Between Stationary Metal Surfaces," Transactions of the ASME, April, 1949.

35. Elliott, D. H., "Thermal Conduction Across Aluminum Bolted Joints," ASME Paper No. 65-HT-53, August, 1965.

36. Koh, B. and John, J. E. A., "The Effect of Interfacial Foils on Thermal Contact Resistance," ASME Paper No. 65-HT-44, August, 1965.

37. Stubstad, W. R., "Thermal Contact Resistance Between Thin Plates in Vacuum," ASME Paper No. 65-HT-16, August, 1965.

38. Blum, H. A. and Glifford Jr., J. M., "Transient Phenomena in Heat Transfer Across Surfaces in Contact," ASME Paper No. 65-HT-59, August, 1965.

39. Kaspareck, W. E. and Dailey, R. M., "Measurements of Thermal-Contact Conductance Between Dissimilar Metals in a Vacuum," ASME Paper No. 64-HT-38, August, 1964.

40. Barzelay, M. E., Tong, K. N. and Holloway, G. F., "Thermal Conductance of Contacts in Aircraft Joints," National Advisory Committee For Aeronautics, Technical Note 3167, March, 1954.

41. Barzelay, M. E., Tong, K. N. and Holloway, G. F., "Effect of Pressure on Thermal Conductance of Contact Joints," National Advisory Committee For Aeronautics, Technical Note 3295, May, 1955.

42. Boeschoten, F. and Van der Held, E.F.M., "The Thermal Conductance of Contact Between Aluminum and Other Metals," Physica, Vol. XXIII, 1957.

Section 3: Subjects Related to Contact Resistance

43. Archard, J.F., "Contact and Rubbing of Flat Surfaces," Journal of Applied Physics, Vol. 24, No. 8, August, 1953.

44. Archard, J.F., "Elastic Deformation and the Laws of Friction," Research Correspondence, Vol. 9, 1956.

45. Archard, J.F., "Single Contacts and Multiple Encounters," Journal of Applied Physics, Vol. 32, No. 8, August, 1961.

46. Bowden, F.P. and Tabor, D., "Friction and Lubrication," London: Metheun and Co., Ltd., New York: John Wiley and Sons, Inc., 1956.

47. Budiansky, Berbard, "A Reassessment of Deformation Theories of Plasticity," Journal of Applied Mechanics, June, 1959.

48. Dorinson, A., "Microtopography of Finely Ground Steel Surfaces in Relation to Contact and Wear," ASLE Transactions, Vol. 8, pp. 100-108, 1965.

49. Furey, M.J., "Surface Roughness Effects on Metallic Contact and Friction," ASLE Transactions, Vol. 6, pp. 49-59, 1963.

50. Goodman, L.E., "Contact Stress Analysis of Normally Loaded Rough Spheres," Journal of Applied Mechanics, pp.515-522, September, 1962.

51. Greenwood, J. A. and Williamson, J. B. P., "The Contact of Nominally Flat Surfaces," Burndy Research Division, Research Report No. 15, July, 1964.

52. Greenwood, J. A. and Tripp, J. H., "Elastic Contact of Rough Spheres," Burndy Research Division, Research Report No. 21, February, 1965.

53. Hoffman, O. and Sachs, G., "Introduction to the Theory of Plasticity for Engineers," McGraw-Hill, New York, 1953.

54. Holm, Ragnar, "Electric Contacts Handbook," Springer-Verlag, Berlin/Gottingen/Heidelberg, 1958.

55. Hunt, F. V., "Elastic-Plastic Instability Caused by the Size Effect and Its Influence on Rubbing Wear," Journal of Applied Mechanics, Vol. 26, No. 7, July, 1955.

56. Jones, Llewellyn, "The Physics of Electrical Contacts," Clarendon Press, Oxford, 1957.

57. Kragelsky, I. V. and Demkin, N. B., "Contact Area of Rough Surfaces," Wear, Vol. 3, pp. 170-187, 1960.

58. Ling, F. F., "Some Factors Influencing the Area-Load Characteristics for Semismooth Contiguous Surfaces Under Static Loading," ASME Paper No. 57-A-246, September, 1957.

59. Ling, F. F., "On Asperity Distributions of Metallic Surfaces," Journal of Applied Physics, Vol. 29, No. 8, August, 1958.

60. Marochkin, V.N., "Friction Coefficient Analysis Applied to Two Rough Surfaces," Friction and Wear in Machinery, Translation ASME.

61. Mindlin, R.D., "Compliance of Elastic Bodies in Contact," ASME Paper No. 48-APM-24, September, 1949.

62. Hill, R.A., "The Mathematical Theory of Plasticity," Oxford University Press, New York, 1950.

63. Nadai, A., "Theory of Flow and Fracture of Solids," Vol. I, McGraw-Hill Book Company, Inc., New York, 1950.

64. Timoshenko, S. and Goodier, J.N., "Theory of Elasticity," McGraw-Hill Book Company, Inc., New York, 1951.

Appendix A

CONTACT SPOT DENSITY FOR NOMINALLY FLAT ROUGH SURFACES

The real area of contact between two nominally flat rough surfaces having a random distribution of asperity heights about a mean line can be approximated by considering the interaction of an ideally flat rigid surface with a nominally flat rough surface having a roughness $\sigma = \sqrt{\sigma_1^2 + \sigma_2^2}$, where σ_1 and σ_2 are the root mean square deviations of surface 1 and 2.

Consider the placement of an ideal flat rigid surface upon a surface having asperities with a random distribution of heights and base angles, and the asperities are distributed ergodically over the surface. Shown below is the ideal flat surface just coming into contact with the rough surface (sectional view).

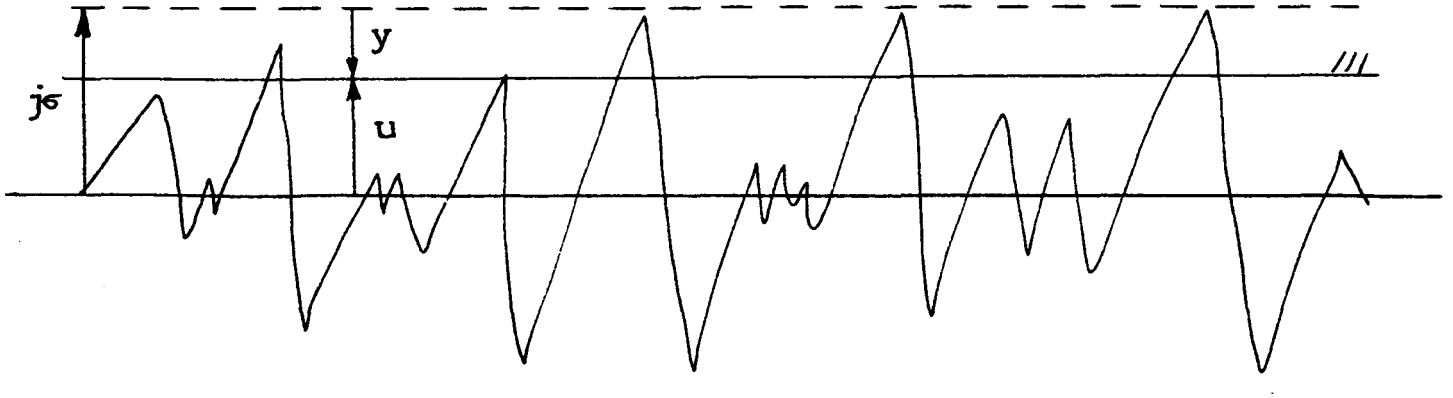

Let N_1 and N_2 be the number of contact points per unit length in mutually perpendicular directions 1 and 2. σ is the standard deviation or root mean square deviation of the heights of the asperities from a median. The maximum height of any asperity in the sample length is given by $j\sigma$ where j is a factor ranging in value from 2.90 to 3.8 depending upon the number of asperities in the sample and the range of asperity heights. I is the interval for which the frequencies have been determined.

For a Gaussian distribution of asperity heights the frequency of contact spots in the 1-direction per unit length is given by

$$n_1 = \frac{N_1 I_1}{\sqrt{2\pi}\ \sigma_1} e^{-\frac{1}{2}\left(\frac{u}{\sigma_1}\right)^2} \qquad \text{(A-1)}$$

where u is the distance measured from the mean line to the ideal plane.

The frequency equation can be rewritten by letting $u + y = j\sigma$ where y is the distance moved by the plane, i.e., the compliance of the two surfaces:

$$n_2 = \frac{N_1 I_1}{\sqrt{2\pi}\ \sigma_1} e^{-\frac{1}{2}\left[j - \frac{y}{\sigma_1}\right]^2} \qquad \text{(A-2)}$$

Similarly in the mutually perpendicular 2-direction

$$n_2 = \frac{N_2 I_2}{\sqrt{2\pi}\ \sigma_2} e^{-\frac{1}{2}\left[j - \frac{y}{\sigma_2}\right]^2} \qquad \text{(A-3)}$$

The number of asperities encountered by the ideal flat plane as it moves a distance y is given by:

$$n = n_1 n_2 = \frac{N_1 N_2 I_1 I_2}{2\pi \sigma_1 \sigma_2} e^{-\frac{1}{2}\left[j_1 - \frac{y}{\sigma_1}\right]^2} e^{-\frac{1}{2}\left[j_2 - \frac{y}{\sigma_2}\right]^2} \quad \text{(A-4)}$$

In this analysis it is assumed that when $y = 0$, there is contact at 3 asperities, i.e., the frequency curve has been arbitrarily truncated. For surfaces which are ergodic and have the same distribution, $I_1 = I_2$, $\sigma_1 = \sigma_2$, $j_1 = j_2$ and $N_1 = N_2$.

$$n = \frac{N^2}{2\pi}\left(\frac{I^2}{\sigma^2}\right) e^{-\left[j - \frac{y}{\sigma}\right]^2} \quad \text{(A-5)}$$

Differentiating this equation one can show that

$$\frac{dn}{dy} = \frac{2nj}{\sigma}\left(1 - \frac{y}{j\sigma}\right) \quad \text{(A-6)}$$

which is found to be important in the following analysis.

Appendix B

REAL TO APPARENT AREA RATIO FOR NOMINALLY FLAT ROUGH SURFACES

Assume that all the asperities can be idealized as cones having base angles whose tangents are given by $k\sigma$ where σ is the r.m.s. deviation of all the tangents and k is a multiplier in the same sense as j in Appendix A.

As the ideal flat plane moves a distance dy into the rough surface, dn asperities are contacted and the following relation

$$Ay + dy = Ay + dA \tag{B-1}$$

can be expressed as

$$(n + \frac{dn}{dy}\, dy)\pi\, (r + dr)^2 = n\pi r^2 + dA \tag{B-2}$$

Assume radius of contact per contact spot is proportional to the displacement of the flat surface, i.e.,

$$r = \frac{y}{\tan\theta}\ , \text{ therefore } dr = \frac{dy}{\tan\theta} \tag{B-3}$$

as a first approximation when $\tan\theta$ is assumed constant with y.

Neglecting terms of $(dy)^2$ and smaller

$$\frac{dA}{dy} = \frac{n\pi}{\tan^2\theta}\left[\ 2\ \frac{dy}{y} + \frac{2j}{\sigma}\ dy - \frac{2ydy}{\sigma^2}\right] \qquad \text{(B-4)}$$

Since

$$Ay = \frac{n\pi y^2}{\tan^2\theta} \qquad \text{(B-5)}$$

$$\therefore\ \frac{dA_y}{A_y} = \left(\ \frac{2\,dy}{y} + \frac{2j}{\sigma}\ dy - \frac{2y\ dy}{\sigma^2}\ \right) dy \qquad \text{(B-6)}$$

The boundary conditions to be satisfied are at

$$y = 0\ ,\ A_y \doteq 0 \qquad \text{(B-7)}$$

and

$$y = j\sigma\ ,\ A_y = A_a \qquad \text{(B-8)}$$

The boundary condition (B-8) states that all the material above the mean line has flowed into the voids below the mean line when the compliance has reached its maximum value $j\sigma$.

Solving Equation (B-6) one can show that

$$\epsilon_1^{\,2} \equiv \frac{A_y}{A_a} = \left(\frac{y}{j\sigma}\right)^2 e^{-j^2}\left(1 - \frac{y}{j\sigma}\right)^2 \qquad \text{(B-9)}$$

The validity of this equation has been checked with values determined by graphical means and the agreement is quite good, Figure 17.

Appendix C

AREA RATIO-HARDNESS RELATIONSHIP FOR PLASTIC DEFORMATION

A simple force balance gives the following relationship

$$dF = HdA \tag{C-1}$$

where F is the applied force and H is the microhardness of the material.

Using Equation (B-6) one can write

$$dW = HA_y\left(2\frac{dy}{y} + \frac{2j}{\sigma}dy - \frac{2y}{\sigma^2}dy\right) \tag{C-2}$$

but

$$A_y = A_a\left(\frac{y}{j\sigma}\right)^2 e^{-j^2}\left(1 - \frac{y}{j\sigma}\right)^2 \tag{C-3}$$

Since the slopes of the asperities are 10^o or less, the hardness of the material is approximately three times the yield strength and constant for any asperity height (46).

Letting H be a constant one can solve Equation (C-3) to show that

$$P_a = \frac{W}{A} = H\left(\frac{y}{j\sigma}\right)^2 e^{-j^2}\left(1 - \frac{y}{j\sigma}\right)^2 \tag{C-4}$$

Appendix D

ELASTIC AND PLASTIC COMPLIANCE RATIO

Consider the interaction of two smooth spherical caps having the same radius of curvature R. The force F acts through the centers of each cap and is perpendicular to the contact plane which is midway between the centers of the caps.

Assuming that the hardness of the surfaces is constant and equal to 3Y, a simple force balance gives

$$c = \left[\frac{F}{3Y\pi} \right]^{1/2} \tag{D-1}$$

where c is the radius of contact.

Since the radius of contact is generally much smaller than the radius of curvature, the compliance can be determined from

$$C_p = \frac{2c^2}{R} = \frac{2}{3\pi} \left[\frac{F}{YR} \right] \tag{D-2}$$

From elastic theory one can immediately write that

$$C_e = 1.23 \left[\frac{F^2}{E^2} \frac{2}{R} \right]^{1/3} \tag{D-3}$$

The ratio of the elastic to plastic compliance is

$$\frac{C_e}{C_p} = 1.55 \frac{Y}{E^{2/3}} \frac{R^{2/3}}{F^{1/3}} \qquad \text{(D-4)}$$

For surfaces which we shall consider, the radius of curvature R can be related to the pitch L and the flatness deviation d by using the following relationship:

$$R \doteq \frac{L^2}{8d} \qquad \text{(D-5)}$$

$$\frac{C_e}{C_p} = 1.93 \frac{Y}{E^{2/3}} \frac{L^{4/3}}{d^{2/3}} \frac{1}{F^{1/3}} \qquad \text{(D-6)}$$

For a stainless steel surface having a pitch of $\frac{1}{4}$-inch and a flatness deviation of 500×10^{-6} inches, the ratio reduces to

$$\frac{C_e}{C_p} = \frac{60.1}{F^{1/2}} \qquad \text{(D-7)}$$

For a load of 100 pounds per contact, the ratio is 13.2, and this is the load that is often encountered when surfaces are brought together under load.

Appendix E

CRITERIA FOR PLASTIC YIELDING OF THE SUBSTRATUM

Cylindrical Waviness

From elastic theory the half width of contact for cylinders which are of the same material, having equal radii and $\nu = 0.3$

$$c_2 = 1.08 \left[\frac{WR}{E} \right]^{1/2} \qquad \text{(E-1)}$$

The maximum shear stress which can be sustained in the substratum before plastic yielding occurs is

$$s_{max} = 0.126 \left[\frac{2WE}{R} \right]^{1/2} \qquad \text{(E-2)}$$

Solving Equations (E-1) and (E-2) and using the approximation $R \doteq L^2/8d$, one can write

$$\epsilon_2 = 1.23m \left[\frac{L}{d} \frac{s_{max}}{E} \right]^{1/2} \qquad \text{(E-3)}$$

where $m^2 = \ell/L$ as defined in the report. The substratum of the wavy cylindrical component will yield plastically when ϵ_2 exceeds the value determined by (E-3).

Spherical Waviness

The radius of contact for two identical spherical caps composed of the same material is

$$c_2 = 1.11\left[\frac{P}{E}\ \frac{R}{2}\right]^{1/3} \qquad \text{(E-4)}$$

and the maximum shear stress which can be sustained by the substratum is given by

$$s_{max} = 0.12\left[PE^2\ \frac{4}{R^2}\right]^{1/3} \qquad \text{(E-5)}$$

solving Equation (E-4) and (E-5) with $R \doteq L^2/8d$

$$\epsilon_2 = 1.16\ \frac{L}{d}\ \frac{s_{max}}{E} \qquad \text{(E-6)}$$

(E-6) gives the value of ϵ_2 which must be exceeded before substratum yielding is important.

It should be noted that the dimensionless number ϵ_2 which is the criterion for whether plastic yielding of the substratum is significant, depends upon the surface geometry and the material properties, but does not depend upon the applied load.

Nominally Flat Rough Surfaces in Contact

The criterion for plastic yielding of the substratum of nominally flat rough surfaces can be determined from

$$\epsilon_1 = 5.40 \frac{s_{max}}{E} \sqrt{n} \frac{j\sigma}{(\tan\theta)^2} \left(1 - \frac{c}{Y_o}\right) \qquad \text{(E-7)}$$

This equation is the result of solving Equations (E-4) and (E-5) with the radius of curvature approximated by

$$R \doteq \frac{j\sigma}{2(\tan\theta)^2} \left(1 - \frac{c}{Y_o}\right) \qquad \text{(E-8)}$$

where σ is r.m.s. of the roughness, $\tan\theta$ is the slope of the asperity, $Y_o = j\sigma$ is the separation at zero load and c is the compliance.

Just as for the other two cases the criterion is based upon the surface geometry and the material properties, but independent of the applied load.

Table 1

Aluminum Specimens A 3 L = 0.25"

d = 1250 μ in σ = 60 μ in r.m.s.

A 4 L = 0.25"

d = 1300 μ in σ = 57 μ in r.m.s.

Date	Time	P_a	Temp	h/k	Load Unloading
9/16/65	7:45 am	246	513	13.85	L
9/16/65	9:50 am	703	475	20.51	L
9/16/65	11:15 am	2200	478	46.7	L
9/16/65	12:40 pm	3600	476	76	L
9/16/65	2:30 pm	5900	448	108.5	L
9/16/65	3:40 pm	3600	468	104	U
9/16/65	5:30 pm	703	506	53.5	U
9/16/65	12:00 pm	246	492	22.4	U

Table 2

Stainless Steel Specimens S 3 L = 0.25"

d = 1000 μ in σ = 42.5 μ in r.m.s.

S 4 L = 0.25"

d = 900 μ in σ = 45.0 μ in r.m.s.

Date	Time	P_a	Temp	h/k	Loading Unloading
9/20/65	11:30 am	246	541	10.8	L
9/20/65	12:50 pm	940	519	16.4	L
9/20/65	1:45	2050	512	33.4	L
9/20/65	2:25	4400	498	62.4	L

Table 3

Magnesium Specimens M 3 L = 0.25"

d = 2000 μ in σ = 55 μ in r.m.s.

M 4 L = 0.25"

d = 1800 μ in σ = 62 μ in r.m.s.

Date	Time	P_a	Temp	h/k	Loading Unloading
9/17/65	5:30 pm	246	500	12.0	L
9/17/65	7:30 pm	703	490	18.5	L
9/18/65	8:30 am	2200	500	50.0	L
9/18/65	10:30 am	3600	490	80.0	L
9/18/65	12:30 pm	2200	485	68.5	U
9/18/65	2:30 pm	703	490	40.0	U
9/18/65	4:30 pm	246	470	20.0	U

Table 4

Aluminum Specimens L = 1 in d = 20 μ in σ = 3-5 μ in r.m.s.

L = 1 in d = 40 μ in σ = 3-5 μ in r.m.s.

L = 1 in d = 120 μ in σ = 3-5 μ in r.m.s.

P_a	h	ϵ_2	h	ϵ_2	h	ϵ_2
100	200	.125	350	.185	750	.280
300	1000	.321	1600	.380	2300	.410
500	2100	.405	3000	.435	4000	.455
700	3400	.442	4500	.464	5900	.483
900	4750	.462	6000	.484	7700	.495

Table 5

Stainless Steel Specimens

L = 1 in d = 40 μ in σ = 3-5 μ in r.m.s.

L = 1 in d = 150 μ in σ = 3-5 μ in r.m.s.

P_a	h	ϵ_2	h	ϵ_2
100	85	.120	95	.134
300	325	.275	170	.200
500	700	.375	230	.230
700			300	.265
900			370	.294

Table 6

Magnesium Specimens L = 1 in d = 105 μ in σ = 3-5 μ in r.m.s.

L = 1 in d = 260 μ in σ = 3-5 μ in r.m.s.

P_a	h	ϵ_2	h	ϵ_2
100	2100	.310	900	.20
300	6800	.434	2200	.316
500	9400	.458	4600	.400
700			8300	.445

Table 7

Brass Specimens L = 1 in d = 780 μ in σ = 3-5 μ in r.m.s.

L = 1 in d = 950 μ in σ = 3-5 μ in r.m.s.

P_a	h	ϵ_2	h	ϵ_2
100	360	.076	250	.055
300	590	.130	405	.110
500	790	.144	500	.135
700	1000	.173	650	.150

Table 8

Material	Temp (^{o}F)	E(psi)	k(BTU/hr-ft^{2}-^{o}F)	Y(psi)
Stainless Steel (303)	100	29×10^{6}	9.0	120,000
	300	27.6×10^{6}	9.8	
	500	26.5×10^{6}	10.6	
Leaded Brass	100	14.2×10^{6}	65.0	68,000
	300	13.0×10^{6}	71.0	
	500	12.5×10^{6}	80.0	
Aluminum (2024 T4)	100	10.5×10^{6}	72.5	66,000
	300	10.0×10^{6}	88.0	
	500	8.5×10^{6}	100.0	
Magnesium (AZ 31B)	100	6.5×10^{6}	46.0	28,000
	300	5.5×10^{6}	54.0	
	500	4.2×10^{6}	58.5	

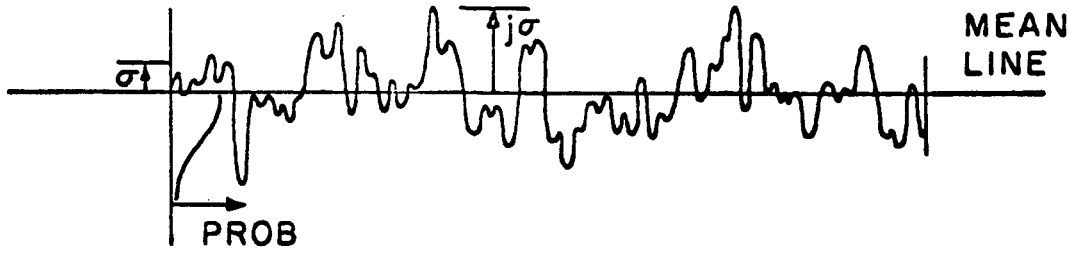

VERTICAL SCALE 5 mm = 59.6 μ in.

HORIZONTAL SCALE 5 mm = 0.00596 in.

FIGURE 1a. TYPICAL SURFACE PROFILE

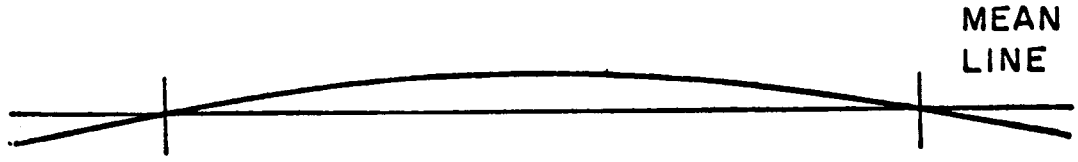

VERTICAL SCALE 5 mm = 59.6 μ in.

HORIZONTAL SCALE 5 mm = 59.6 μ in.

FIGURE 1b. TYPICAL ASPERITY

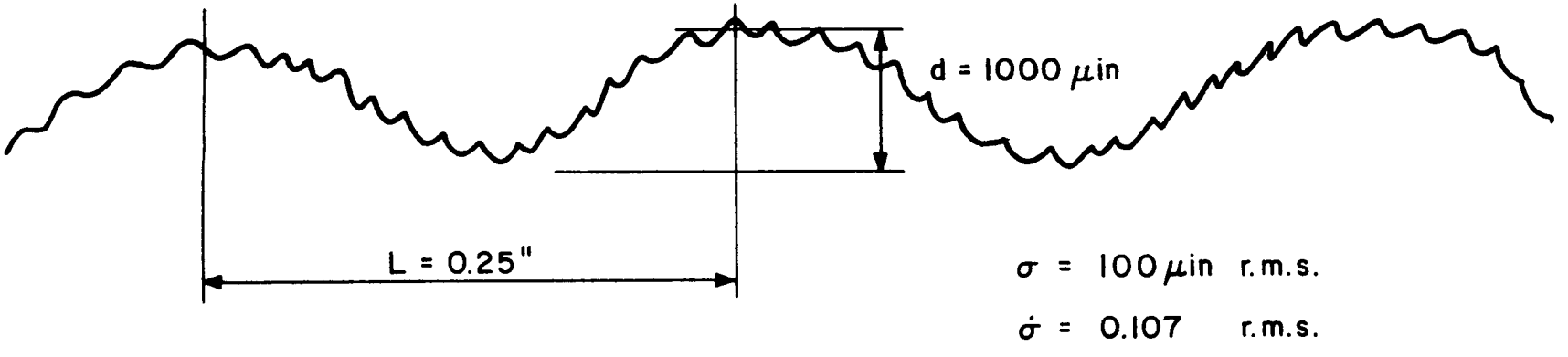

FIGURE 2 WAVY-ROUGH SURFACE PROFILE

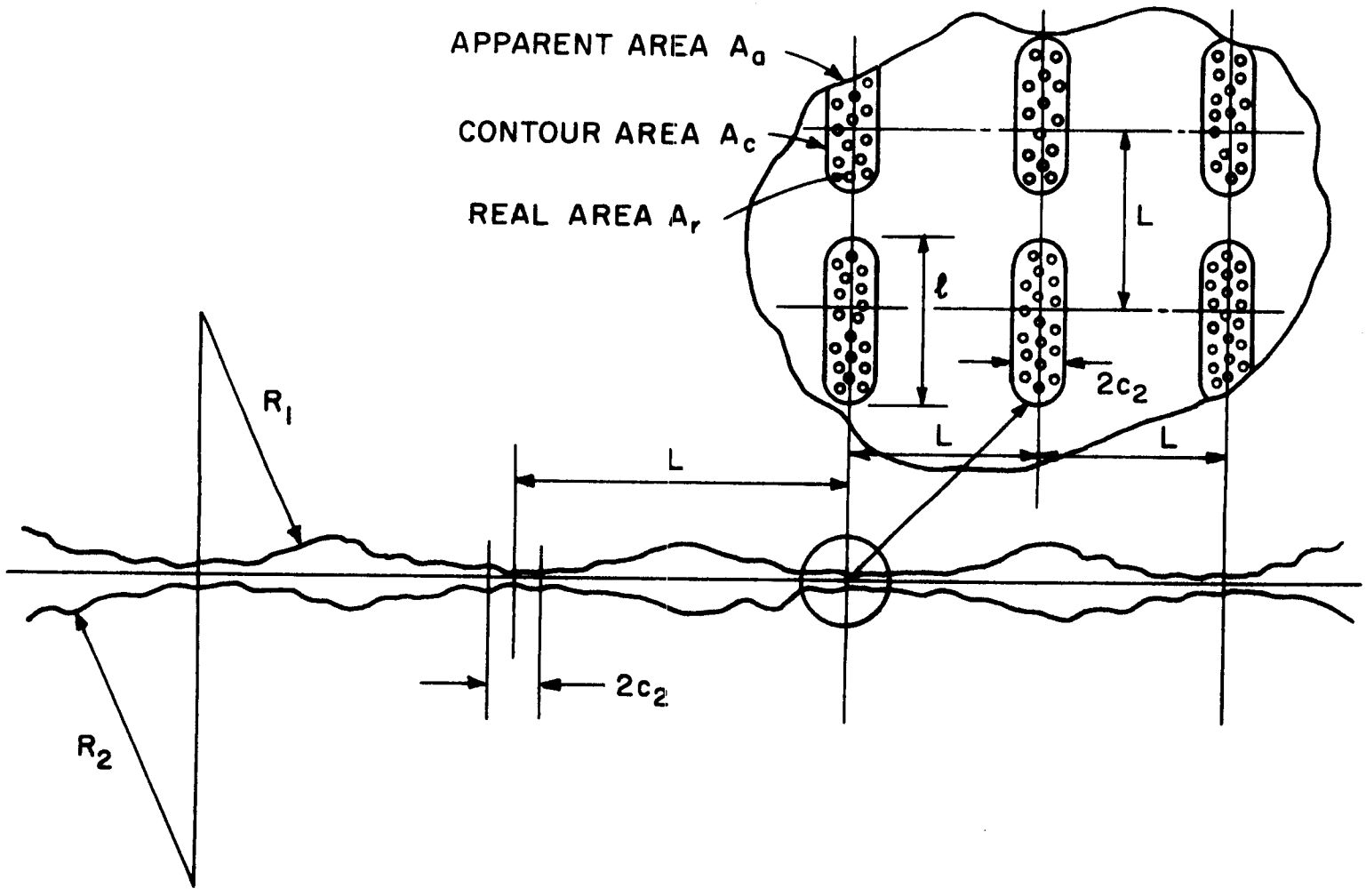

FIGURE 3. CYLINDRICAL CONTACT MODEL

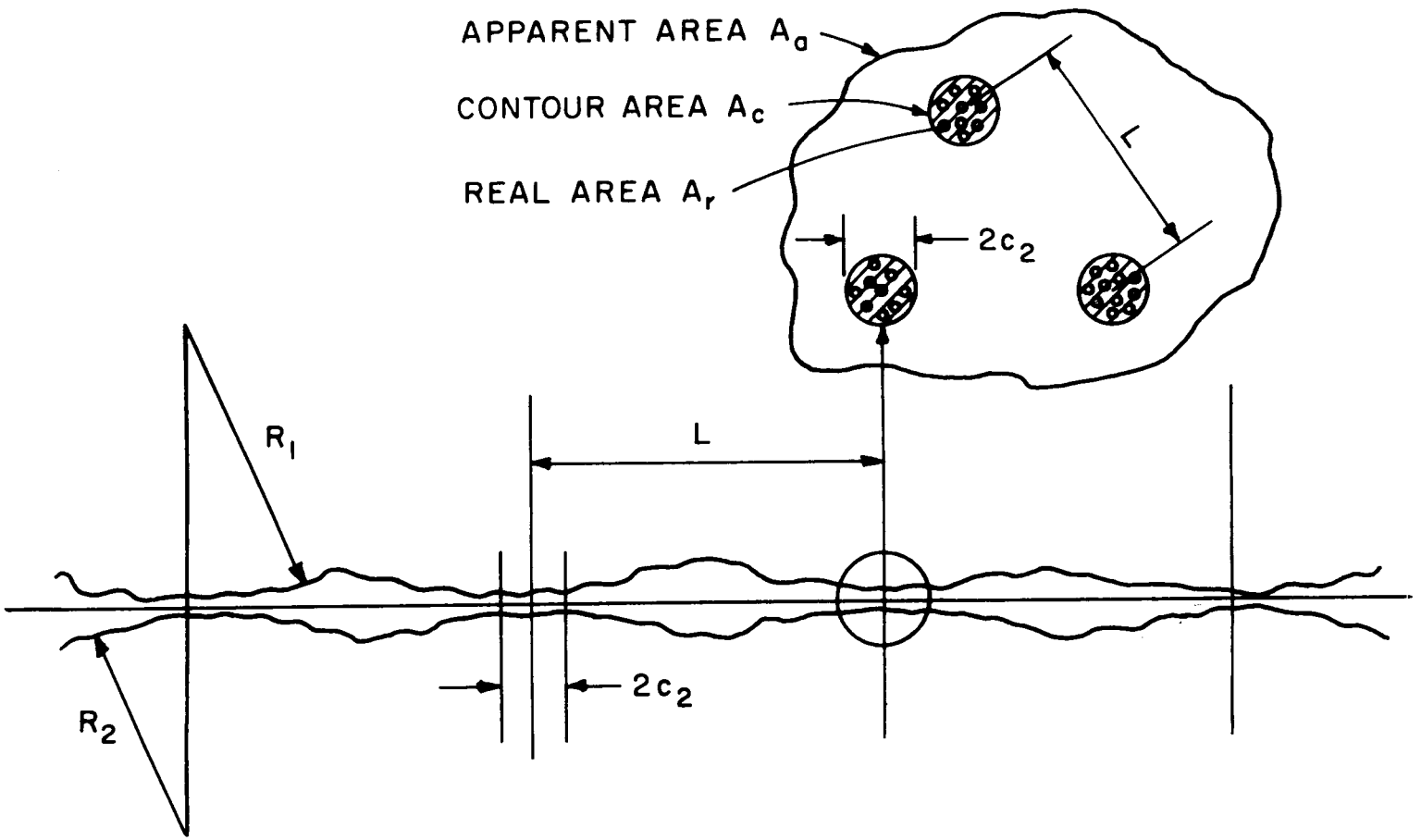

FIGURE 4. SPHERICAL CONTACT MODEL

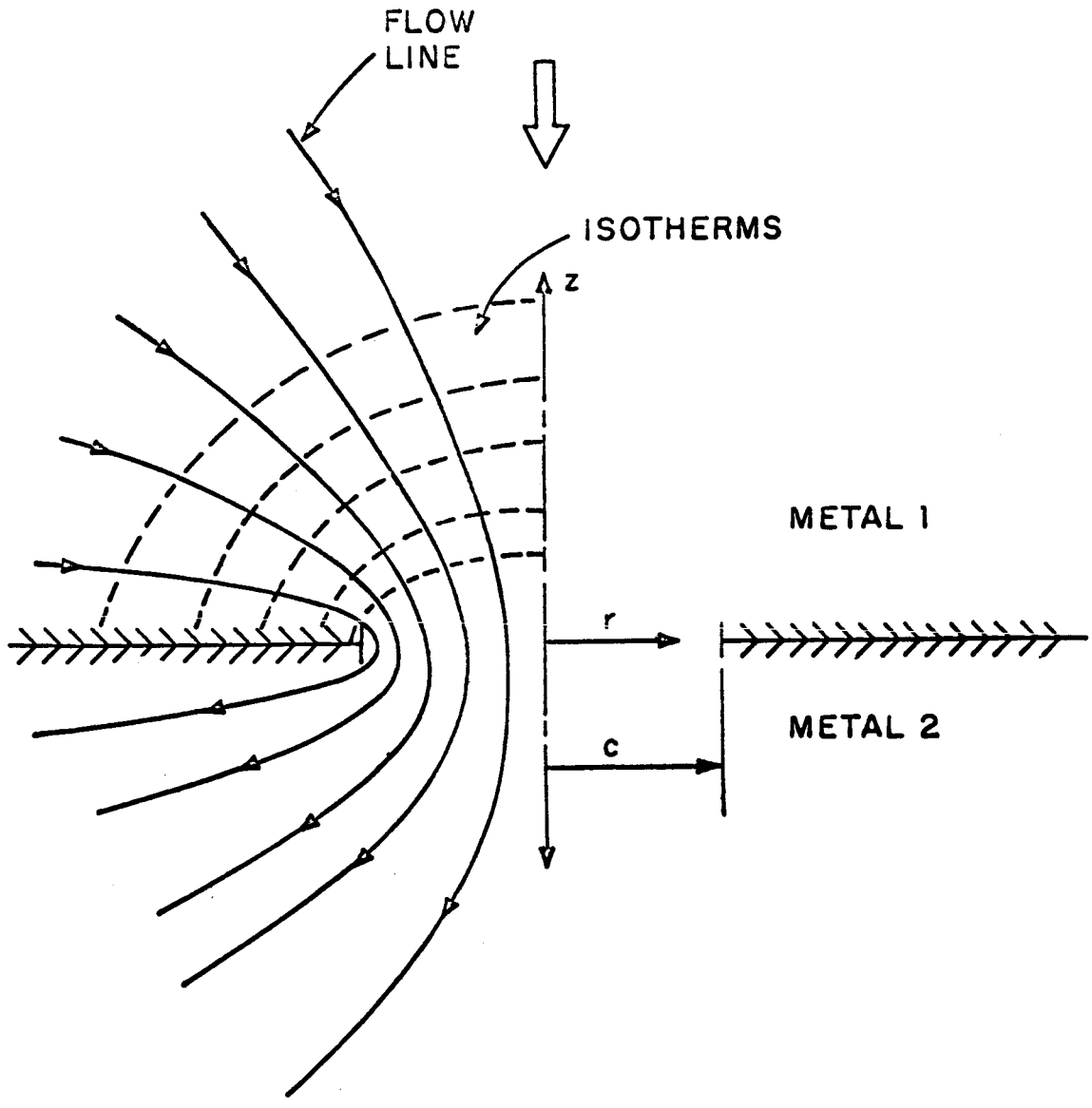

FIGURE 5. CONTACT MODEL FOR LIGHT APPARENT PRESSURE

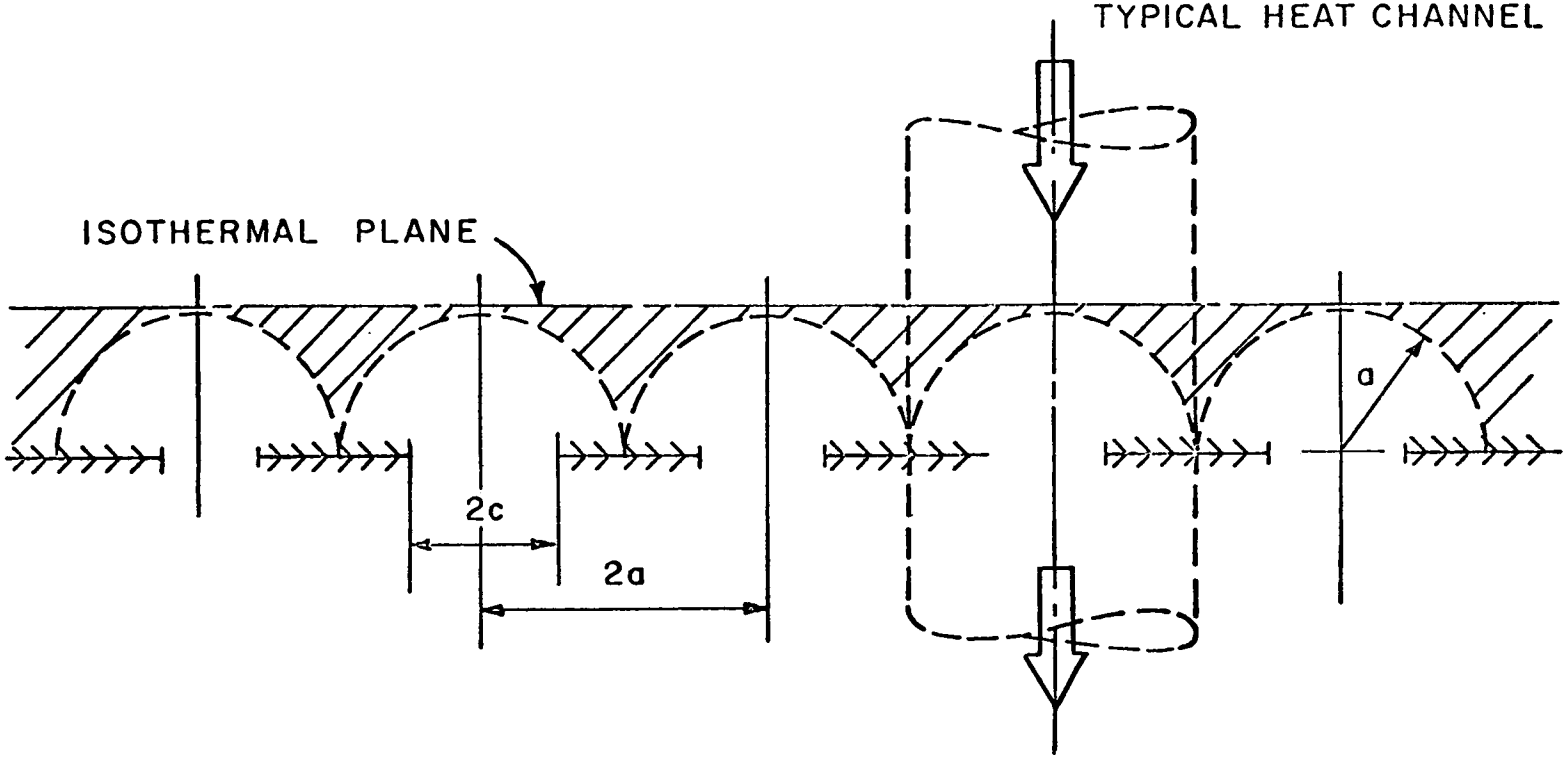

FIGURE 6. CONTACT MODEL FOR MULTIPLE CONTACTS

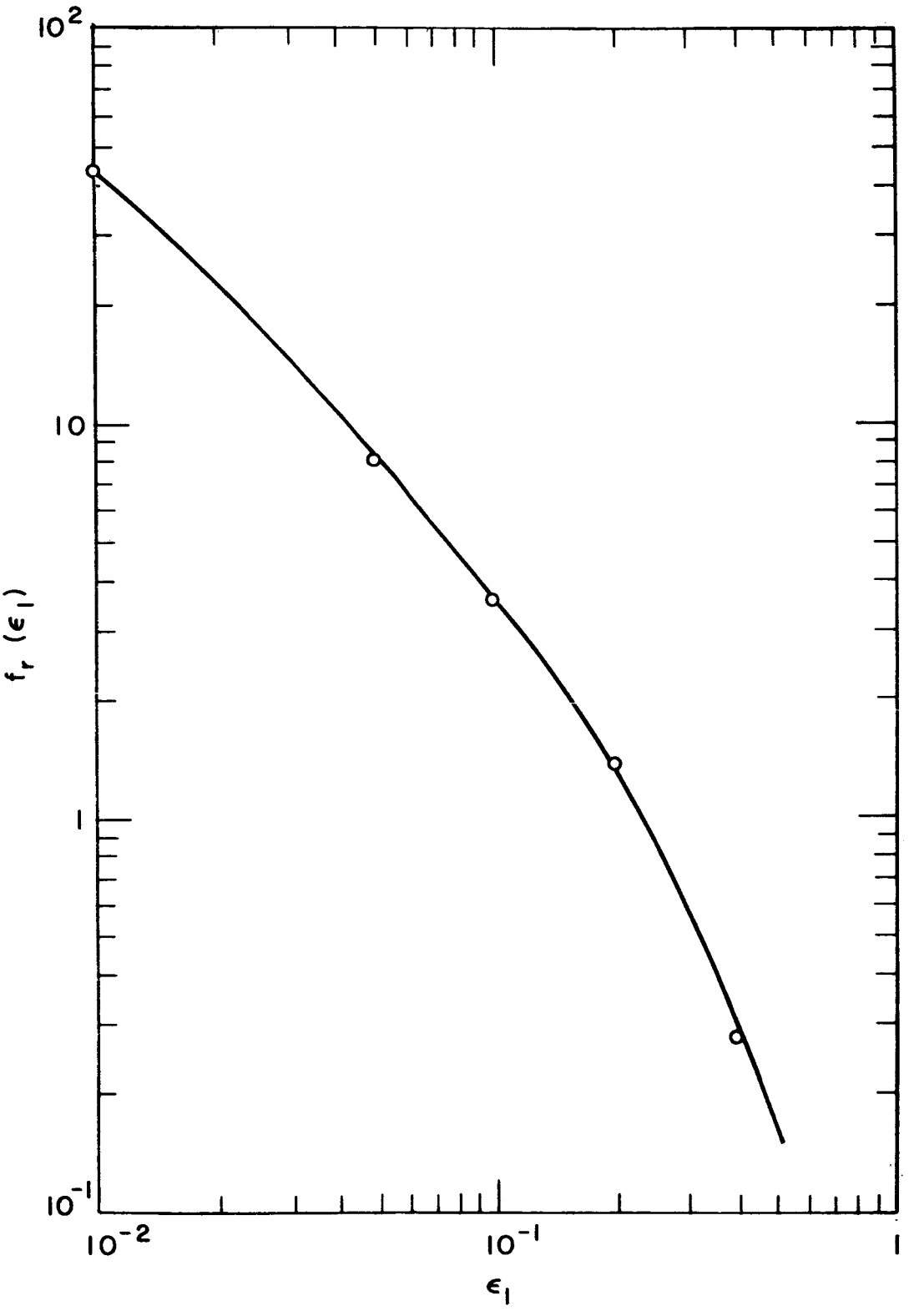

FIGURE 7. CONTACT CONDUCTANCE FACTOR FOR NOMINALLY FLAT ROUGH SURFACE VERSUS THE AREA RATIO

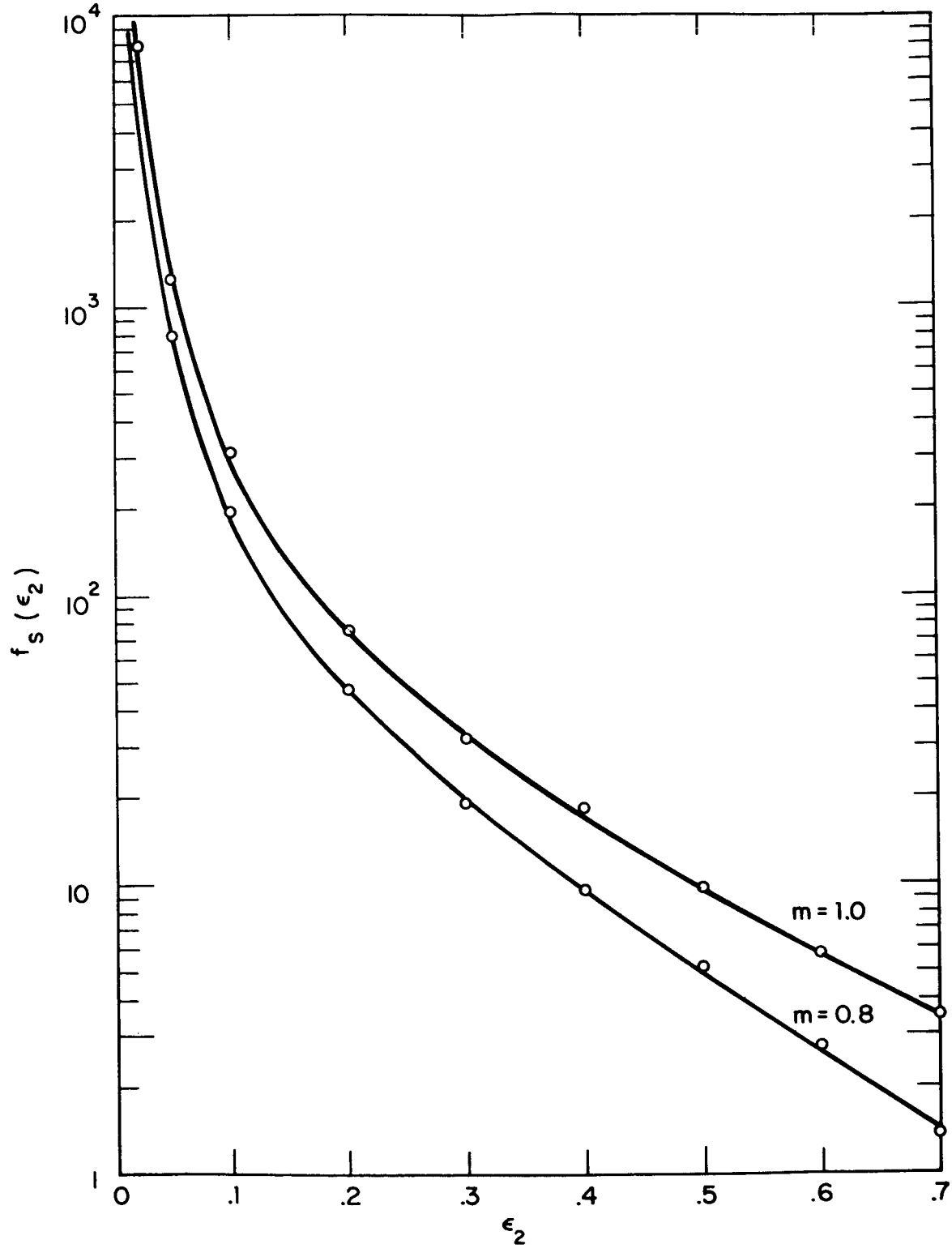

FIGURE 8. CONTACT CONDUCTANCE FACTOR FOR CYLINDRICAL WAVINESS

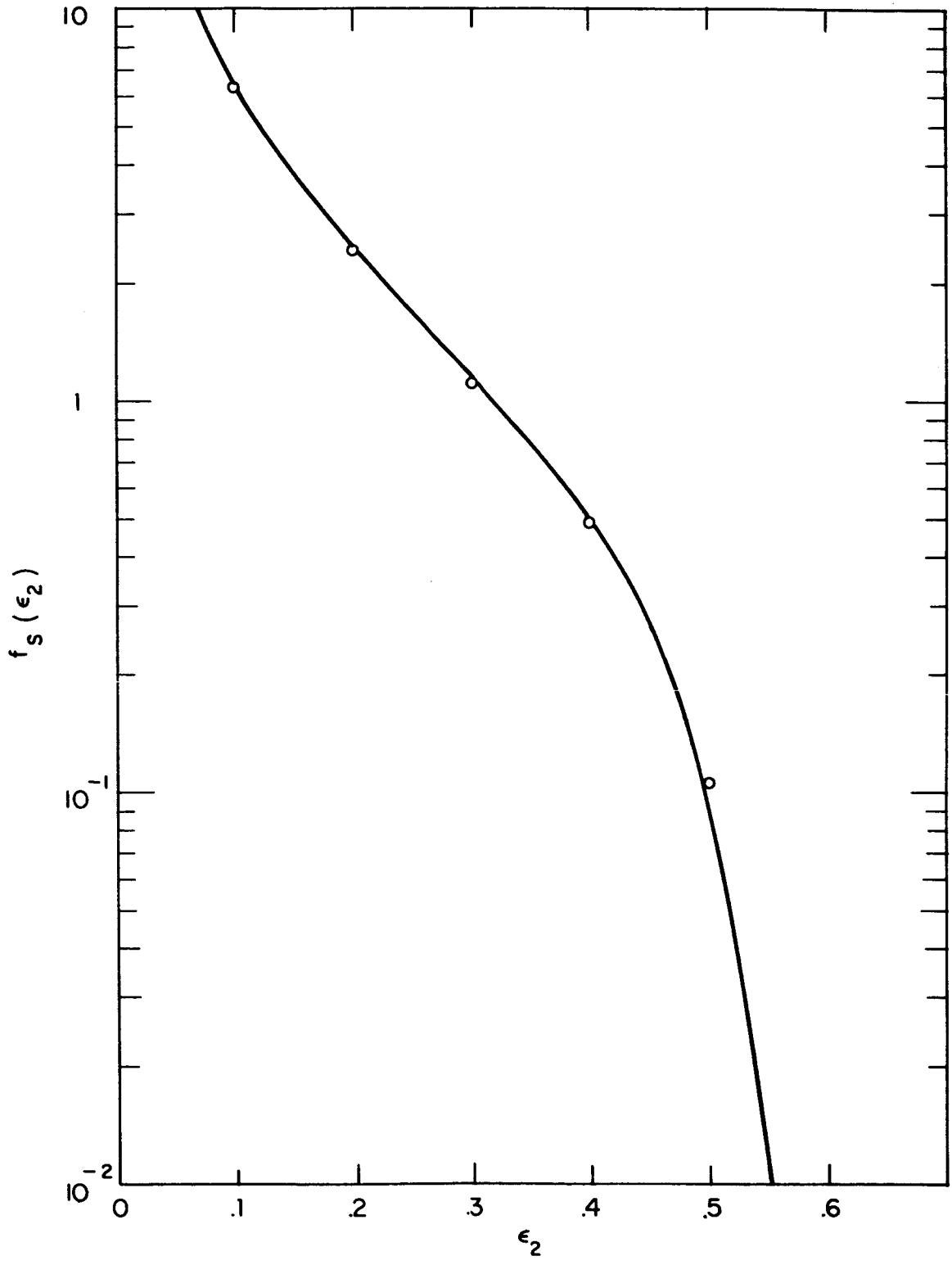

FIGURE 9. CONTACT CONDUCTANCE FACTOR FOR SPHERICAL WAVINESS

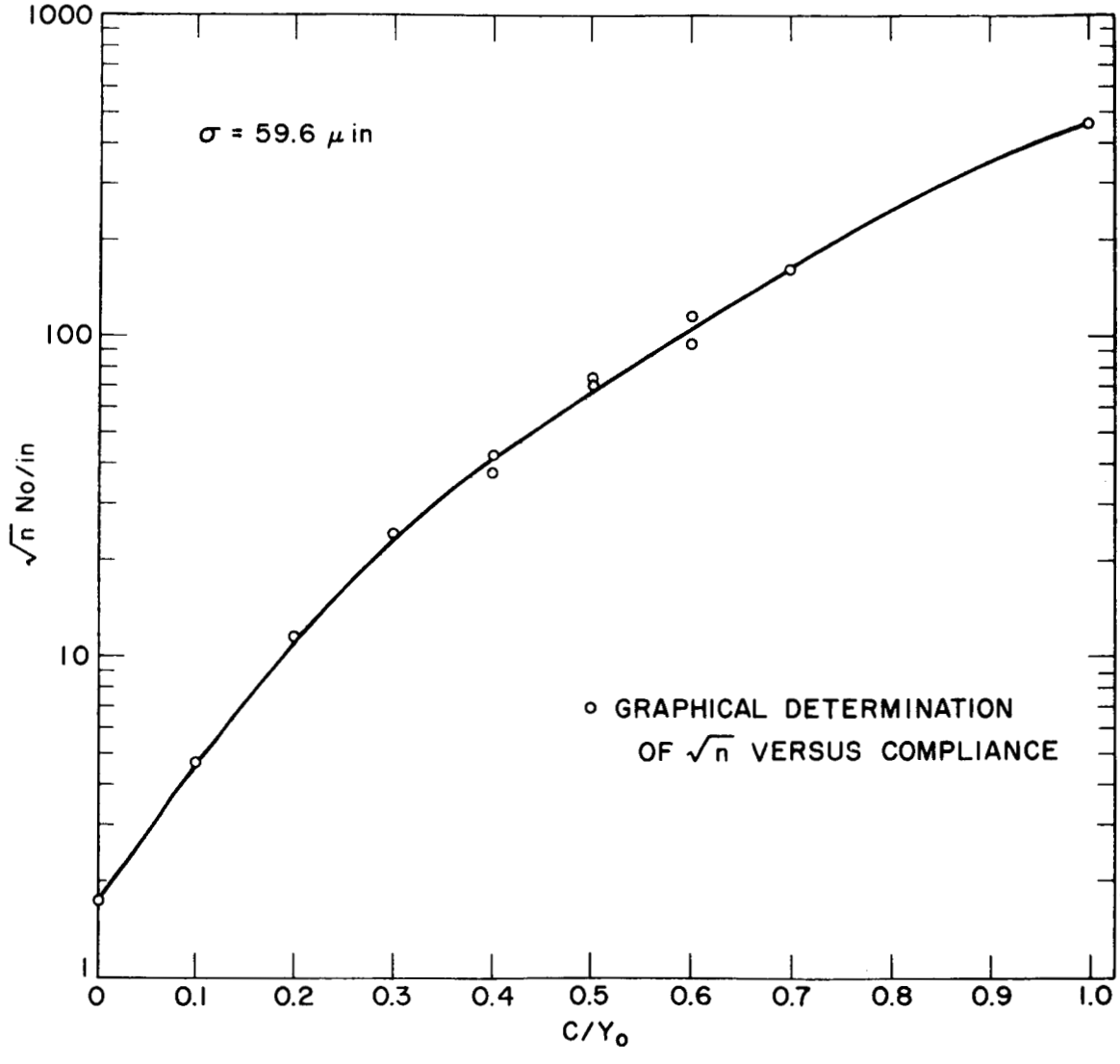

FIGURE 10. NUMBER OF CONTACT SPOTS VERSUS COMPLIANCE

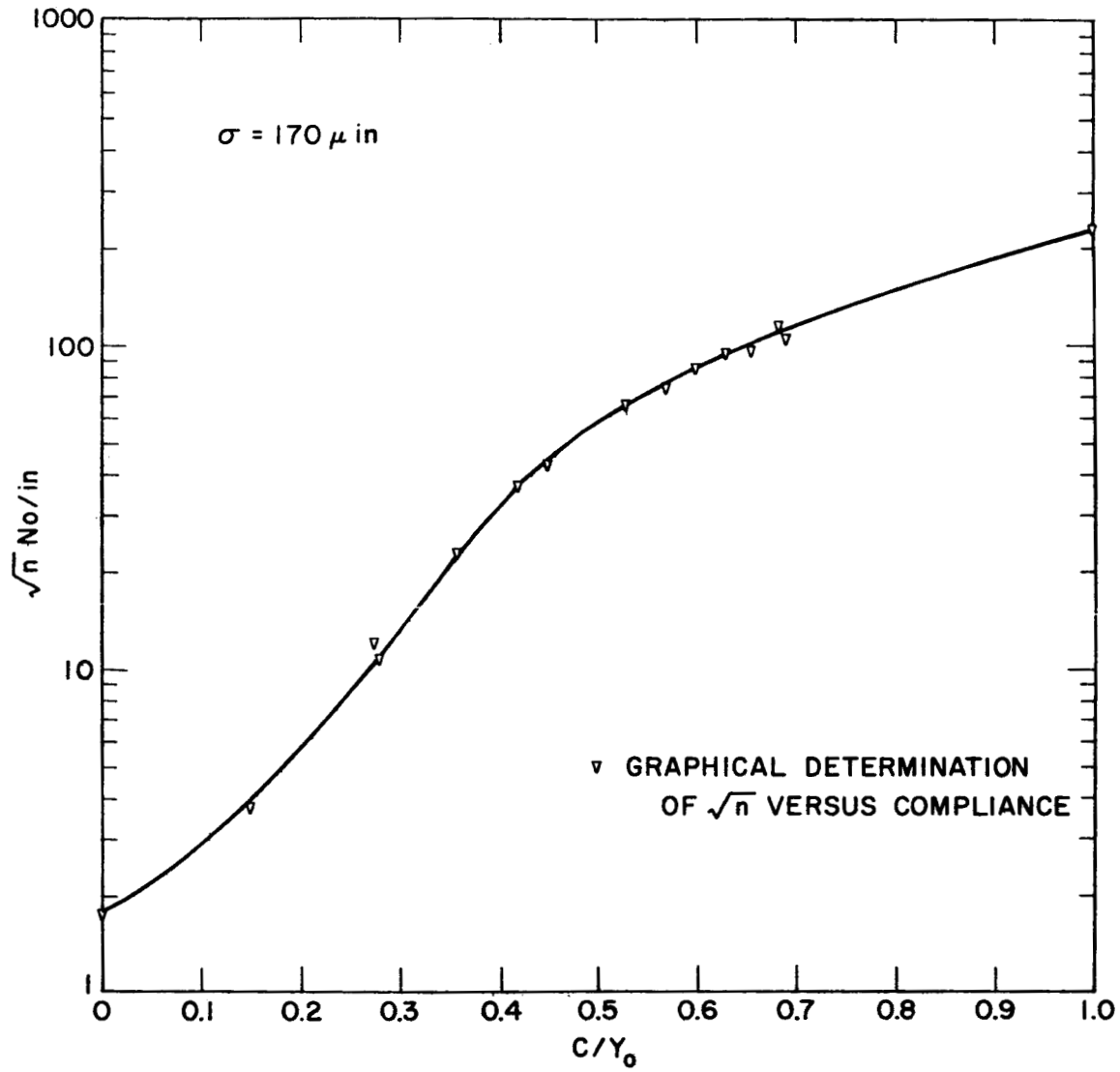

FIGURE 11. NUMBER OF CONTACT SPOTS VERSUS COMPLIANCE

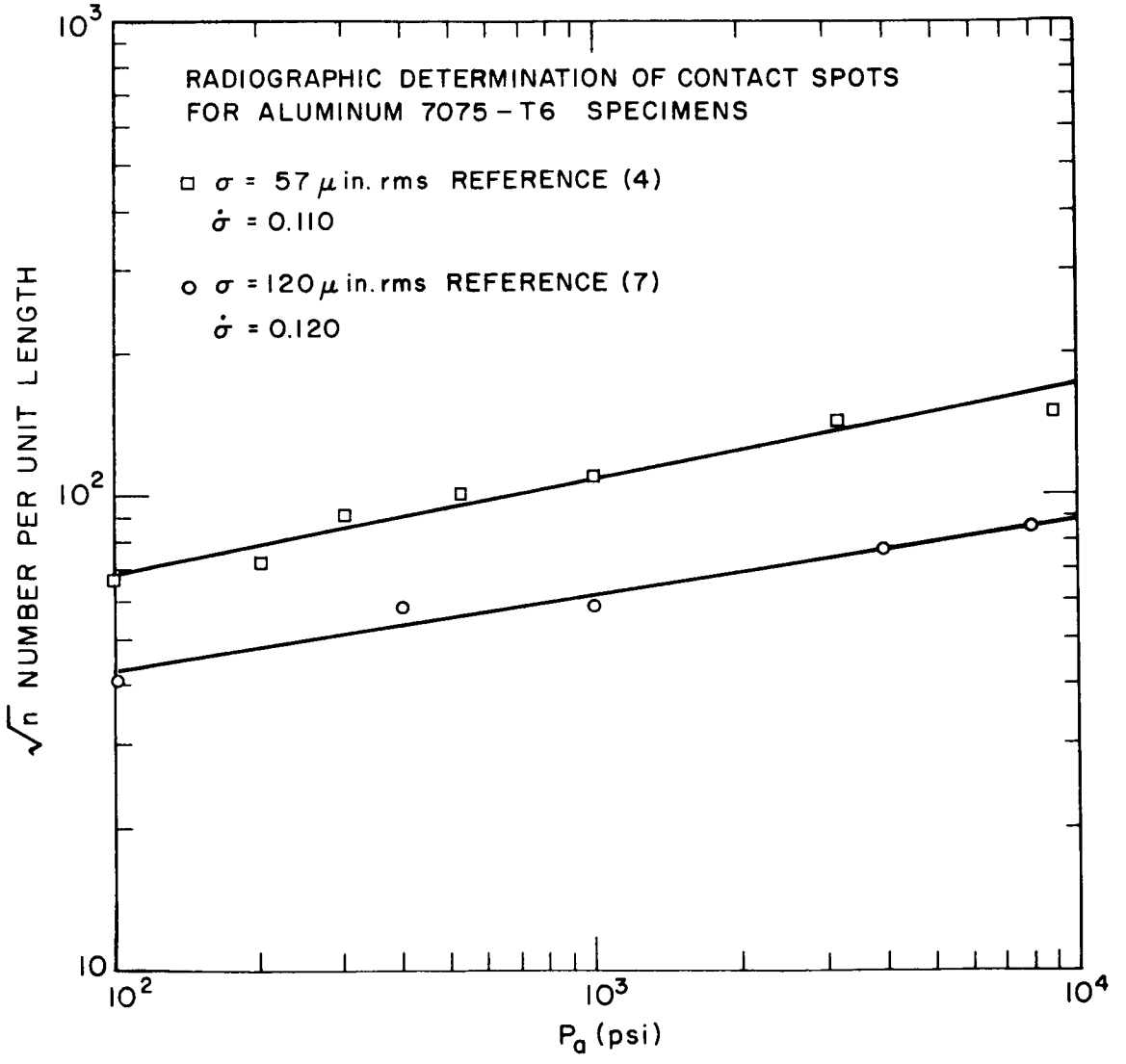

FIGURE 12. NUMBER OF CONTACT SPOTS VERSUS APPARENT PRESSURE

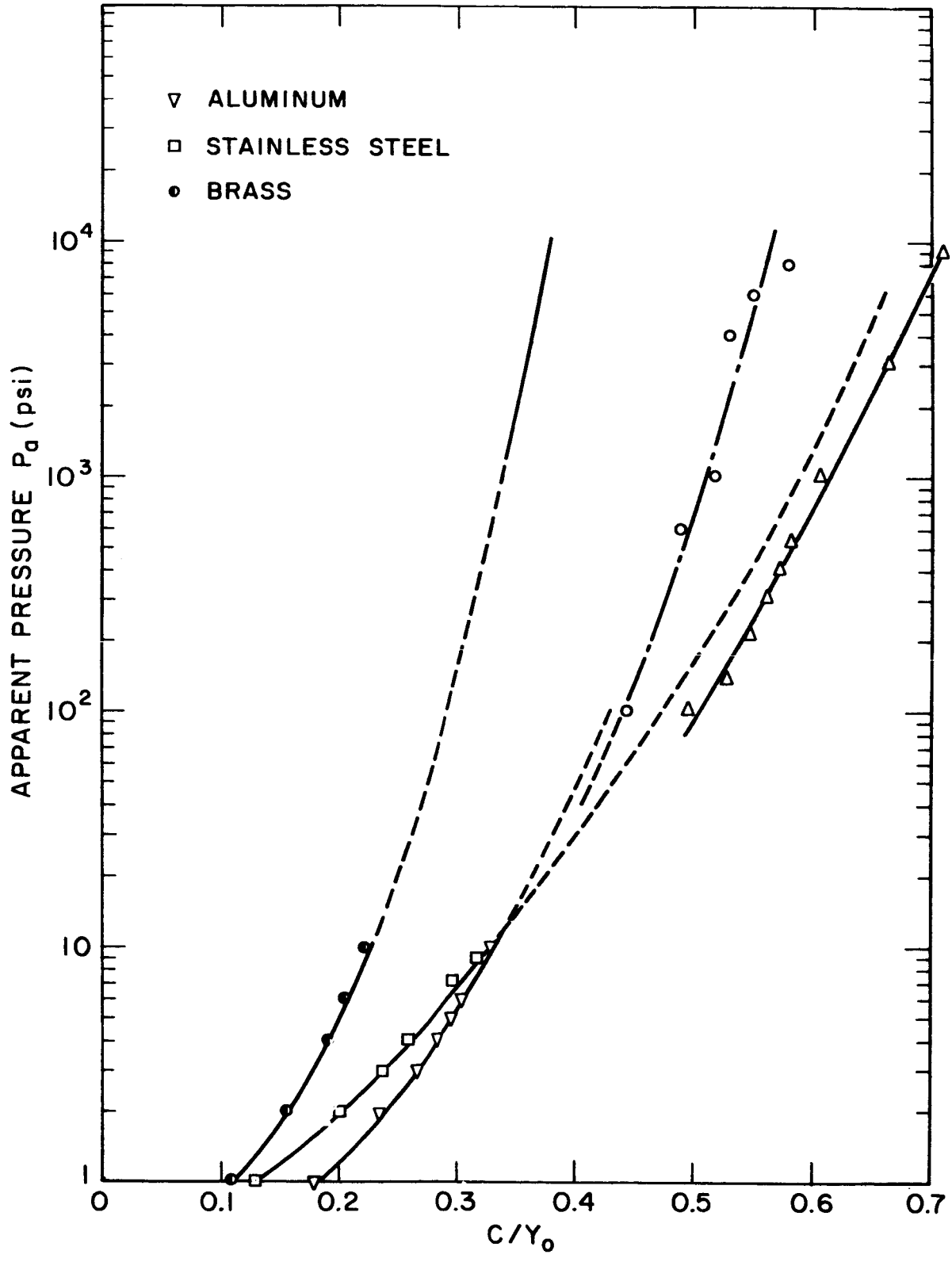

FIGURE 13. APPARENT PRESSURE VERSUS COMPLIANCE

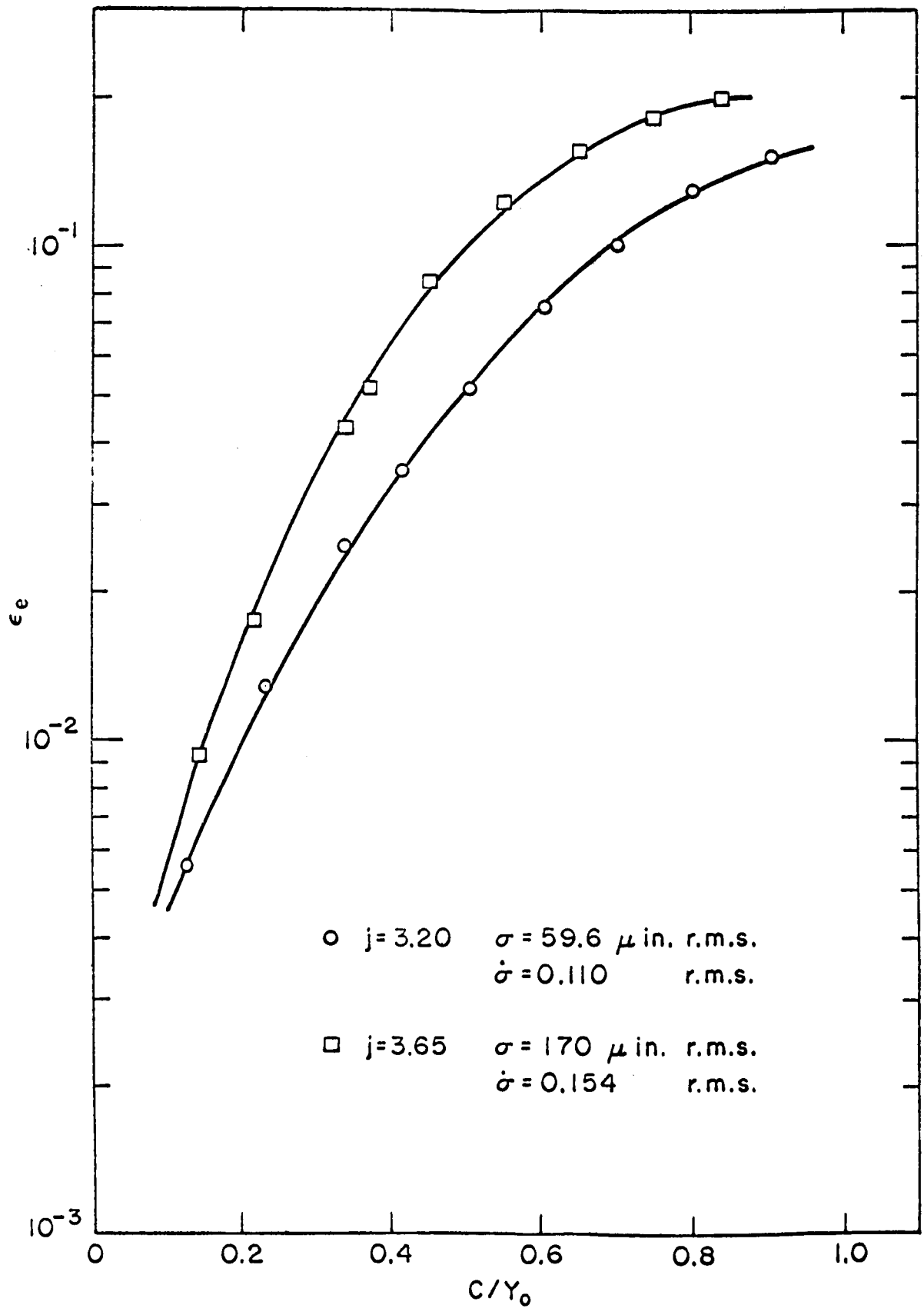

FIGURE 14. AREA RATIO VERSUS COMPLIANCE RATIO

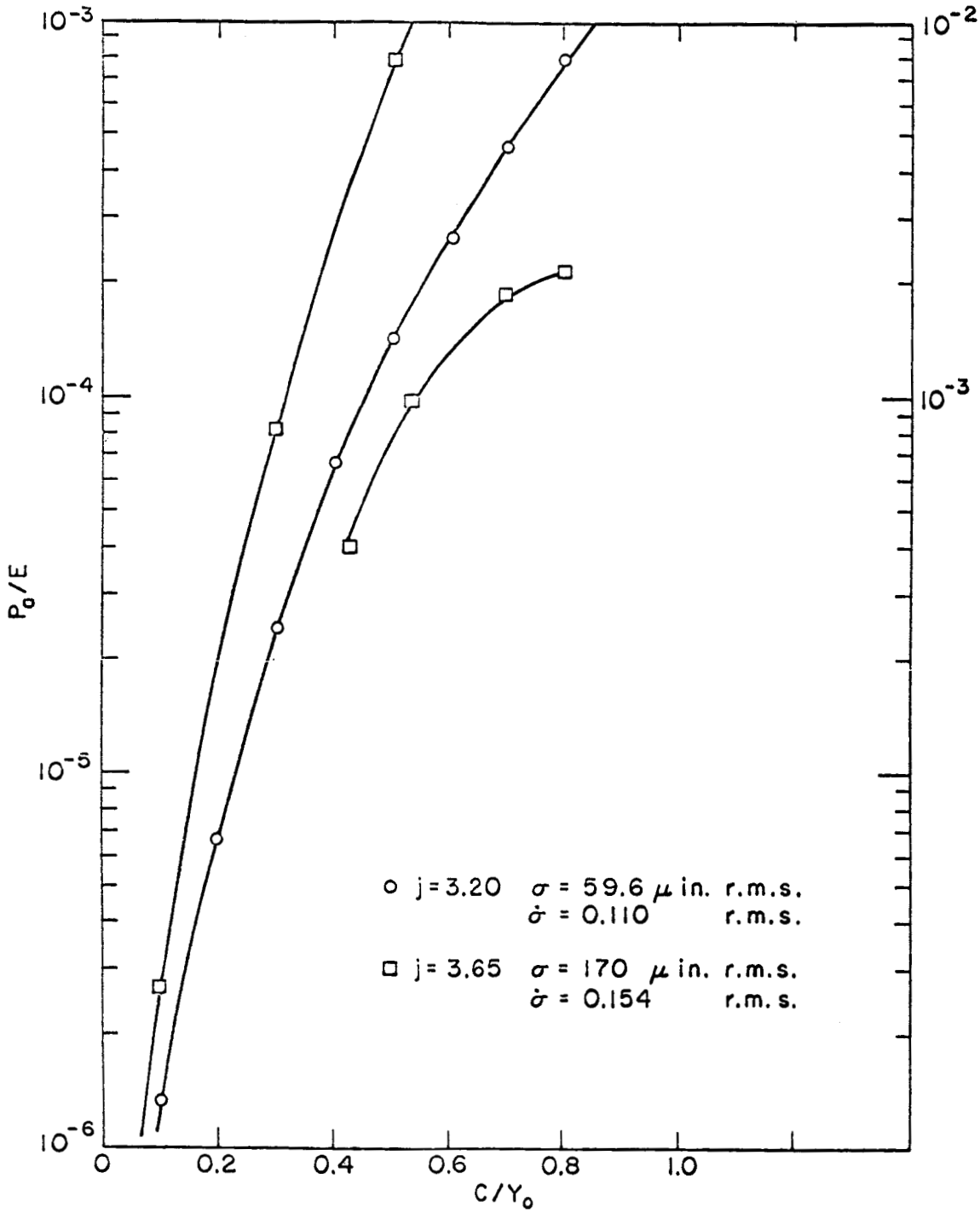

FIGURE 15. APPARENT PRESSURE VERSUS COMPLIANCE RATIO

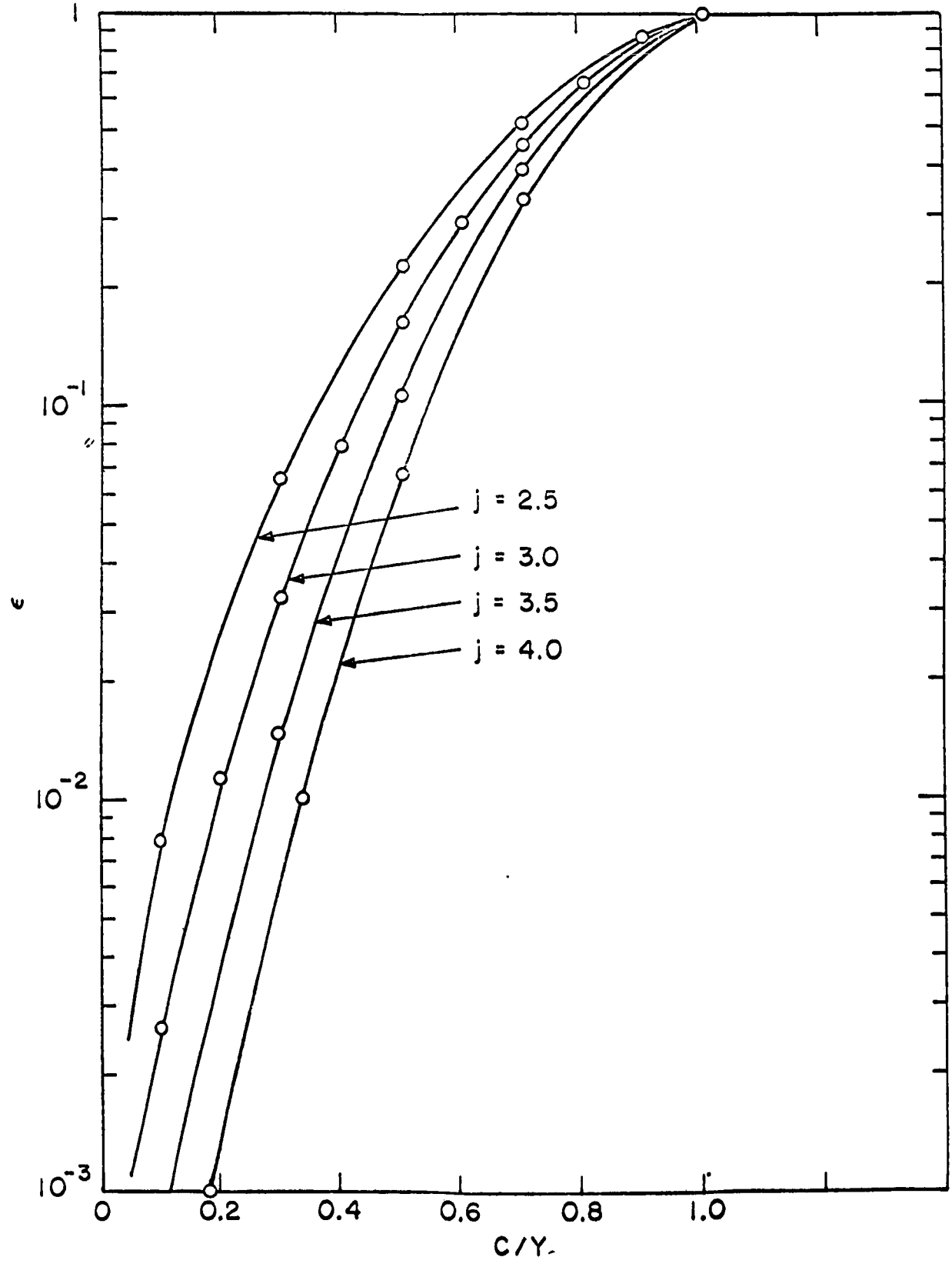

FIGURE 16. AREA RATIO VERSUS COMPLIANCE RATIO

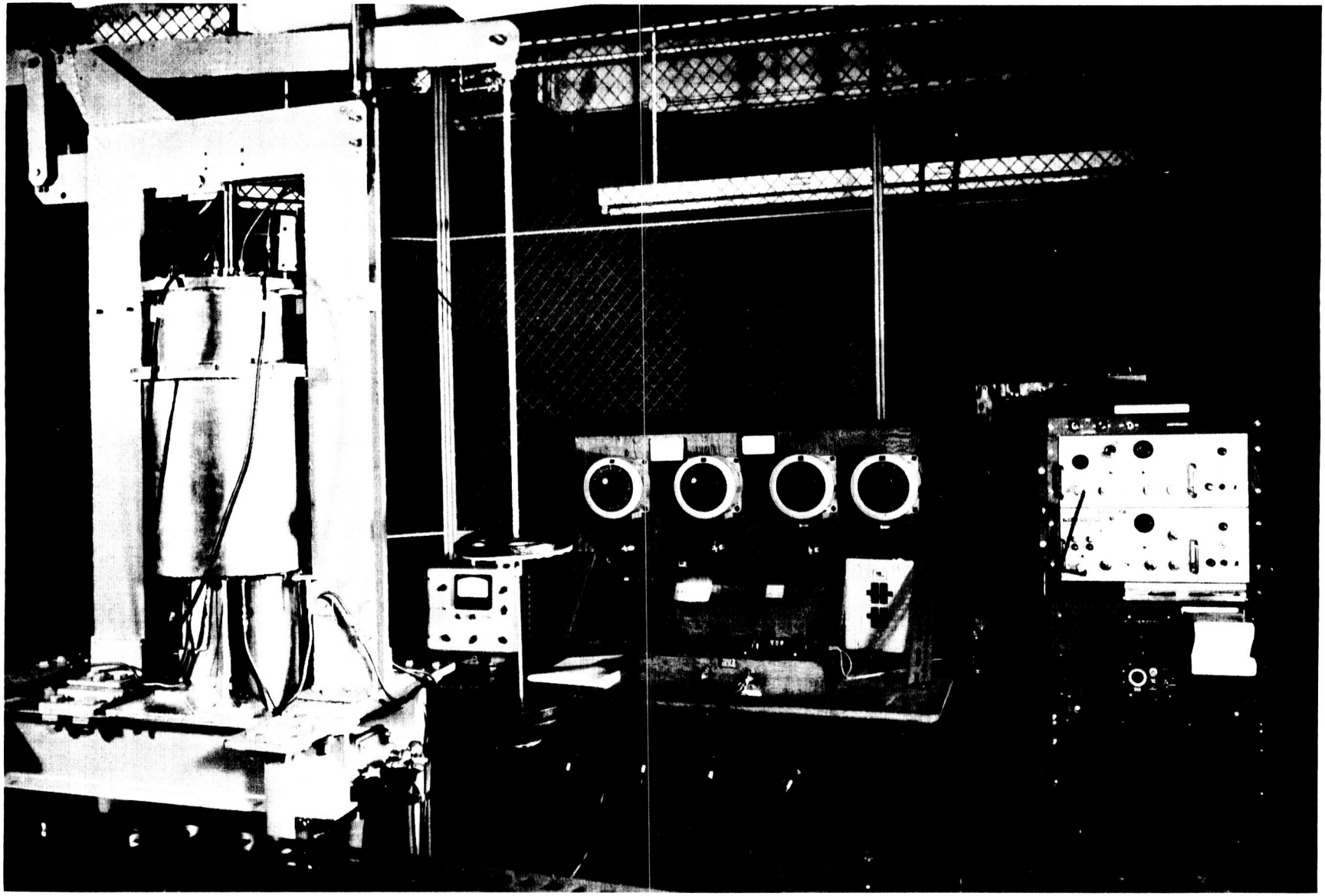

FIGURE 17: CONTACT RESISTANCE APPARATUS

PARTS LIST FOR FIGURE 18

Part No.	
1	Top Plate
2	Loading Mechanism
3	Bellows
4	Upper Main Cooler
5	Spacer of Optional Conductivity
6	Transite Spacer
7	Upper Main Heater
8	Upper Heat Meter
9	Upper Sample
10	Lower Sample
11	Guard Ring: Upper Guard Ring Cooler
12	Upper Guard Ring Heater
13	Lower Guard Ring Heater
14	Radiation Shield
15	Guard Ring: Lower Guard Ring Cooler
16	Lower Heat Meter
17	Lower Main Heater
18	Transite Spacer
19	Dynamometer - Aluminum Cylinder
20	Lower Main Cooler

Part No.	
21	Base Plate

Top Plate Mountings (Not Shown on Figure 18)

1	Adjustable Vacuum Leak
2	Upper Main Heater Power Feedthrough (2 Terminals)
3	Upper Guard Ring Heater Power Feedthrough (2 Terminals)
4	Upper Main Cooler Feedthrough (Inlet and Outlet)
5	Upper Guard Ring Cooler Feedthrough (Inlet and Outlet)
6	Thermocouple Feedthroughs (2 with 8 Thermocouples Each)

Base Plate Mountings (Not Shown on Figure 18)

1	Lower Main Heater Power Feedthrough (2 Terminals)
2	Lower Guard Ring Heater Power Feedthrough (2 Terminals)
3	Lower Main Feedthrough (Inlet and Outlet)
4	Lower Guard Ring Cooler Feedthrough (Inlet and Outlet)
5	Thermocouple Feedthrough (For Up to 8 Thermocouples)
6	Dynamometer Signal Feedthrough

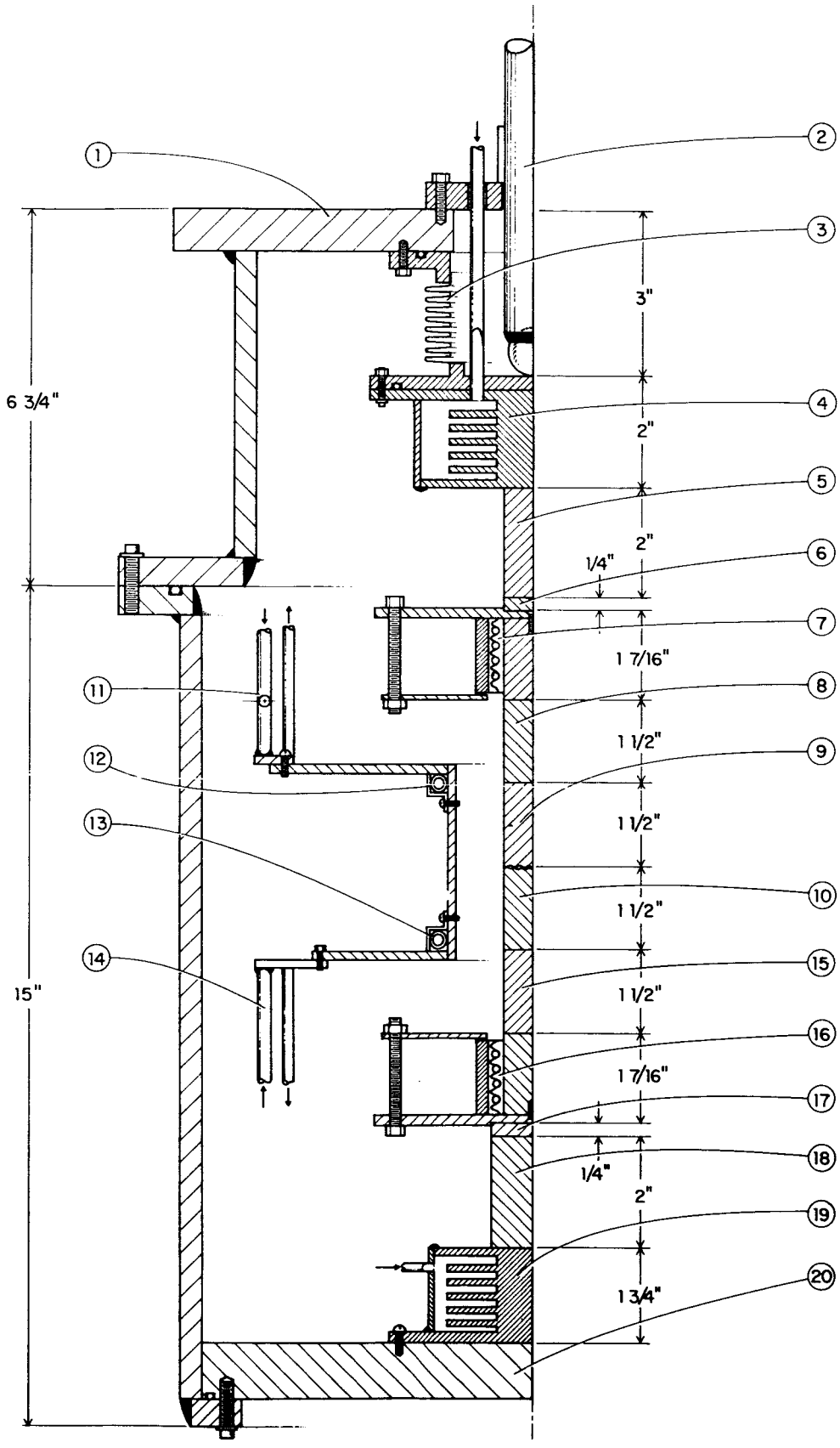

FIGURE 18. TEST SECTION AND CHAMBER

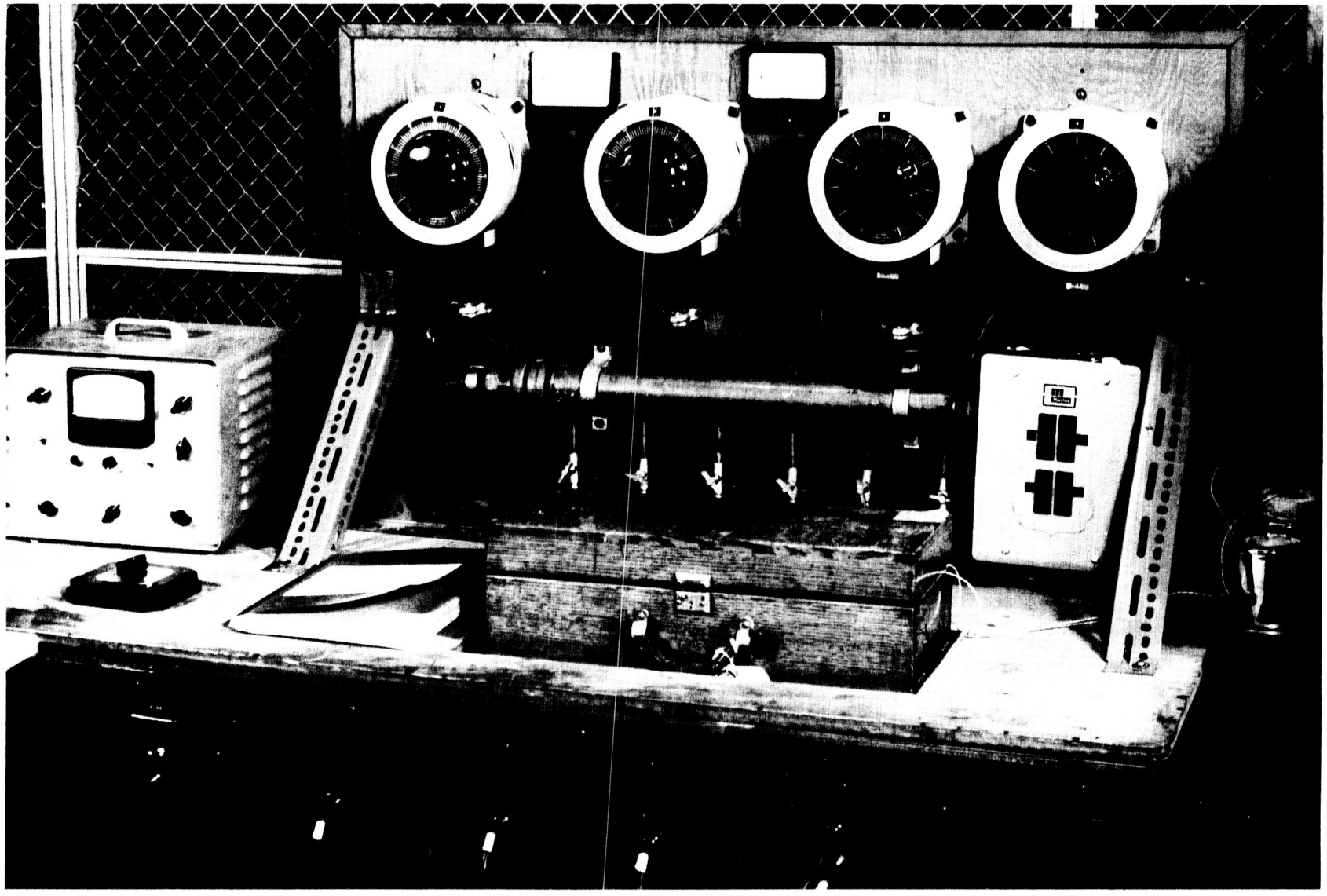

FIGURE 19. INSTRUMENT CONSOLE

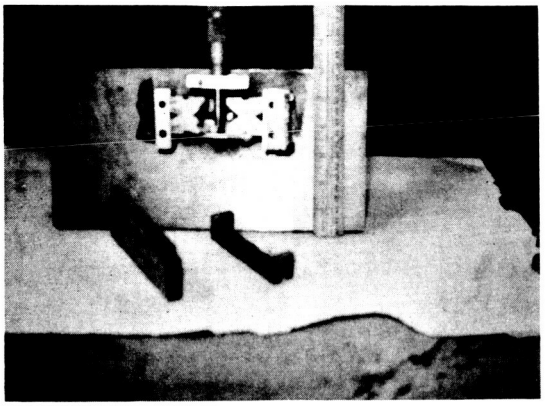

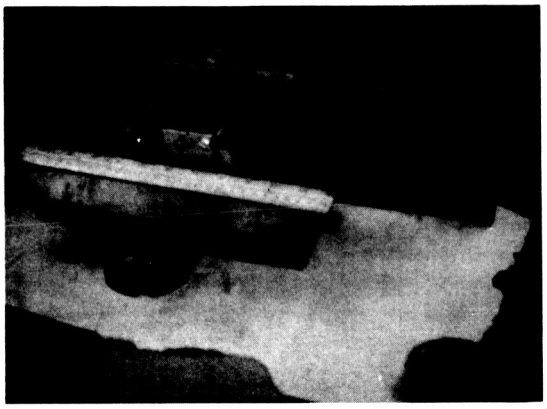

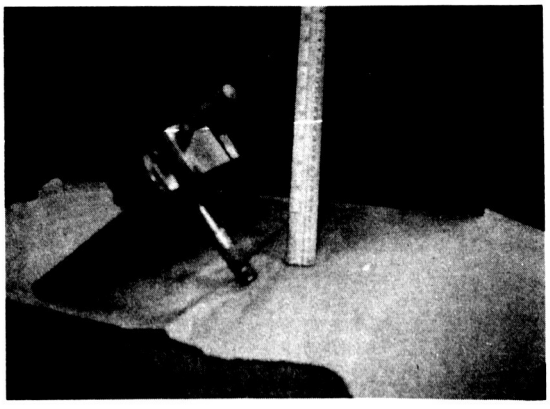

FIGURE 20. WAVINESS GENERATOR

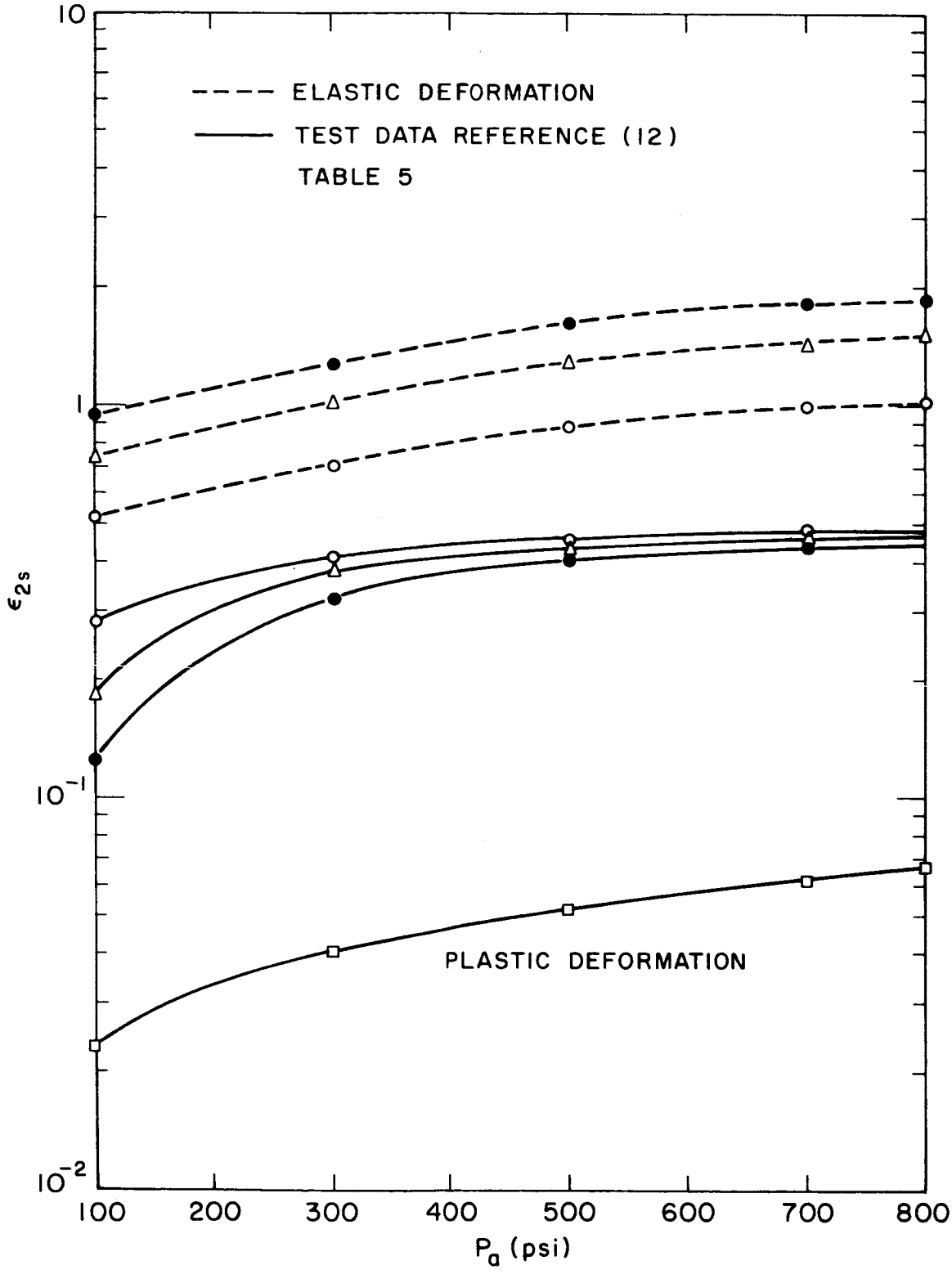

FIGURE 21. ϵ_{2s} VERSUS APPARENT PRESSURE ALUMINUM

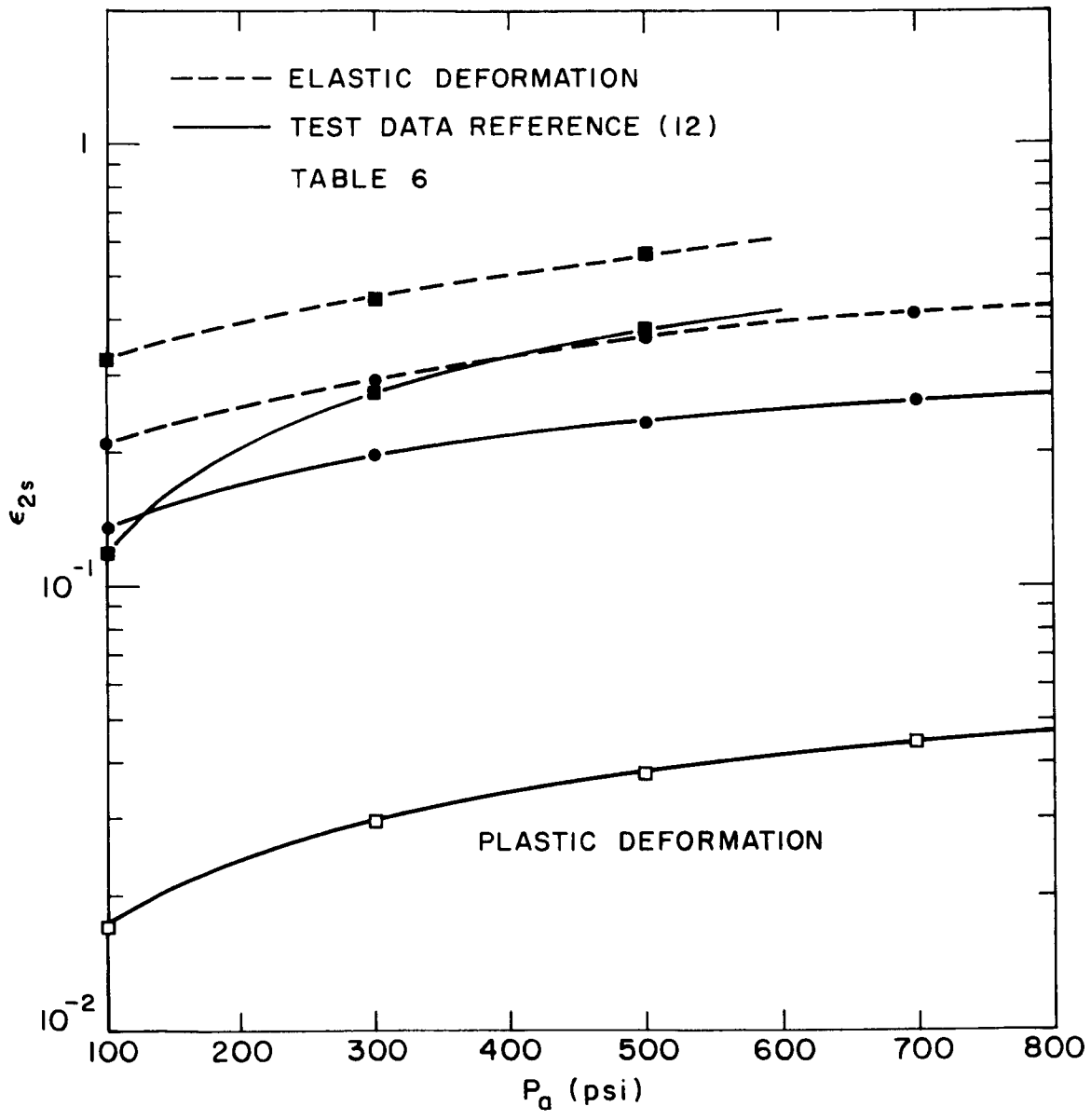

FIGURE 22. ϵ_{2s} VERSUS APPARENT PRESSURE STAINLESS STEEL

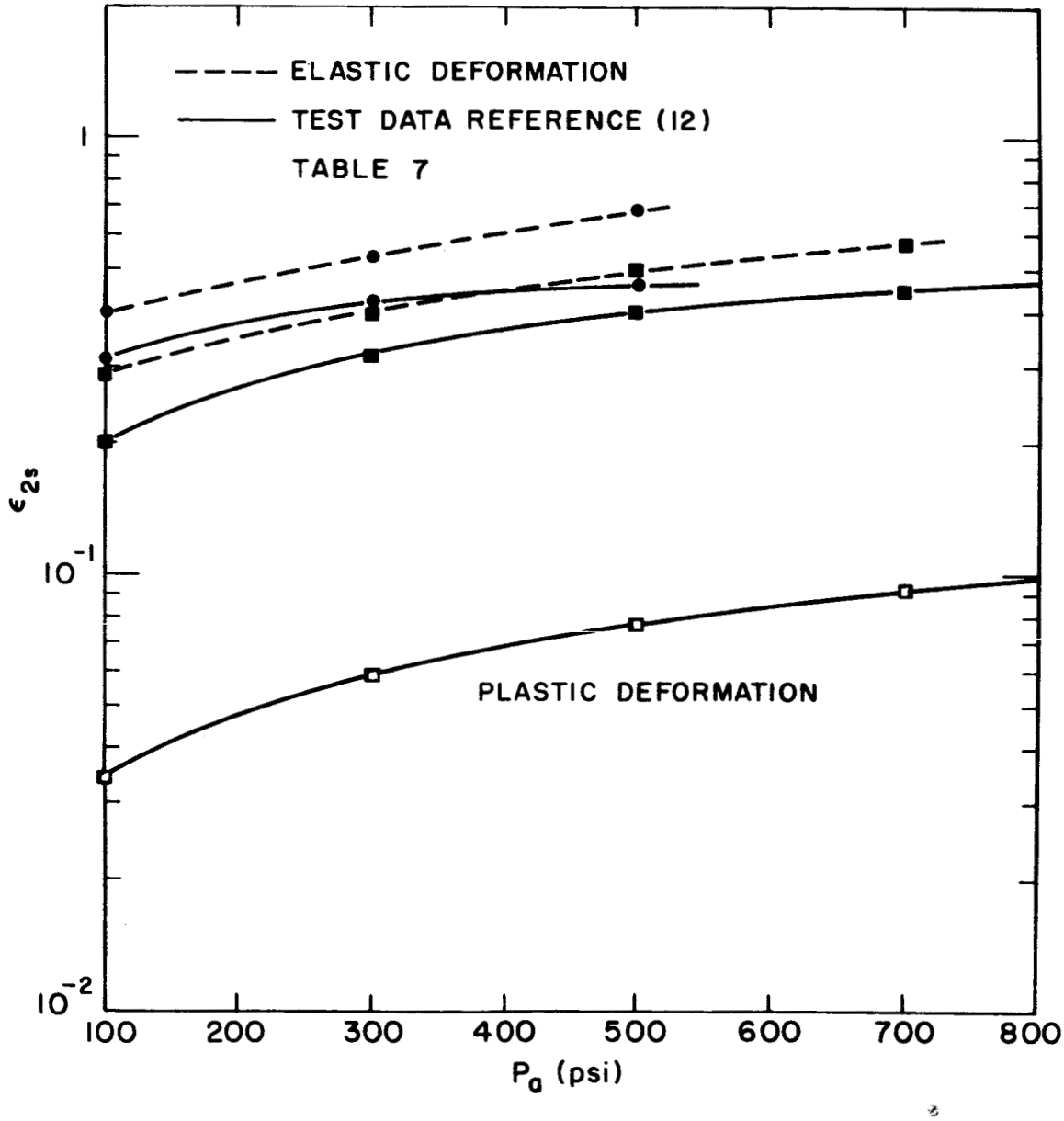

FIGURE 23. ϵ_{2s} VERSUS APPARENT PRESSURE MAGNESIUM

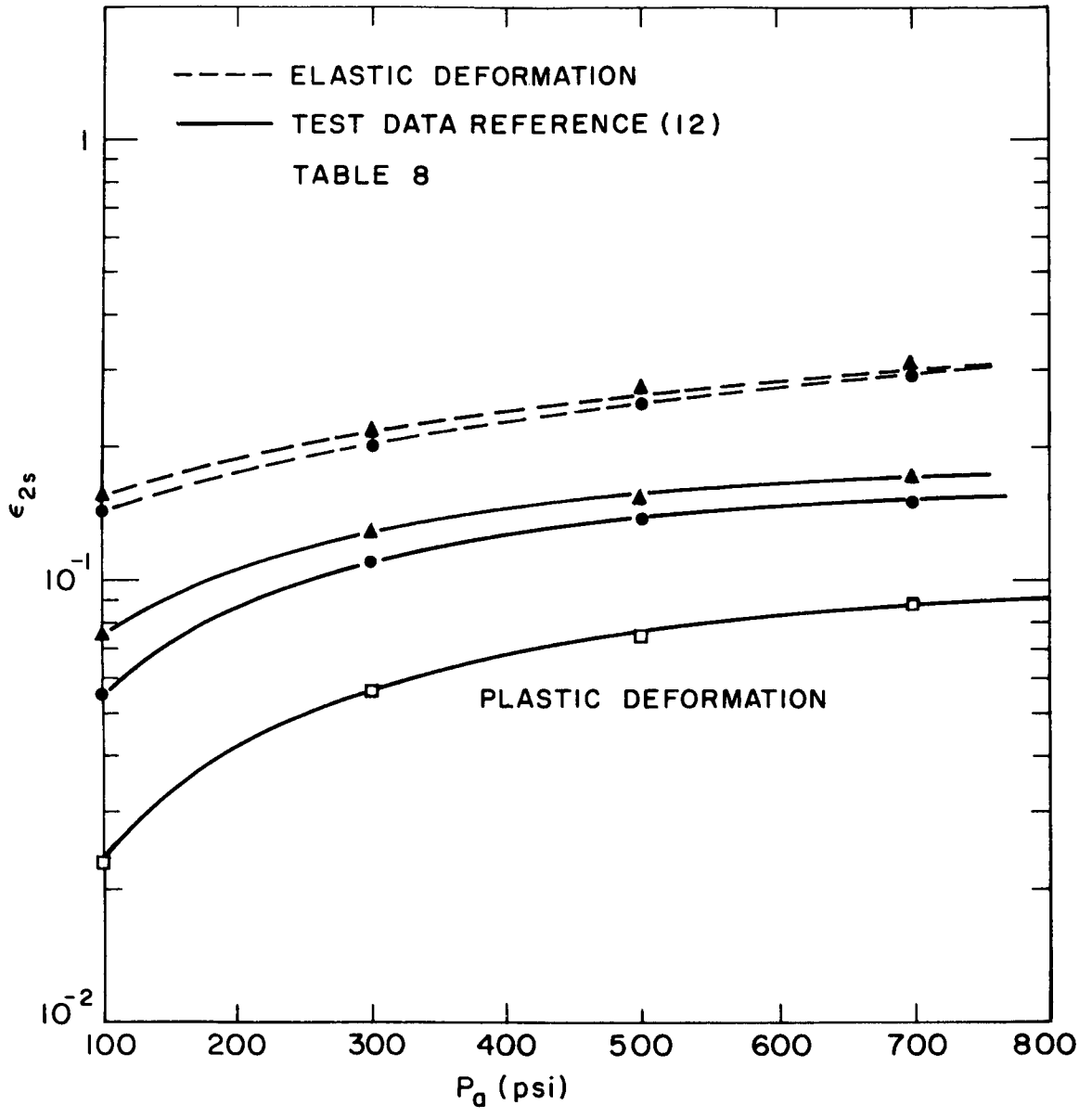

FIGURE 24. ϵ_{2s} VERSUS APPARENT PRESSURE BRASS

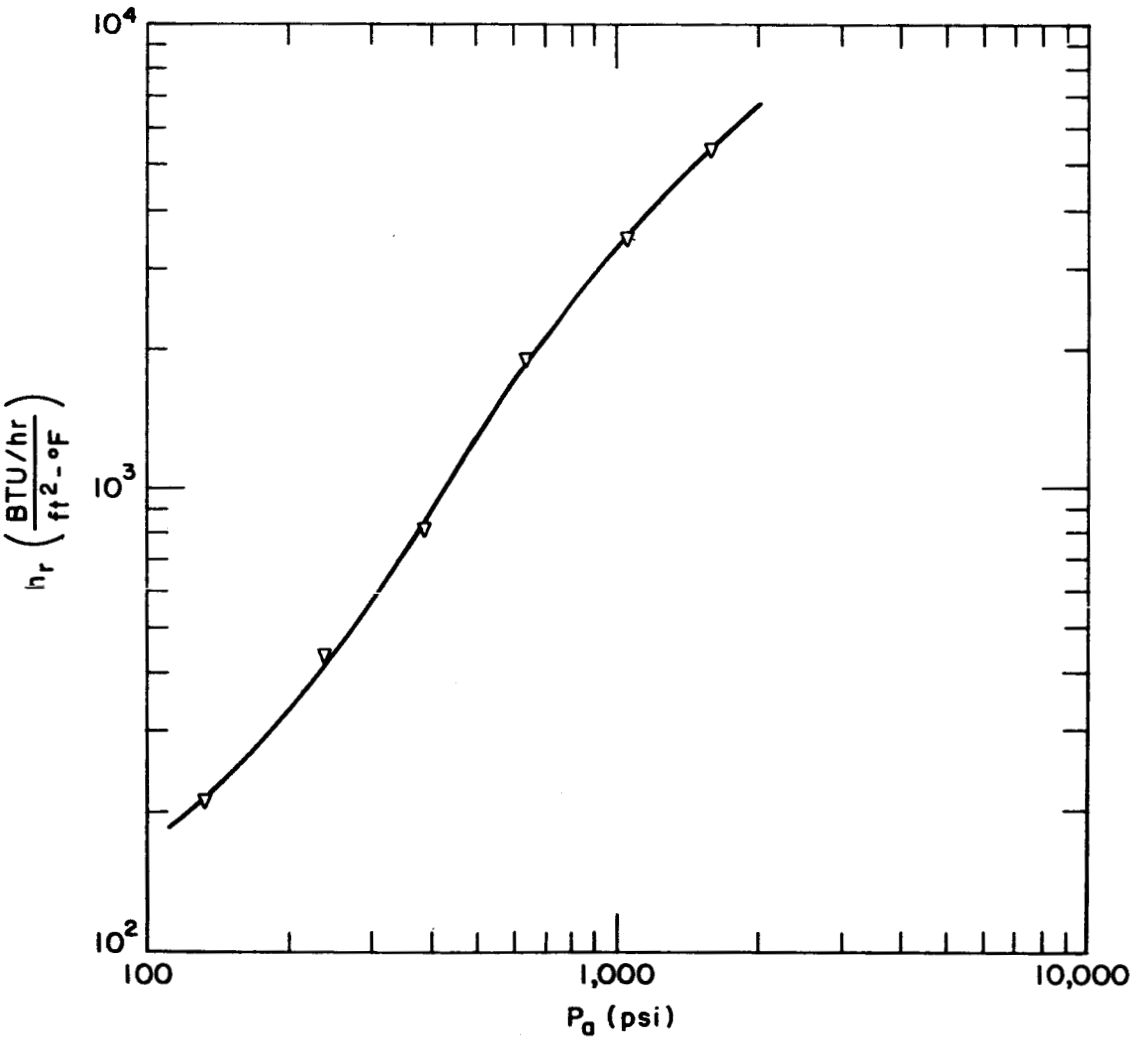

FIGURE 25. CONDUCTANCE VERSUS APPARENT PRESSURE STAINLESS STEEL

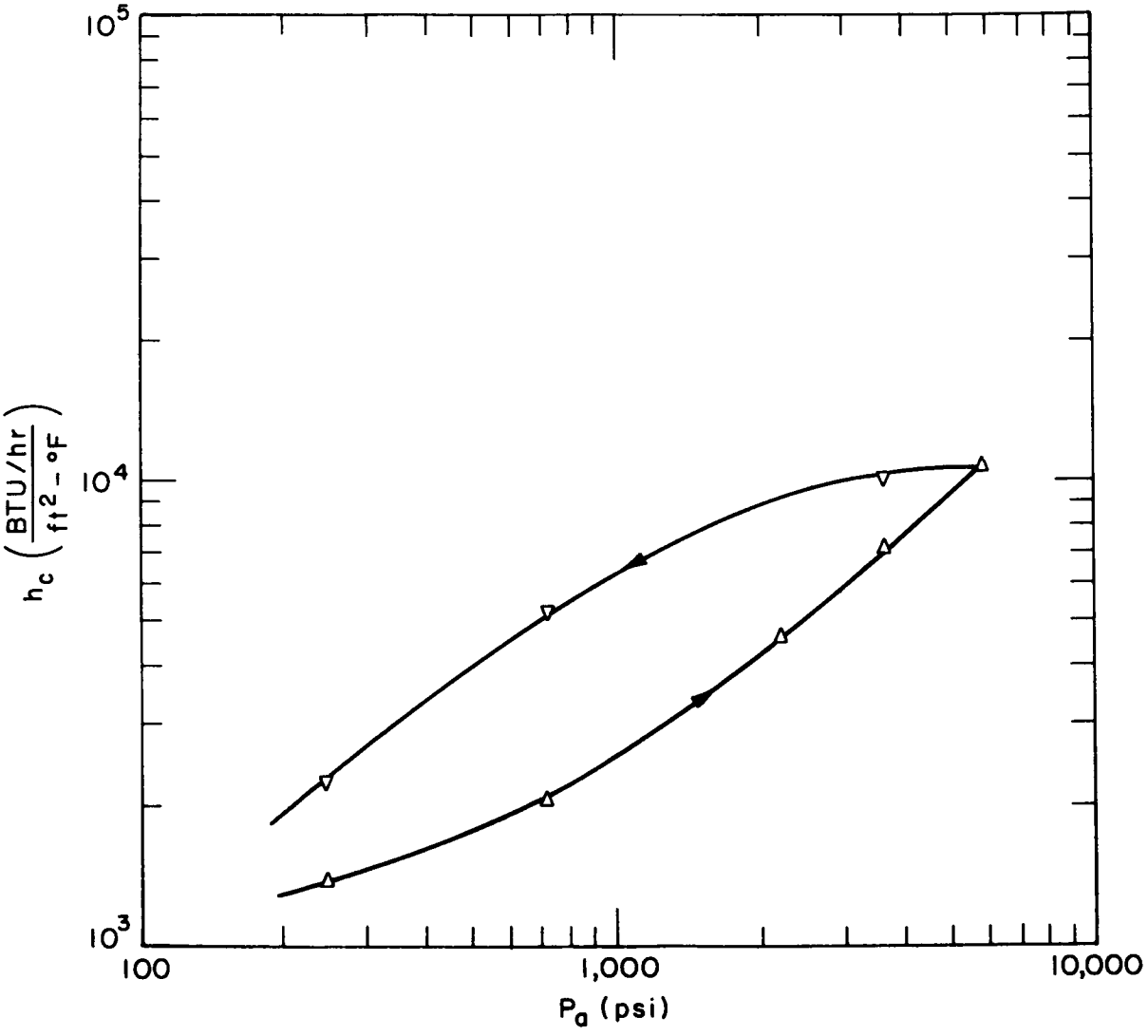

FIGURE 26. CONDUCTANCE VERSUS APPARENT PRESSURE ALUMINUM

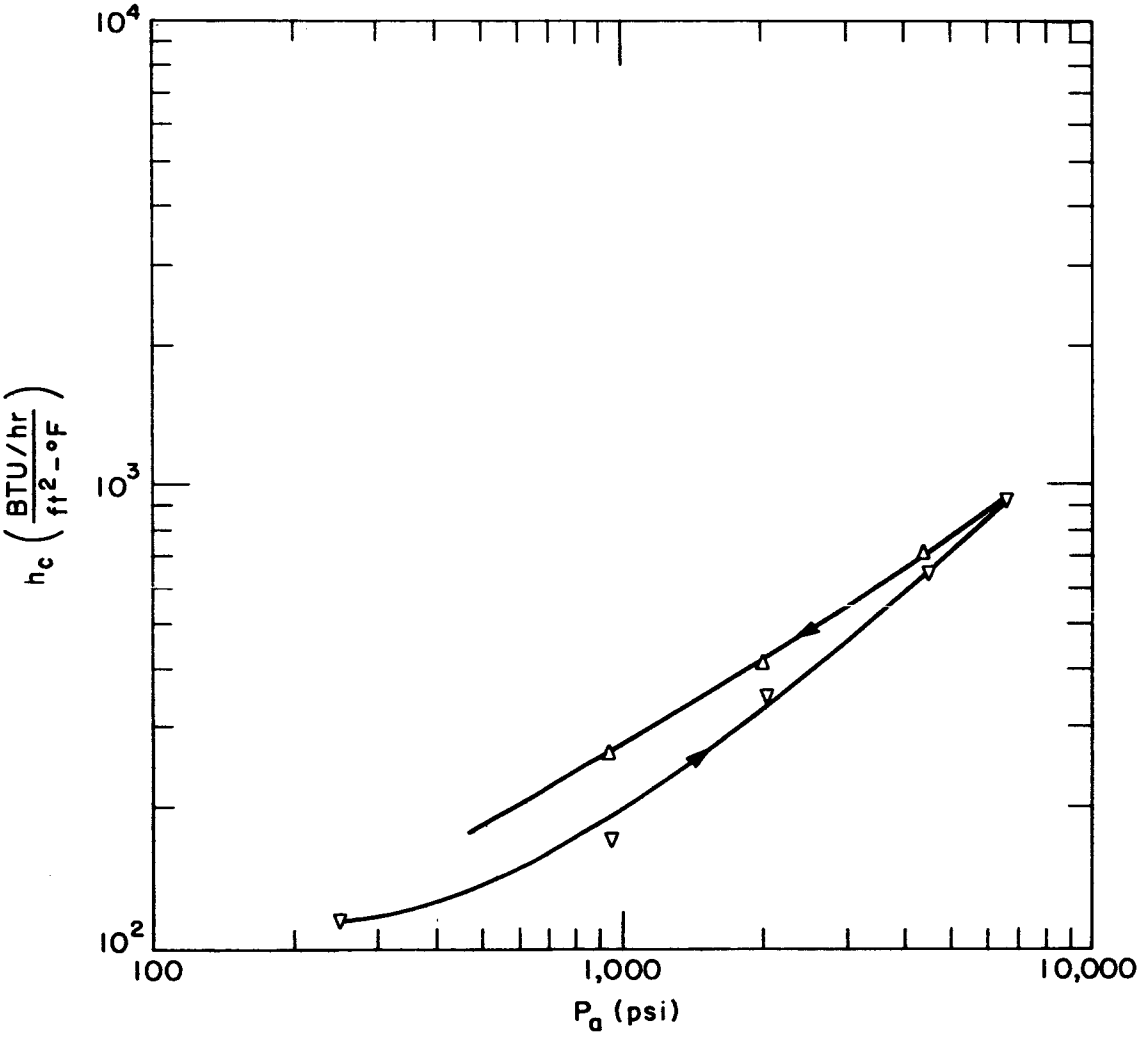

FIGURE 27. CONDUCTANCE VERSUS APPARENT PRESSURE STAINLESS STEEL

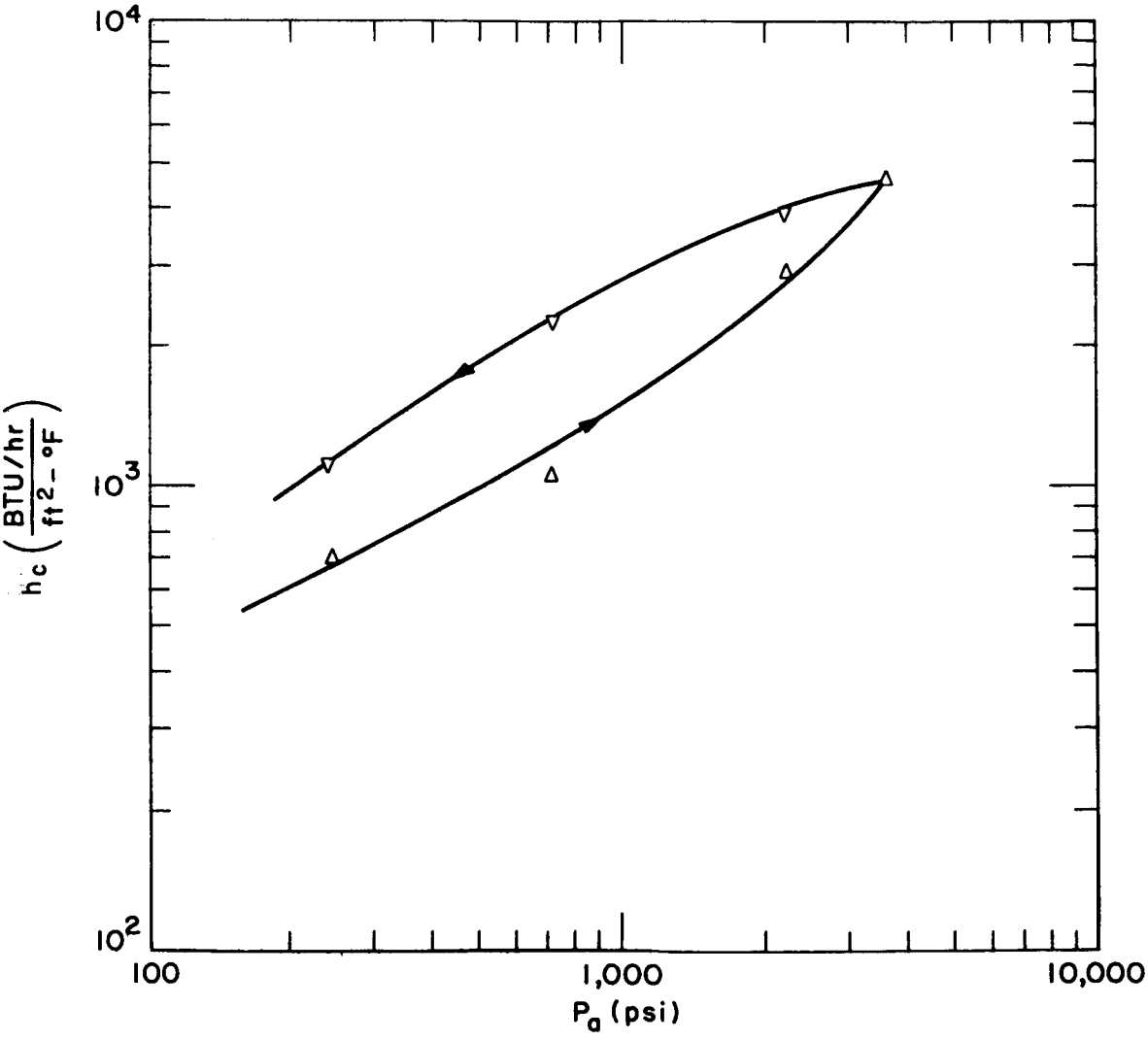

FIGURE 28. CONDUCTANCE VERSUS APPARENT PRESSURE MAGNESIUM

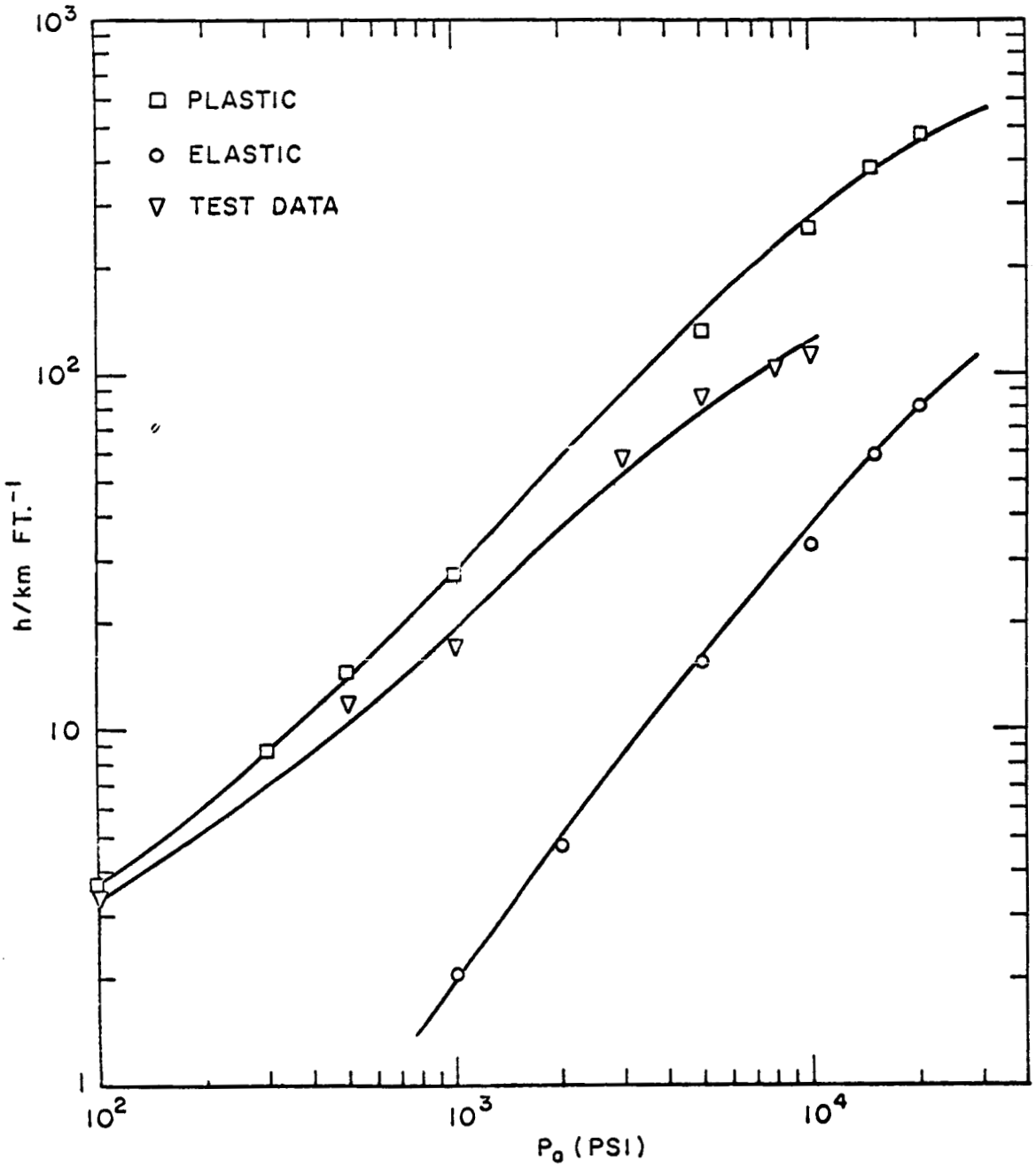

FIGURE 29. HEAT TRANSFER COEFFICIENT VERSUS APPARENT PRESSURE

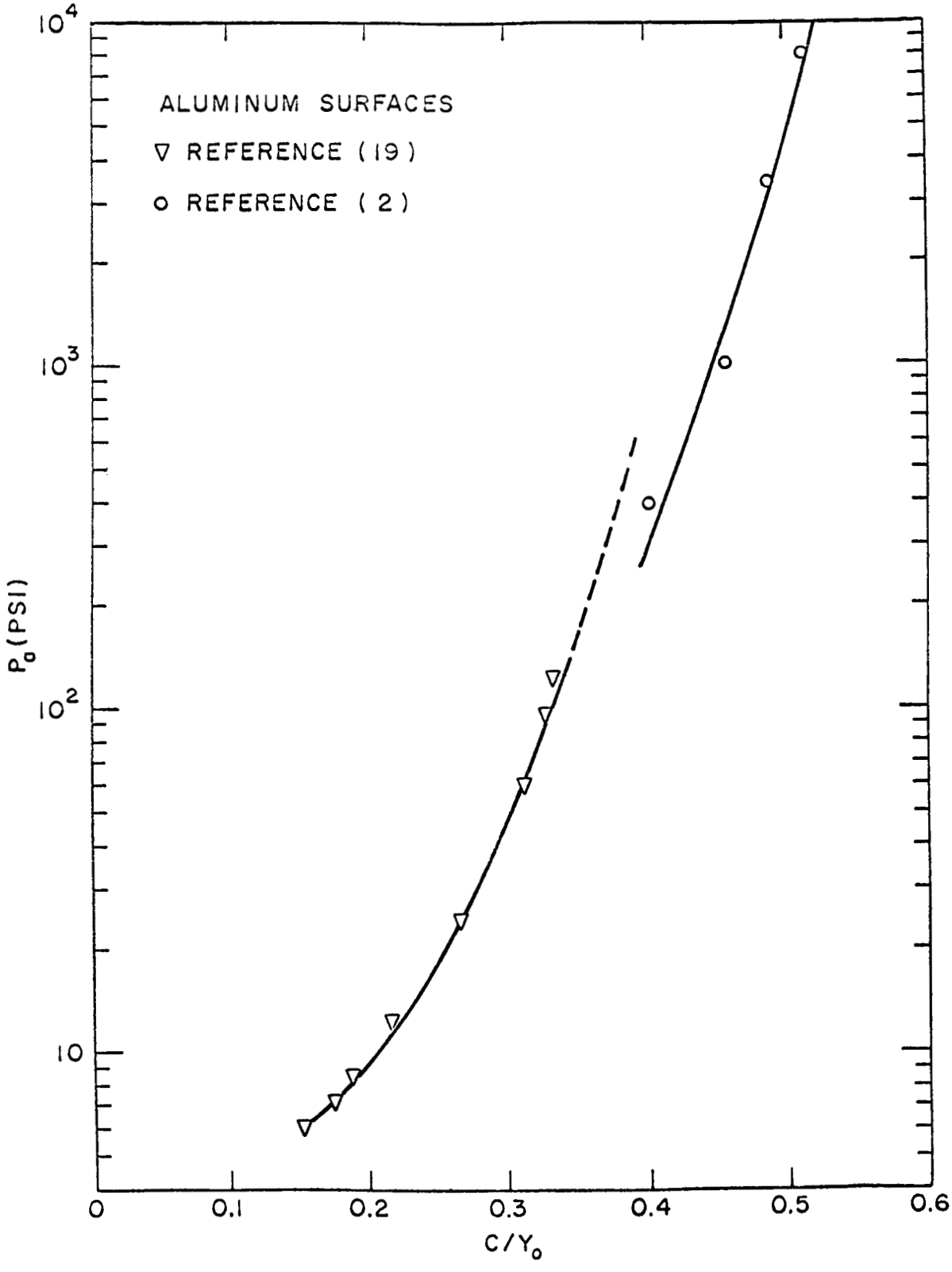

FIGURE 30. APPARENT PRESSURE VERSUS COMPLIANCE RATIO

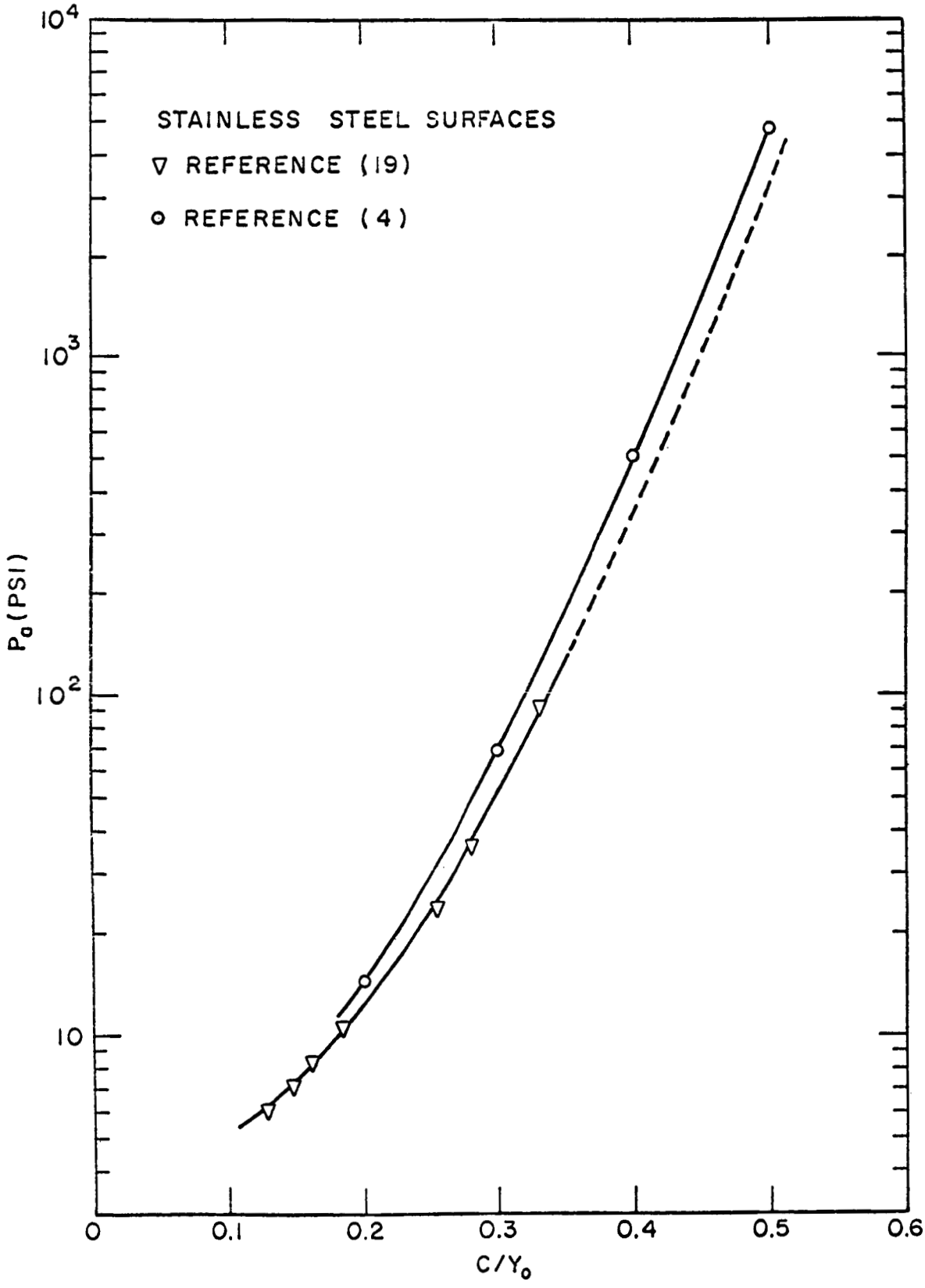

FIGURE 31. APPARENT PRESSURE VERSUS COMPLIANCE RATIO

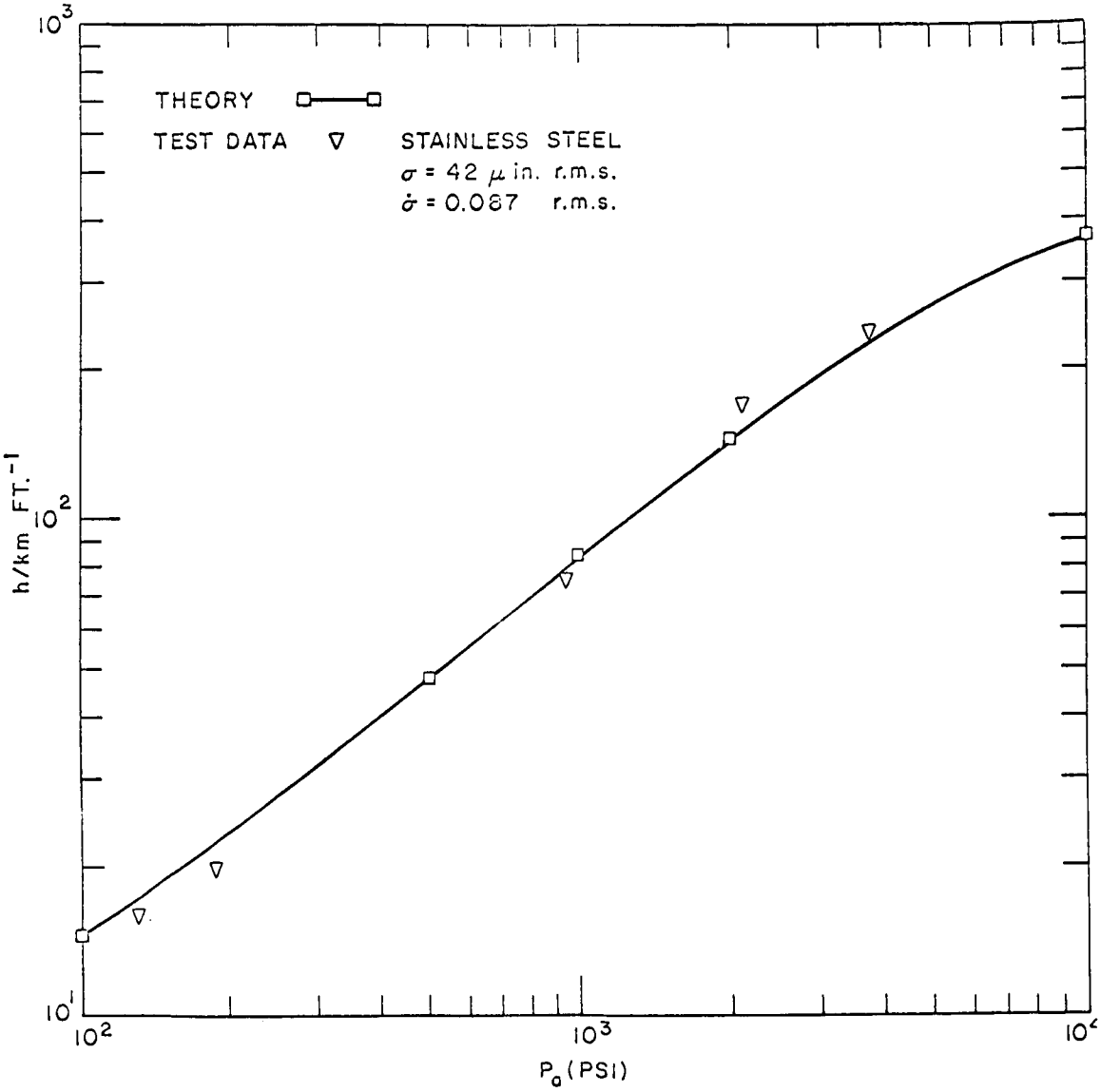

FIGURE 32. HEAT TRANSFER COEFFICIENT VERSUS APPARENT PRESSURE